Discrete Dynamics in Nature and Society

Advanced Dynamic Simulations in Transportation

Guest Editors: Wei Guan, Xuedong Yan, Essam Radwan, Sze Chun Wong, and Xiaoliang Ma

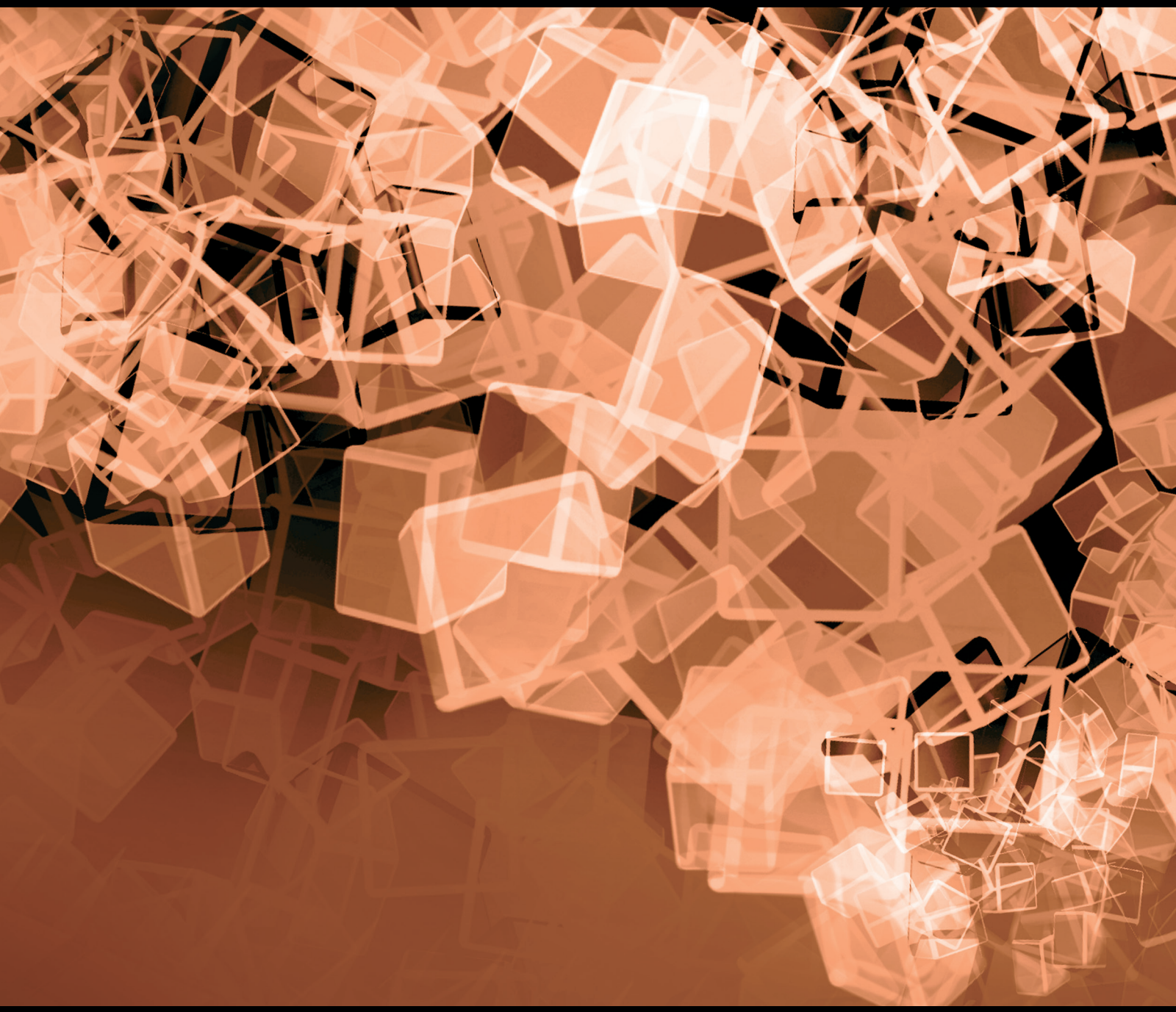

Advanced Dynamic Simulations in Transportation

Discrete Dynamics in Nature and Society

Advanced Dynamic Simulations in Transportation

Guest Editors: Wei Guan, Xuedong Yan, Essam Radwan, Sze Chun Wong, and Xiaoliang Ma

Editorial Board

Contents

Hindawi Publishing Corporation
Discrete Dynamics in Nature and Society
Volume 2015, Article ID 675263, 2 pages
http://dx.doi.org/10.1155/2015/675263

Editorial

Advanced Dynamic Simulations in Transportation

Wei Guan,[1] Xuedong Yan,[1] Essam Radwan,[2] Sze Chun Wong,[3] and Xiaoliang Ma[4]

[1]*MOE Key Laboratory for Urban Transportation Complex Systems Theory and Technology, Beijing Jiaotong University, Beijing 100044, China*
[2]*Center for Advanced Transportation Systems Simulations, University of Central Florida, Orlando, FL 32816, USA*
[3]*Department of Civil Engineering, The University of Hong Kong, Pokfulam, Hong Kong*
[4]*Department of Transportation Sciences and Centre for Traffic Research (CTR), Royal Institute of Technology (KTH), 100 44 Stockholm, Sweden*

Correspondence should be addressed to Wei Guan; weig@bjtu.edu.cn

Received 6 July 2015; Accepted 7 July 2015

Advanced simulation methods have been widely applied in the field of transportation for driving behavior investigation, planning, design and operation of transportation systems, evaluation of transportation policy, and innovation of intelligent transportation systems (ITS). With the development of computer technologies, dynamic simulations even in a real time manner become more and more powerful and sophisticated in either practical applications or scientific research in the transportation field. This special issue aims to discuss and share experience in theoretical analyses, state-of-the-art techniques, and cutting-edge case studies of advanced dynamic transportation simulations.

In this special issue, we collect seven papers that involve different aspects of advanced simulation techniques to explore the mechanism of transportation operation, effectiveness of intelligent transportation systems, driving behavior and traffic operation, and transportation logistics system performance under various scenarios.

In the field of transportation logistics, closed-loop supply chain distribution network system has become a new research point since people pursue circular economy and social sustainable development. X. Yuan and X. Zhang establish use of Vensim software to simulate three-loop supply chain distribution network system model and investigate the relationship among supplier, manufacturer, retailers, and products (parts) recycler with the government policy. In a competitive environment, transportation costs are an important part of the costs of logistics enterprises. Q. Yan and Q. Zhang present a biobjective transportation cost model for solving a multiobjective vehicle routing problem with soft time-window constraints that specify the earliest and latest arrival times of customers.

Traffic flow big data strongly shows temporal, spatial, and historical correlations. H. Lu et al. use speed and occupancy data to develop the traffic flow state clustering model. Using a bilevel optimization model, the authors calculate the number of temporal-spatial-historical correlation variables and traffic flow state formulation of regional traffic flow. Traffic sensors (e.g., magnetic detectors, cameras, and bluetooth detectors) provide real-time data for traffic operation surveillance and arterial travel time estimation. Considering the restriction in the sensors' installation cost, Q. Yu et al. propose a sensor location model to find the optimal sensor placement for minimizing the travel time estimation error in signalized arterial.

As the economy develops rapidly, deepening urbanization and the increasing urban population lead to a large demand for urban rail transit in many cities. The modern streetcar system is considered as an important mode of urban transit systems in China. However, its construction and development face massive challenges due to the conflicts between streetcars and other vehicles at the intersections in urban road networks. B. Wang et al. develop a segmented signal progression model for modern streetcar system in order to ensure high streetcar system efficiency and minimize its negative impacts on transit and vehicular traffic.

On the other hand, many urban rail systems have been plagued by heavy passenger flow, and thus it is critical to design an efficient and economical timetable for a heavily congested urban rail corridor. Y.-T. Zhu et al. propose a model for timetable design of urban rail line with capacity constraints to identify the departure time of trains at the start terminal and minimize the system cost, including passenger waiting cost and operating cost. A two-stage simulation-based genetic algorithm is developed to solve the model.

Interestingly, while most of the simulation models are explored for motor vehicles, Zhou et al. improve the Nagel-Schreckenberg (NS) CA model and the multivalue CA (M-CA) model for both regular bicycles and electric bicycles and provide useful simulation tools for mixed traffic operation analyses. A two-stage simulation-based genetic algorithm is developed to solve the model. In this study, different bicycle driving behaviors with characteristics of the slowing down probability and lane-changing probability were simulated using the proposed models. The results show that the M-CA model exhibits more stable performance than the two-lane NS model and provides results that are closer to real bicycle traffic performance.

Transportation simulation is a multidisciplinary area. The editors acknowledge that this special issue cannot fully cover all cutting-edge technologies and methods emerging in this field. However, these papers reveal both the promise and the challenges faced by the field of dynamic simulations in transportation. Through this special issue, we encourage more transportation researchers, educators, students, practitioners, and policy makers to seek and explore advanced dynamic simulation techniques to enhance transportation operation, safety, and environment quality.

Acknowledgments

We sincerely acknowledge all of the authors and anonymous reviewers' great contributions to this special issue.

Wei Guan
Xuedong Yan
Essam Radwan
Sze Chun Wong
Xiaoliang Ma

Hindawi Publishing Corporation
Discrete Dynamics in Nature and Society
Volume 2015, Article ID 854089, 13 pages
http://dx.doi.org/10.1155/2015/854089

Research Article

Simulation-Based Sensor Location Model for Arterial Street

Qinxiao Yu, Ning Zhu, Geng Li, and Shoufeng Ma

Institute of Systems Engineering, College of Management & Economics, Tianjin University, Tianjin 300072, China

Correspondence should be addressed to Geng Li; ligeng345@126.com

Received 25 December 2014; Accepted 26 May 2015

Academic Editor: Essam Radwan

Traffic sensors serve as an important way to a number of intelligent transportation system applications which rely heavily on real-time data. However, traffic sensors are costly. Therefore, it is necessary to optimize sensor placement to maximize various benefits. Arterial street traffic is highly dynamic and the movement of vehicles is disturbed by signals and irregular vehicle maneuver. It is challenging to estimate the arterial street travel time with limited sensors. In order to solve the problem, the paper presents travel time estimation models that rely on speed data collected by sensor. The relationship between sensor position and vehicle trajectory in single link is investigated. A sensor location model in signalized arterial is proposed to find the optimal sensor placement with the minimum estimation error of arterial travel time. Numerical experiments are conducted in 3 conditions: synchronized traffic signals, green wave traffic signals, and vehicle-actuated signals. The results indicate that the sensors should not be placed in vehicle queuing area. Intersection stop line is an ideal sensor position. There is not any fixed sensor position that can cope with all traffic conditions.

1. Introduction

Traffic sensors (e.g., magnetic detectors, cameras, and bluetooth detectors) are widely used in transportation system for systematic surveillance. Various traffic applications need different sensor data. OD estimation may require the traffic counting information on links. Travel time estimation asks for information about link travel time or path travel time. These information can be obtained either from float vehicle such as taxi or cameras which are able to read plate license number. One of the most intuitive pieces of information for advanced traveler information system is travel time. Therefore, a simple and implementation-wise easy method is needed to estimate travel time.

Attempt to estimate arterial street travel time is very challenging. Arterial street traffic is highly dynamic and the movement of vehicles is disturbed by signals and irregular vehicle maneuver. Zhang [1] developed a travel time and journey speed estimation method for freeways by the utilization of volume to capacity ratio, volume, and occupancy. Skabardonis and Geroliminis [2] employed Kinematic wave theory to model the spatial-temporal queueing at the signals. Liu and Ma [3] proposed that loop detector data and signal phase changes information, which in a high-resolution data context are required to estimate travel time. Without using traditional traffic flow theory, Takaba et al. [4] developed some heuristic models for travel time estimation by using loop detector and license plate reader. A neural network framework is developed to fuse probe vehicle data and loop detector data by Cheu et al. [5]. Dailey and Cathey [6] employed probe sensor to define vehicle speed function. Currently, Li et al. [7] studied that most of the travel time estimation methods or algorithms require many sources of real time data. Investment in these transportation surveillance devices is costly, and thus providing these pieces of real time information is expensive. Among all these traffic sensors, loop detectors are relatively cheap and popular. In addition, loop detectors are also widely used in travel time estimation field [8, 9]. Due to the high cost of transportation infrastructure, it is necessary to find a way to save investment.

Sensor location problem works for this purpose. It aims to find an optimal sensor placement pattern either in transportation network or freeway. The purpose of sensor placement is mainly for various flow estimations which are OD trips estimation, link flows estimation, path flows estimation, and its related application. Yang and Zhou [10] proposed four sensor location rules in transportation network mainly for OD estimation. This paper can be seen the seminal paper in

the sensor location literature. Bianco et al. [11] introduced a linear system approach for sensor location problem modeling. Gentili and Mirchandani [12] extended linear system approach by introducing active and passive sensors. Ehlert et al. [13] presented several models to cover as many flows as possible. OD estimation using generalized least-square method is applied to seek for the optimal sensor placement pattern by Fei et al. [14] and Eisenman et al. [15]. In addition to OD estimation, path estimation or identification is another hot topic. Normally, license plate reader is employed to recognize route or estimate route travel time by Castillo et al. [16] and Mínguez et al. [17]. Modeling techniques adopted are integer program. Commercial software or heuristics is used for solving these problems. Hu et al. [18] studied the link sensor placement problem to infer all link flow information of the network of interests. Viti et al. [19] investigated partial observation problems and gave a simple metric for quantify the quality of a sensor placement pattern. Other sensor location problems include mobile sensor routing problem (Zhu et al. [20]), bottleneck identification oriented sensor location problem (Liu and Danczyk [21]), and sensor location problem considering time-spatial correlation (Liu et al. [22]).

Sensor location problem on freeway is relatively limited, particularly for travel time estimation. Kim et al. [23] adopted genetic algorithm to find an optimal sensor placement location on freeway with the minimization of mean absolute relative error. Kianfar and Edara [24] used clustering technology for optimizing freeway traffic sensors. Other freeway sensor location problems employ empirical study methods (Kwon et al. [25]), simulation (Thomas [26]), and dynamic programming (Ban et al. [27]).

Due to the complexity of urban transportation system, none of current studies consider combining travel time estimation method with a sensor location pattern to seek an optimal sensor placement pattern. Another important characteristic of urban transportation system is traffic signal control. This paper attempts to find optimal sensor location pattern with traffic signals. A simulation tool is used to generate basic traffic flow data. The rest of this paper is organized as follows. Section 2 offers a description of travel time estimation method and partition rule in arterial street. Section 3 presents optimal sensor location pattern on a single link. Section 4 gives results for multiple links and also with traffic signal control. Section 5 concludes the whole paper.

2. Sensor Location Model Description

2.1. Section Partition Rule for Arterial Street. In our model, a signalized arterial street is partitioned into sections. Each section is associated with a sensor, and the speed of section is represented by the average instantaneous speed (normally, it is collected from the 30s time interval) at the sensor spot. The estimated travel time of each section is calculated by the length and speed of the section. By summing up estimated travel time across all sections, the estimated arterial travel time can be obtained.

In our study, the boundary of section is determined by three sensors, which are located at the section and the adjacent upstream and downstream section, respectively. The total length of signalized arterial is set to L, the total number of sensors is n, the location of the sensor i is x_i, and the length of section i is l_i which is calculated as follows:

$$l_i = \begin{cases} x_1 + \dfrac{x_2 - x_1}{2}, & i = 1 \\ \dfrac{x_{i+1} - x_{i-1}}{2}, & 1 < i < n \\ L - x_n + \dfrac{x_n - x_{n-1}}{2}, & i = n. \end{cases} \tag{1}$$

2.2. Travel Time Estimation Model. There are many travel time estimation models, among which the speed-based travel time estimation model is easy-to-operate and widely applied [6–9, 28–30]. These three models proposed by Li et al. [7] are adopted in our study. The principle of all these three models is to calculate travel time according to the spot-speed obtained by sensors.

The first model is instantaneous model. A vehicle is supposed to enter the arterial street at time k. The detected speed at time k is considered as the average speed of vehicles at that section. The travel time of vehicle at section i is denoted as $t(i, k)$:

$$t(i,k) = \frac{l_i}{v(i,k)}, \tag{2}$$

where l_i is the length of the section i and $v(i, k)$ is the measured speed of section i at time k. The travel time $T(k)$ of vehicle passing through the entire signalized arterial street is the sum of all sections' travel times:

$$T(k) = \sum_{i=1}^{n} t(i,k). \tag{3}$$

In the instantaneous model, speeds from only one point on each section are used to estimate travel time, while ignoring the speed variations within a section. This does not meet the authentic traveling situation of vehicles. However, from the perspective of calculation, when the travel time is fixed, its corresponding average speed is fixed. Therefore, the sensor location pattern is very critical. A suitable senor location pattern can accurately capture the average travel time of its spatial influence area. On the other hand, all speeds are collected at the time of vehicle entering the arterial. The speed associated with the downstream section will not change dramatically when the vehicle traverses the arterial. These two reasons result in travel time estimation error. The other two speed estimation models are Time Slice Model and Dynamic Time Slice Model.

The difference among the three travel time estimation models lies in the calculation method for vehicle speed on each section, which is the main factor that affects error. These three models all use the speed measured by sensors, so the travel time estimation error is caused by not only inevitable calculation error, but also the error arising from the location of sensor in arterial street. Different combinations of sensor locations generate different section partitions, thus, resulting in different estimation errors.

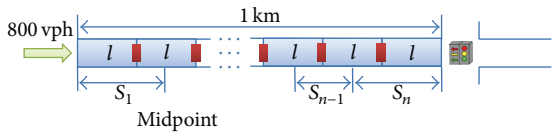

FIGURE 1: Partitioned arterial street with traffic signal.

To compare the differences among these three models, numerical experiments are conducted for the identical sensor location pattern. In our study, a traffic simulation tool is used for a street with length 1 km as shown in Figure 1. Intersection signal cycle is 100 s, green light duration is 60 s, and the vehicle enters the street with a speed of 3.6 km/h. The maximum speed is 57.6 km/h. The vehicle's arrival rate is 800 vph and obeys Poisson distribution. Sensors are evenly distributed on the road at equal interval of l. The influential area of each sensor is shown in Figure 1. The number of sensors is increased from 1 to 10. Travel time is estimated with above-mentioned three methods, respectively.

In order to compare the resulted obtained by these three methods, we use three measures for evaluation which are the mean absolute error (MAE), root mean square error (RMSE), and mean absolute relative error (MARE), respectively.

$$\begin{aligned} \text{MAE} &= \frac{1}{n}\sum_{i=1}^{n}\left|\text{ett}_i - \text{gttt}_i\right|, \\ \text{RMSE} &= \sqrt{\frac{1}{n}\sum_{i=1}^{n}\left(\text{ett}_i - \text{gttt}_i\right)^2}, \\ \text{MARE} &= \frac{1}{n}\sum_{i=1}^{n}\frac{\left|\text{ett}_i - \text{gttt}_i\right|}{\text{gttt}_i}. \end{aligned} \tag{4}$$

ett_i refers to the estimated travel time, gttt_i refers to the ground-truth travel time, and n refers to the number of vehicles. Through 10 traffic simulations, 10 groups of travel time $\{S_r \mid S_r = (\text{gttt}_{r1}, \text{gttt}_{r2}, \ldots, \text{gttt}_{rn}), r = 1, 2, \ldots, 10\}$ are obtained. These three travel time estimation methods were used to calculate the corresponding estimated travel time and the MAE_r, MARE_r, and RMSE_r respectively. Finally, 10 sets of three measures are obtained for each travel time estimation method. The mean values and standard deviations are calculated according to these 10 sets of data. The experimental results are shown in Figure 2.

As shown in Figure 2, the three estimation models have little differences in most cases. Particularly, the time slice model and dynamic time slice model almost obtain the same results. The instantaneous model outperforms other two estimation models, although instantaneous model (IM) only makes estimation according to the traffic condition when vehicle enters the street. But under the traffic signal control, the traffic flow has certain reproducibility. The vehicle's travel time can be accurately estimated when the vehicles traverse the arterial street smoothly. Therefore, in subsequent experiments, IM method is adopted to estimate the travel time.

3. Sensor Location Setting in Single Link

In the urban transportation network, the movement of vehicles is with some regularity due to the traffic signal control. Generally it can be summarized as, after passing through previous intersection, vehicles enter the street at low speed or original speed. Then, the vehicles accelerate to the maximum allowable speed and keep moving. When approaching the next intersection, it determines whether to slow down or keep moving at the original speed according to traffic signals. The speed contour profile is shown in Figure 3.

The key point of estimating vehicle's travel time on a certain link is to find the vehicle's average speed on that link. Vehicle moves with different speed at different positions of the link. In order to accurately estimate travel time, we need to find an appropriate location for the sensor, making sure that the instantaneous speed is close to the average speed. Therefore, the location of sensor has great impact on the travel time estimation error. Figure 4 shows the relationship between travel time estimation error (MARE) and different sensor locations when a sensor is placed on a 1 km link under different arrival rates.

As can be seen from Figure 4, the smallest travel time estimation error is obtained when the sensor is placed at the 50 m, and the mean travel time estimation error of the four arrival rates is about 8%. In the link from 100 m to 850 m, the sensor location has little impact on travel time estimation and the error is about 29%. In the 100 m of downstream section, the travel time estimation error increases about 120%.

Sensor location pattern is closely related to the vehicle's trajectory on the link. (i) If a vehicle enters the intersection at a slow speed and the sensor is placed at the inlet (0 m) position, where the average speed is small, the estimation error will be large. (ii) If the vehicle accelerates to the maximum speed after entering the link, the vehicle speed varies greatly within this distance (from 3.6 to 56.6 km/h), so it is easy to find a position that can represent the average speed of the link. (iii) The vehicle runs at the limited speed in the middle section of the link, and the speed fluctuation is small. Therefore, no matter where the sensor is placed, the detected speed is almost equal to the maximum speed. Thus, it cannot reflect the average speed on the link. (iv) Within the 100 m in the downstream, vehicles enter the queuing area. The length of queue increases as the arrival rate increases. When the sensor is closer to the intersection, the sensor is likely to be occupied by vehicles. When the sensor is occupied, it cannot detect speed. The estimation error is large. However, when the arrival rate is less than the saturation volume, the number of queuing vehicles is small. All the vehicles can pass through the intersection in a signal cycle. The proportion of sensor's occupied time is small. Therefore, the travel time can be estimated. When the arrival rate is greater than the saturated volume, vehicles at the tail of the queue need to wait for two or more signal cycles before passing through the intersection. The sensor is more likely to be occupied and cannot obtain vehicle speed during a long period of time.

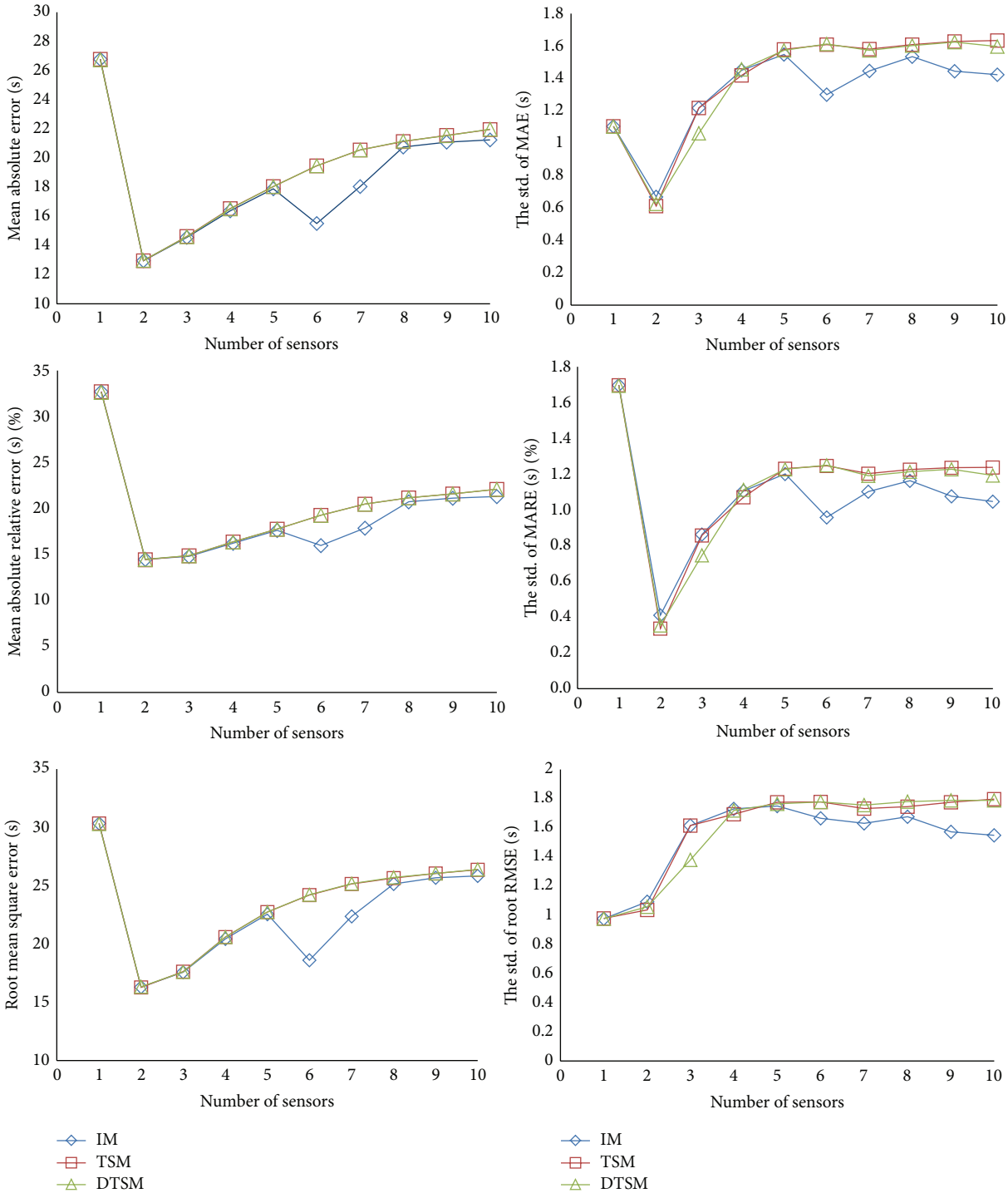

Figure 2: Errors and their standard deviations versus number of sensors.

4. Sensor Location in Arterial Street

4.1. Sensor Location Model Description. A signalized arterial street is usually composed of many links, and there is a traffic signal between every two links. In order to study sensor placement pattern in such a signalized arterial street, we divide arterial street into equal-length cells, as shown in Figure 5. If a cell is equipped with a sensor, then the sensor will be placed on the cell's right boundary. Section is defined as the influential area of the sensor. The partition method is given in previous section.

Assume that the entire horizon of the study is T and a total of M vehicles pass through the entire street. K sensors will be placed on the arterial street; that is, there will be K sections.

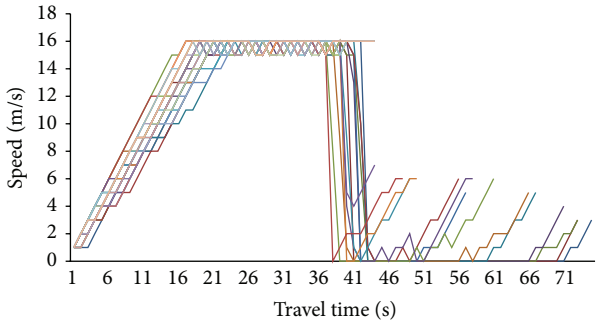

Figure 3: Speed contour profile in a signal cycle.

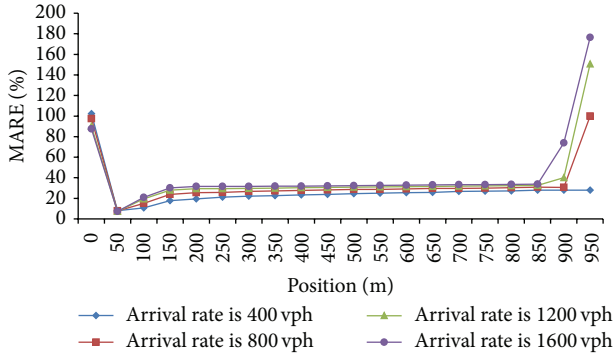

Figure 4: Estimate error versus different sensor locations.

The actual travel time of the mth vehicle that passes through the arterial is GTTT_m, which is obtained by simulation. The estimated travel time is ETT_m, which is the total sum of K sections' estimated travel time ETT_{mk}. The goal of sensor location model is to minimize the error between estimated travel time and actual travel time. The decision variable of the model is $x_i \in \{0, 1\}$, which indicates whether the sensor is placed on ith cell. The model is shown as follows and is called M1:

M1:

$$\min \quad \frac{1}{M}\sum_{m=1}^{M}\left|\frac{\left(\sum_{k=1}^{K}\mathrm{ETT}_{mk}\right)-\mathrm{GTTT}_m}{\mathrm{GTTT}_m}\right|, \tag{5a}$$

$$\text{subject to:} \quad \sum_{i=1}^{N} x_i = K, \tag{5b}$$

$$x_i \in \{0, 1\}, \tag{5c}$$

$$Y \text{ is set of the index of } x_i$$

$$\text{where } x_i = 1, \tag{5d}$$

$$y_k \text{ is the } k\text{th element in } Y,$$

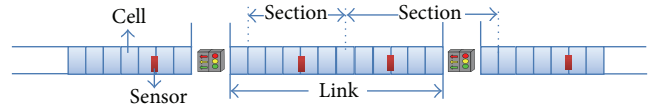

Figure 5: Partitioned arterial street.

$$s_k = \begin{cases} \dfrac{y_{k+1} - y_{k-1}}{2}, & k = 2, \ldots, K-1 \\ y_1 + \dfrac{y_2 - y_1}{2}, & k = 1 \\ y_K + \dfrac{N - y_K}{2}, & k = K, \end{cases} \tag{5e}$$

$$\mathrm{ETT}_k = \frac{s_k}{v_k} \cdot l. \tag{5f}$$

In M1, M is the number of total vehicles, N is the number of cells, and K is the number of sensors, namely, the budget constraint. x_i is the decision variable, and $x_i = 1$ indicates that the ith cell has a sensor; otherwise, $x_i = 0$. y represents the set of cells that are installed with sensors, wherein the total number of elements is K. For instance, if the entire arterial street is divided into 10 cells, budget constraints are three sensors, $Y = \{3, 6, 8\}$ means that sensors are placed in the 3th, 6th, and 8th cells. y_k refers to the kth element of set Y, and S_k is the coverage area of kth sensor, namely, the number of cells contained in the kth section, which is determined by the position of adjacent upstream and downstream sensors. When the positions of a group of sensors are given, the length of K sections can be calculated. Also taking $Y = \{3, 6, 8\}$ as an example, s_1 covers 4.5 cells, s_2 covers 2.5 cells, and s_3 covers 3 cells. V_k is the average speed of section k which is calculated according to the speed detected by corresponding sensor. After solving this model, the optimal sensor placement pattern can be obtained. Due to the complexity of the combinational optimization problem, exact algorithm is very hard. Thus, in our study, genetic algorithm is employed.

In this section, a mathematic model is proposed to solve the sensor placement problem in arterial street. It is a 0-1 programming model. The objective function is to minimize the relative travel time estimation error between estimated and actual travel time. The input data of the model is travel time information of all vehicles in computer simulation which is treated as ground-truth travel time. Once the ground-truth travel time information is given, and our proposed mathematical programming model can decide the optimal sensor placement pattern that minimizes the relative travel time estimation error. Therefore, our model is a mathematical model. In addition, the model is deterministic.

4.2. Case Study. In this study, we only consider the influence of vehicle arrival rate and traffic signal strategy on sensor placement pattern which are two major factors that affect travel time on urban network. In the simulation, the signalized arterial street is set as 3 km long, and it is composed of 6 links. Each link is 0.5 km long. Each link is divided into

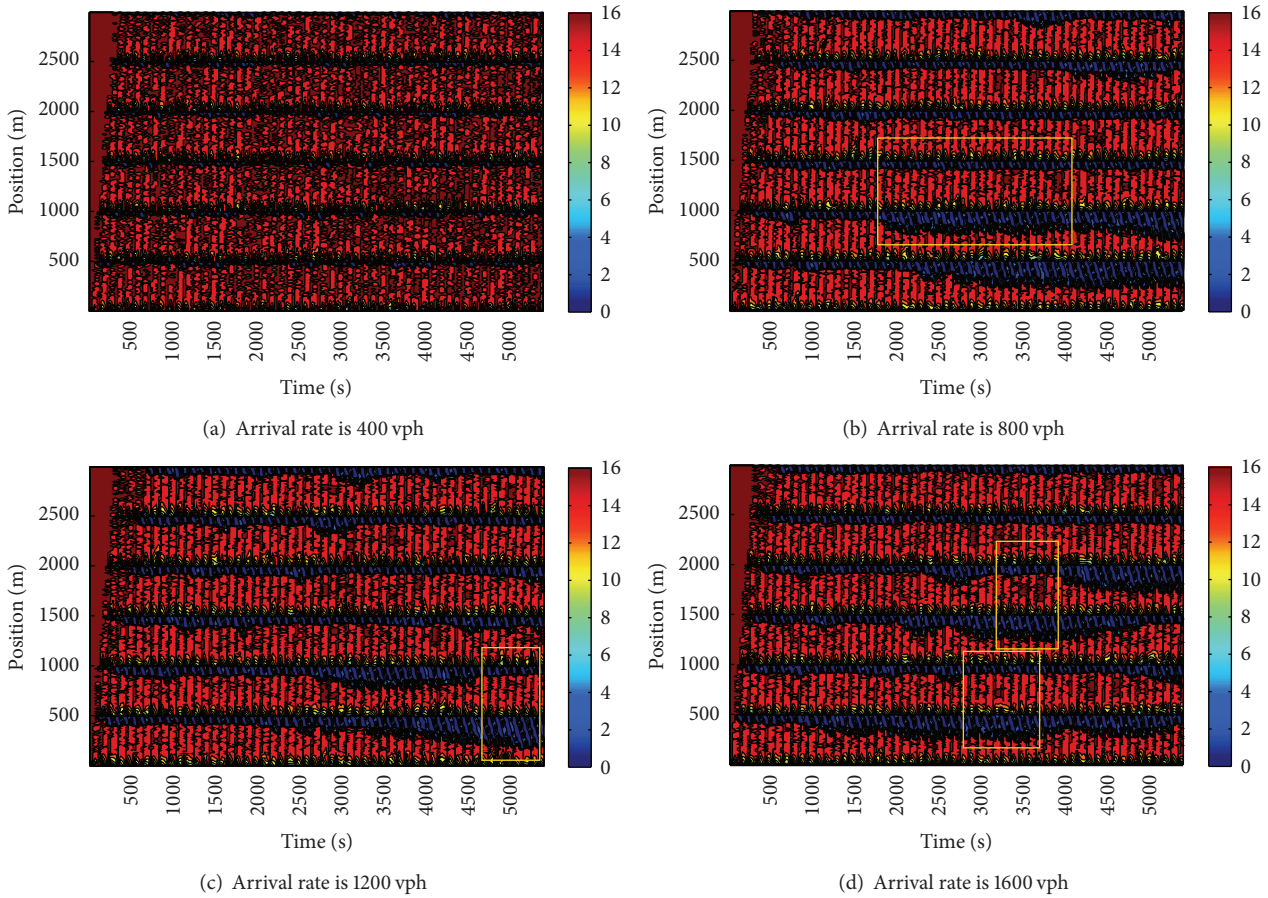

Figure 6: Speed contour plot in synchronized traffic signals.

five cells, and each cell is 0.1 km long. The limited speed is 57.6 km/h. Vehicle arrival rate at the entrance is set as 400 vph, 800 vph, 1200 vph, and 1600 vph, respectively, and arrival rate obeys Poisson distribution. When the arrival rate exceeds the intersection capacity, there will be congestion. In each simulation, the arrival rate is fixed. In the urban transportation network, traffic signals strategy can greatly affect the capacity of each intersection and thereby affect the trajectory of vehicle after entering the arterial street. Therefore, we need to consider different traffic signals strategies. In this study, we consider three common traffic signals strategies: synchronized traffic signals, green wave traffic signals, and vehicle-actuated signals. In the experiment, we analyzed three strategies separately under different vehicle arrival rates.

4.2.1. Synchronized Traffic Signals. Synchronized control refers that all intersections of the arterial street use the same signal configuration and display the same traffic signal at the same time. In the simulation, the signal cycle is set as 100 s, and green ratio is 50%. Vehicle's speed trajectories under different arrival rates are shown in Figure 6. The x-axis represents time, and the y-axis represents the vehicle position. Speed is represented by different colors. Color change from red to blue refers to the gradual decrease of speed. Each row represents the speed variation of the same position at different time points. Each column represents the speed of each position at the same time.

According to Figure 6(a), the arrival rate is 400 vph, which is far less than the intersection capacity. In the whole simulation horizon, the number of vehicles that arrive at the intersection is small, and all vehicles can pass through the intersection within one signal cycle, so the queue length of each intersection is short. In Figure 6(b), the vehicle arrival rate is approximately equal to the intersection capacity. Because the arrival rate obeys Poisson distribution, vehicles have different actual arrival rates in each signal cycle. Some arrival rates are greater than the intersection capacity, and some are less than the intersection capacity. When the arrival rate is greater than the intersection capacity in a signal cycle, there will be multiple queues. While the queuing at the downstream intersection spreads to the upstream, it reduces the actual capacity of upstream intersection, making the queuing at upstream section much longer as the first and second intersections after 2000 s shown in Figure 6(b). When the arrival rate is much greater than the intersection capacity, some queuing vehicles may not be able to pass through the intersection within one signal cycle. Vehicle release rate will be exactly equal to the intersection capacity; that is, the arrival rate of the next intersection is equal to the intersection

Table 1: Comparison among different arrival rates.

Arrival rate (vph)	Number of sensors	Sensor location pattern
400	6	500, 600, 1100, 1700, 2900, 3000
800		500, 600, 2000, 2300, 2500, 3000
1200		1000, 1100, 1300, 2100, 2500, 2900*
1600		200, 500, 800, 1600, 2500, 2600
400	5	1100, 1200, 1300, 1500, 1700
800		200, 600, 1100, 1800, 2200
1200		1000, 1200, 2000, 2300, 2900*
1600		100, 600, 1600, 2200, 2800
400	4	500, 800, 1900, 2300
800		500, 2100, 2700, 3000
1200		200, 500, 1100, 2800
1600		200, 400*, 600, 2900

*The sensor is located in the queuing area.

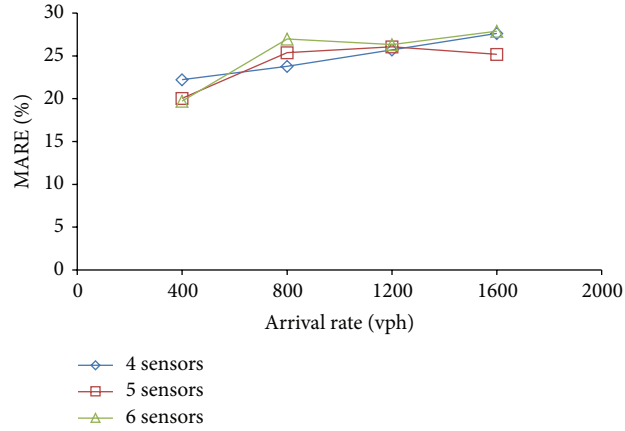

Figure 7: Comparison among MARE in different number of sensors for synchronized traffic signals.

capacity. This intersection will not form a secondary queue. As shown in the yellow rectangle of Figures 6(b), 6(c), and 6(d), if the queue of vehicles at the upstream intersection is too long, then the queue of vehicles at the downstream intersection is short.

Table 1 shows the optimal sensor placement pattern of certain number of sensors at different arrival rates. Some observations can be summarized as follows; (i) among the 12 optimal sensor placement patterns, only three patterns set the sensor in the queuing area (blue area in Figure 6). The bold numbers in Table 1 represent the queuing area, and the corresponding influence areas of the 3 sensors are very short which are 300 m, 400 m, and 200 m, respectively. In these three areas, blue area takes up a large proportion; that is, the average speed of vehicles is small. The queuing is fairly severe. Thus, when sensor is placed in the queuing area, the corresponding influence area is with long queuing length. This is because the average speed in queuing area is small. It has great impact on the estimated travel time. The sensor should not be placed in the queuing area. When sensor is placed in the queuing area, its corresponding detection range should not be too large, and it should be able to accurately capture the length of the queuing. (ii) Among the 12 optimal placement patterns, 9 patterns set sensors at one or more stop line positions (positions 500, 1000, 1500, 2000, 2500, and 3000). Compared with other locations, the average speed of vehicles at stop lines has the largest variations, and the speed profile at stop line is repetitive with regard to cycle time. When the red traffic light is on, the speed is 0. When the green light is turned on, the speed gradually increases to the maximum speed of 57.6 km/h. When the arrival rate is small, the number of queuing vehicles is small, and then the average speed is high. When the arrival rate is large, the number of queuing vehicles is large, and then the average speed is low. In addition, speed variation is determined by both the upstream queuing and downstream traffic congestion situation. Thus, when there are a lot of vehicles queuing at both the upstream and downstream links, the sensor at stop line can timely and flexibly detect the variation of traffic situation. (iii) When the number of sensors is fixed, the corresponding sensor placement patterns of different arrival rates vary greatly. This is because different arrival rates leads to different queue lengths, so the position of sensor should be determined by the road conditions.

In Figure 7, each point represents the travel time estimation error under the optimal sensor placement pattern. This pattern is obtained under certain arrival rate and certain number of sensors. When the arrival rate is 800 vph, 4 sensors are better than 5 or 6 sensors. When the arrival rate is 1600 vph, 5 sensors are better than 6 sensors. Therefore, optimizing the sensor placement pattern can reduce errors and number of sensors. When the number of sensors is 4, MARE is in proportional with the arrival rate; that is in this case, the estimation error cannot be reduced by changing sensor location. However, the estimation error can be reduced by increasing the number of sensors.

4.2.2. Influence of Green Ratio. Green ratio is an important parameter in traffic signals strategy. Congestion occurs when traffic volume is greater than the intersection capacity. In order to timely dissipate queuing vehicles, green ratio should be lengthened. When traffic volume is less than the intersection capacity, the green ratio should be carefully reduced. Green ratio will directly affect intersection capacity. When the arrival rate is a constant, vehicle queuing will change, thus affecting the position of sensor.

In order to study the influence of sensor location on estimated travel time under different green ratios, we set three green ratios, which are 40%, 50%, and 60%, respectively. Other parameters are the same as previous section. By using genetic algorithm, the optimal sensor placement pattern and the travel time estimation errors are obtained. As shown in Figure 8, each point represents the travel time estimation error of the optimal sensor placement pattern. It can be seen from Figure 8 that, regardless of the number of sensors, small green ratio causes larger travel time estimation error. The reason could be explained as that traffic condition becomes

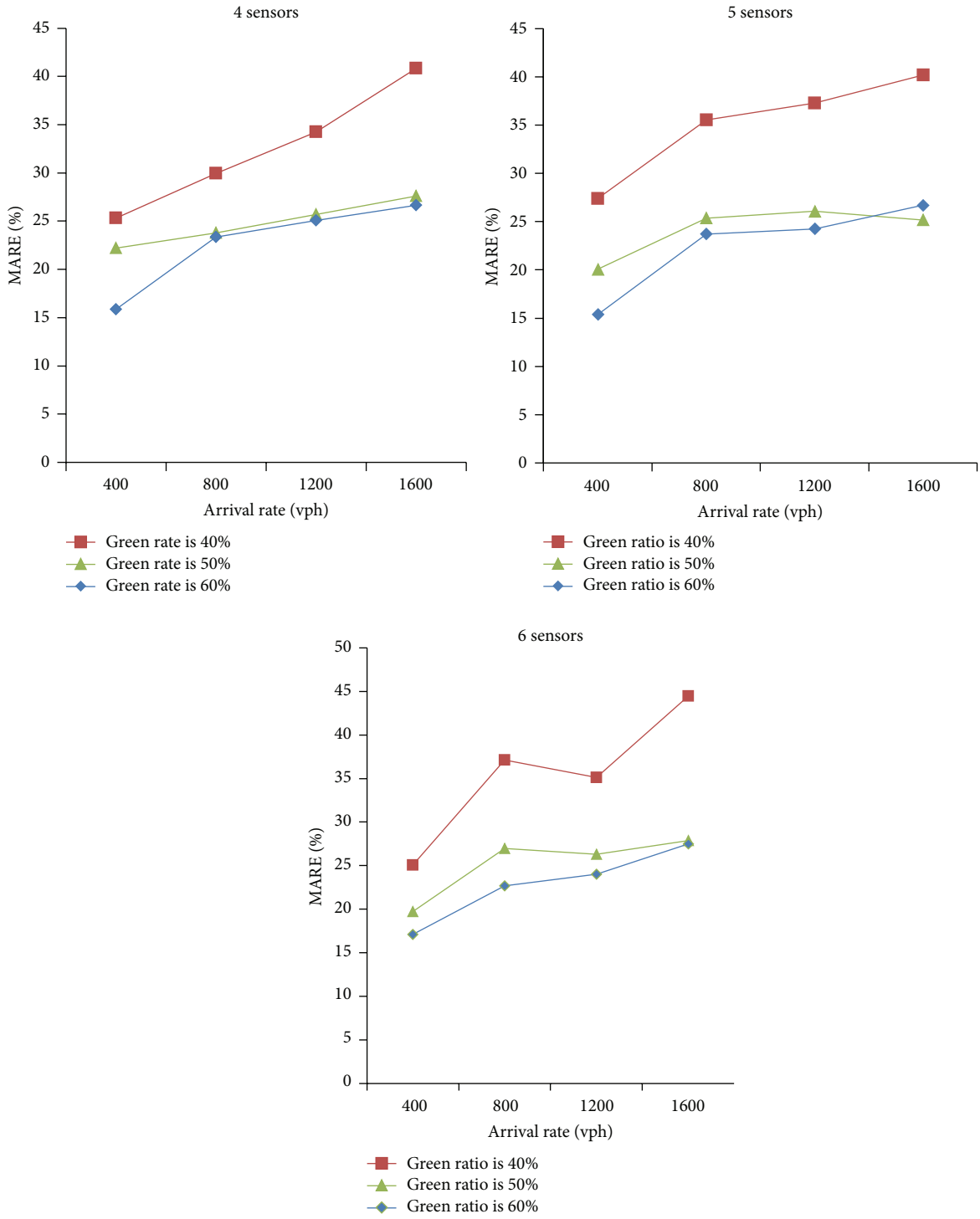

Figure 8: Comparison among different green ratios.

congested and complicated as the green ratio reduced. Therefore, it is hard to predict the travel time.

4.2.3. Green Wave Traffic Signals. Green wave control means that if a vehicle passes through one intersection at a given speed with a green light phase, it will pass through all the downstream intersections at green light phase [31]. The offset time of adjacent intersection's traffic signal equals to the length of the section divided by the given speed. If the vehicle meets a red light phase at the intersection, it will stop and wait. When the light turns green, the vehicle accelerates from zero to the limited speed and moves to the next intersection. The average speed of vehicle on the link is slightly less than the

Table 2: Comparison among different arrival rates.

Arrival rate (vph)	Number of sensors	Sensor location pattern
400	6	600, 700, 900, 1500, 2600, 3000
800		700, 1000, 1300, 1400, 2300, 2700
1200		1500, 1700, 1800, 2100, 2600, 2800
1600		800, 1200, 1400, 2300, 2400, 2800
400	5	1400, 1900, 2200, 2500, 3000
800		900, 1300, 2700, 2800, 3000
1200		900, 1300, 1400, 2500, 2900
1600		700, 800, 1600, 2400, 3000
400	4	1200, 1500, 2200, 2800
800		600, 800, 1100, 1300
1200		1200, 1500, 2700, 2800
1600		1300, 1500, 2600, 3000

limited speed and travel time is slightly larger than the offset time. Therefore, during the green light period, if the number of queuing vehicles exceeds the intersection capacity, vehicles in the front of queue can successfully pass through the next intersection. However, vehicles in the tail part of the queue will meet red light at the next intersection.

In our simulation, the signal cycle is set as 100 s. Green ratio is 50%. Each link is 0.5 km long. The limited vehicle speed is 57.6 km/h. The relative offset time between adjacent intersections is 32 s. Therefore, there will be a band along with the arterial street. As long as the vehicle arrives within the band and keeps moving at the limited speed of 57.6 km/h, it can travel smoothly through the all intersections. Figure 11 shows the speed trajectories under four different arrival rates. Generally speaking, vehicles can move at the maximum speed on the road most of the time and can smoothly pass through each intersection. If the arrival rate is greater than the intersection capacity, the first intersection will have a small number of queuing vehicles; this is, because some vehicles enter the arterial street at a smaller speed, their travel time on the link is greater than the travel time of vehicle which moves at the limited speed (offset time). They will meet red light at the first intersection.

Table 2 shows the corresponding optimal sensor placement patterns of fixed number of sensors for different arrival rates. All sensors are set after the first intersection. This is because the first link has stable traffic condition without any fluctuations under different arrival rates. This can be seen from the four subgraphs of Figure 9. In the section from 0 m to 500 m, the vehicle accelerates to maximum speed and moves to the first intersection after entering the arterial. In this section, the speed trajectory is very similar. Besides, like the synchronized traffic signal strategy, 10 out of the 12 patterns set the sensor on one or more stop lines.

Figure 10 shows the estimation error under the optimal sensor placement pattern for green wave traffic signal control. Compared with other two signals strategies, it is easier to estimate the travel time under green wave control. The estimation error is less than 2%. Regardless of the arrival rate, the travel time estimation error is minimized when the number of detectors is 4. This is because that the traffic condition is simple under the green wave traffic signals. When the traffic is not complicated, less sensors should be placed. When traffic condition is very complicated, more sensors should be placed.

4.2.4. Vehicle-Actuated Traffic Signals. The above two traffic signals strategies are fixed traffic signal control method. They are developed based on historical data. The disadvantage of these strategies is that it is unable to meet real-time changes of traffic flow. In order to overcome this deficiency, vehicle-actuated signals [32] are adopted. This strategy changes the green time adaptively according to real-time traffic volume.

In the simulation of vehicle-actuated control, we set each intersection's signal cycle as 100 s. The minimum green time is 50 s. The maximum green time is 70 s. The unit extension interval is 3 s. When the arterial street gets the access right, the signal system will first give the signal phase a minimum green time of 50 s, enabling the vehicle that has arrived at the intersection to pass through the intersection. If there is no vehicle after this, the access right will be transferred to the subsequent link. If a vehicle is detected within the green time, the green time will be extended a unit time interval of 3 s. The maximum extension can be 70 s.

Figure 11 is the speed trajectory for 4 different arrival rates. Compared with the synchronized traffic signals control, the queuing length at the intersection is shorter, and large-scale long queue appears only once when the arrival rate is 1600 vph. When the traffic volume is large, the signal system can detect the changes of volume, increasing the green time in a timely manner. As a result, intersection capacity is improved and vehicle queue length is reduced. By comparing Figures 6 and 11, it can be seen that, under the vehicle traffic signals control, the average vehicle queue length is short.

The optimal sensor location pattern under vehicle-actuated traffic signals control is shown in Table 3. The corresponding travel time estimation error of each optimal sensor mode is shown in Figure 12. Similar to synchronized traffic signals control, among the 12 optimum placement patterns, only three patterns set the sensor in the queuing area (see the bold numbers in the table). Two of these three sensors have small detection coverage area, which are 250 m and 400 m, respectively. 12 sensor location patterns all choose to place the sensor on a stop line. As can be seen from Figures 11(c) and 11(d), blue area takes up a large proportion in these two areas; that is, the average speed of vehicles is small and the queuing situation is severe. Thus, when the sensor is located in queuing area, its corresponding influence area is the area with long queues. This is because the average speed of queuing area is small which has great impact on the estimation of travel time. The sensors should be avoided from being placed in queuing area. When the sensor is placed in the queue area, its corresponding influence area should not be too large. It should accurately correspond to the length of the queue. In addition, it can be seen from Figure 12 that (i) the travel time estimation error calculated by different number of sensors differs slightly for different arrival rates. (ii) As for a fixed number of sensors, travel time estimation error increases as the arrival rate increases. (iii) Regardless of

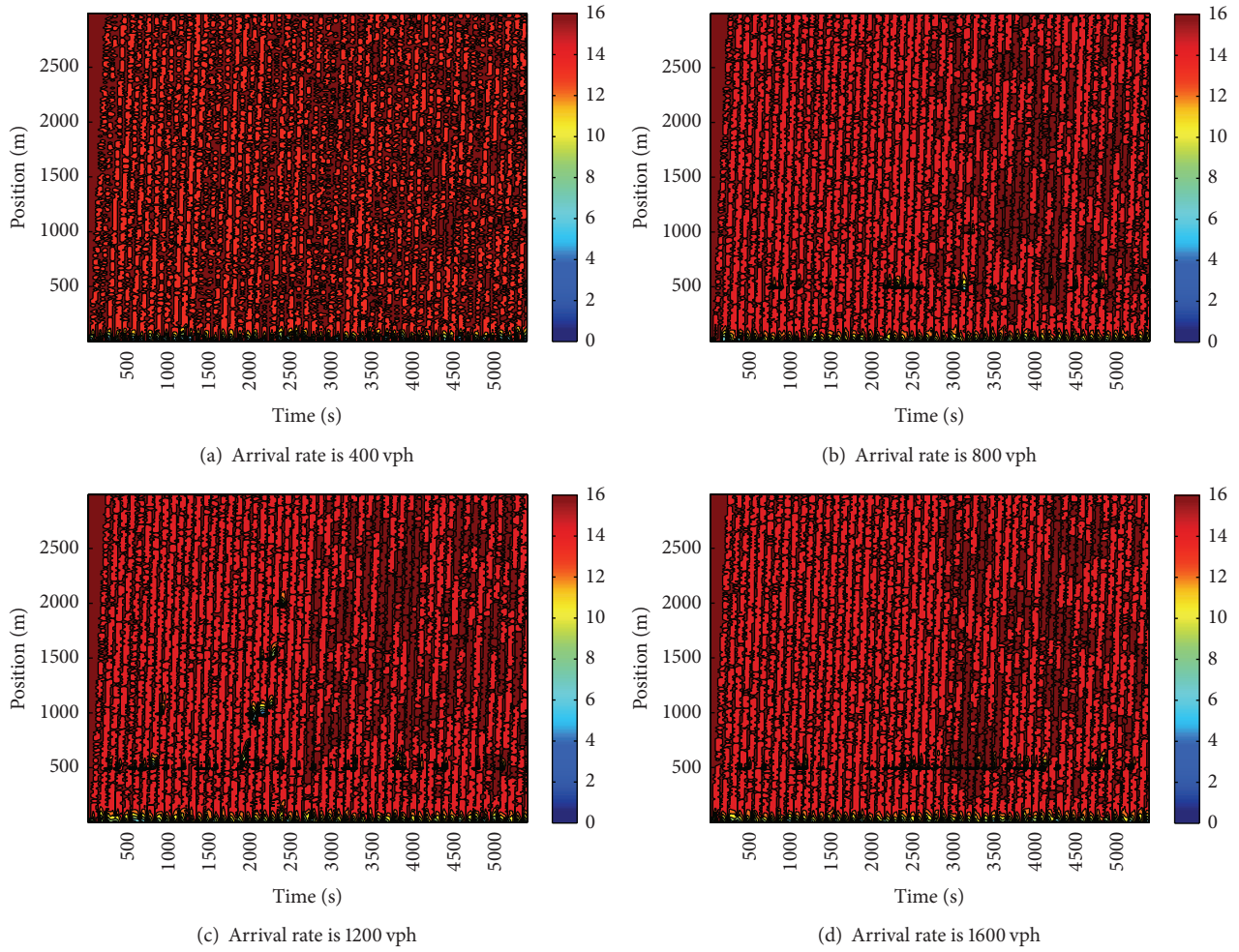

Figure 9: Speed contour plot in green wave traffic signals.

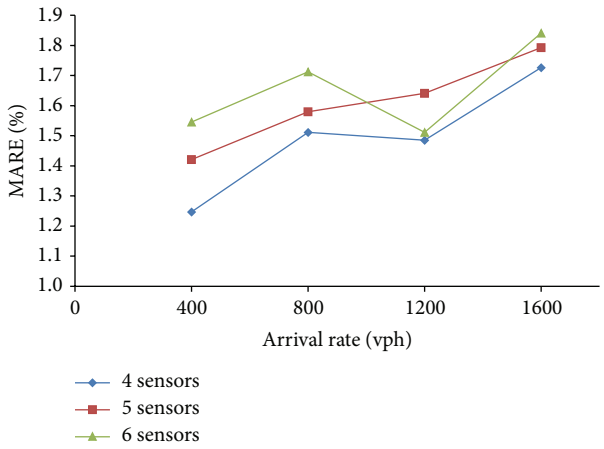

Figure 10: Comparison among MARE in different number of sensors for green wave traffic signals.

arrival rate, the estimated travel time predicted by 6 sensors is the most accurate. The number of arrived vehicles within one signal cycle changes the green time length adaptively, resulting in the change of intersection capacity. The traffic condition of each link becomes more dynamic and random which differs greatly from the cyclical and repetitive traffic condition under synchronized control. Therefore, it requires more sensors to estimate travel time.

Through experimental analyses of these three traffic signals strategies, observations are stated as follows: (i) when the sensor is located in the queuing area, its corresponding influence area is short. Its length should be close to the queuing length. Therefore, when a sensor is located in the queuing area, some sensors should be set in the adjacent upstream and downstream areas in a cooperative manner. (ii) Stop line is an ideal sensor position place. Compared with other location places, the average speed of vehicles at stop lines has the largest variations. Small arrival rate may cause fewer queuing vehicles. The average speed is high. A large arrival rate may cause more queuing vehicles, where the average speed is low. The sensor can timely and flexibly reflect the traffic conditions. (iii) Under simple traffic situation where vehicle speed is stable with small speed fluctuation, few sensors can accurately estimate travel time. Otherwise, more sensors are needed.

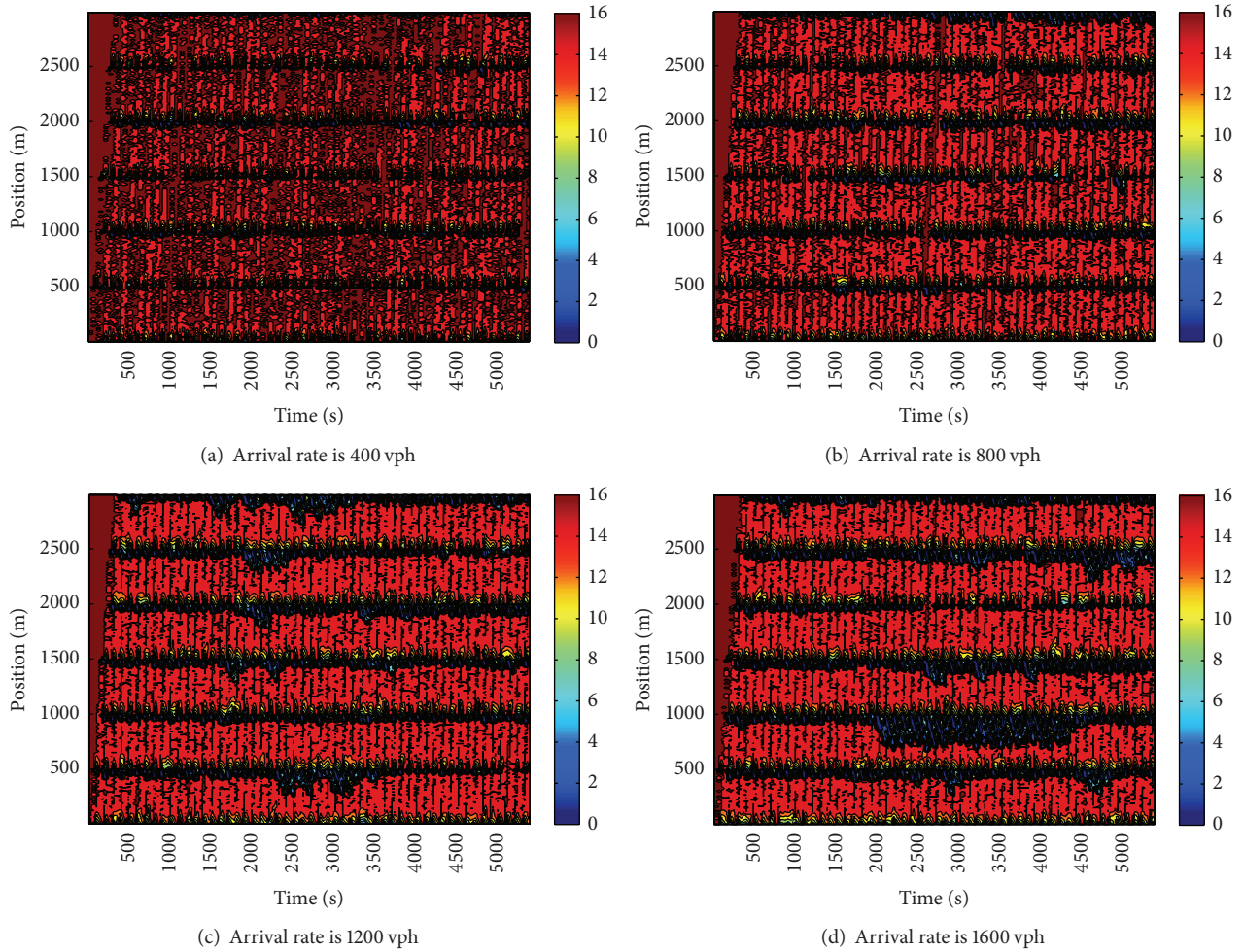

Figure 11: Speed contour plot in vehicle-actuated traffic signals.

Table 3: Comparison among different arrival rates.

Arrival rate (vph)	Number of sensors	Sensor location pattern
400	6	200, 300, 500, 1100, 1400, 1800
800		400, 500, 1200, 1400, 1900, 2800
1200		500, 600, 1900, 2200, 2600, 2900*
1600		500, 900*, 1300, 1400, 2100, 2600
400	5	600, 700, 1300, 1500, 2200
800		600, 900, 1100, 1500, 1900
1200		100, 500, 1800, 2100, 2400
1600		900*, 1000, 1900, 2300, 3000
400	4	600, 1000, 1100, 1700
800		400, 500, 1400, 2600
1200		100, 500, 1300, 1900
1600		300, 700, 1000, 2100

*The sensor is located in queuing area.

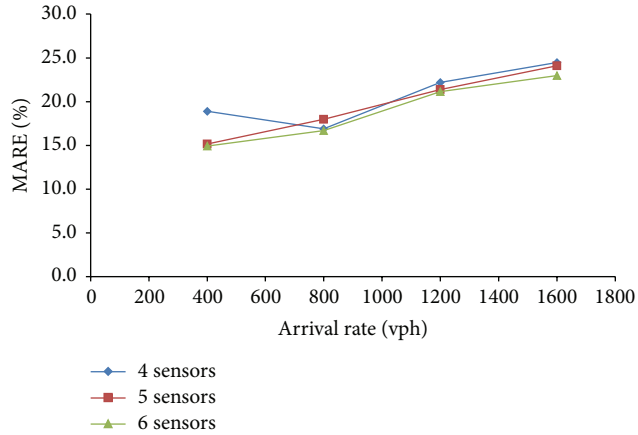

Figure 12: Comparison among MARE in different number of sensors for vehicle-actuated traffic signals.

5. Conclusion

The paper studies the sensor location problem in urban arterial street for travel time estimation and proposes optimal sensor location model (M1) to obtain the minimum travel time estimation error. Based on this model, the influence of traffic signals strategies on sensor location is also discussed.

By comparing the synchronized traffic signals, green wave traffic signals, and vehicle-actuated signals, it is found that sensor should not be placed in vehicle queuing area. If the sensor is located in the queuing area, its associated coverage area should include the vehicle queuing area as precise as possible. Intersection stop line is an ideal sensor position. There is not any fixed sensor position that can cope with all traffic conditions, and the sensor location should be determined according to the characteristics of traffic flow on the road. Under simple traffic situation where vehicle speed is stable and speed fluctuation is small, few sensors can accurately estimate travel time. In case of complex traffic conditions with large fluctuations of vehicle speed, more sensors are required to estimate travel time.

The future research direction can be considered as follows: (i) our study only takes into account the traffic condition of single lane with fixed traffic volume, and the future research can consider more complex traffic situations, such as the dynamic changes of multilane road with dynamic traffic volume and other real phenomena that match with actual road conditions. (ii) The future research can take this study on urban arterial street as background, taking into account the vehicle turnings, and study the sensor location under the road network layout. (iii) A more efficient model for algorithm should be explored in the future research, although the genetic algorithm used in the paper is an effective solution model. (iv) The study only seeks the optimal sensor location for travel time estimation. Future research can focus on optimized combination of more traffic information applications or more information applications.

Conflict of Interests

The authors declare that there is no conflict of interests regarding the publication of this paper.

Acknowledgments

This research was supported by the National Natural Science Foundation Council of China under Projects 71301115, 71431005, 71271150, and 71101102 and Specialized Research Fund for the Doctoral Program of Higher Education of China (SRFDP) under Grant no. 20130032120009.

References

[1] H. M. Zhang, "Link-journey-speed model for arterial traffic," *Transportation Research Record*, vol. 1676, no. 1, pp. 109–115, 1999.

[2] A. Skabardonis and N. Geroliminis, "Real-time estimation of travel times on signalized arterials," *Transportation and Traffic Theory*, no. LUTS-ARTICLE-2009-003, pp. 387–406, 2005.

[3] H. X. Liu and W. Ma, "A virtual vehicle probe model for time-dependent travel time estimation on signalized arterials," *Transportation Research Part C: Emerging Technologies*, vol. 17, no. 1, pp. 11–26, 2009.

[4] S. Takaba, T. Morita, T. Hada, T. Usami, and M. Yamaguchi, "Estimation and measurement of travel time by vehicle detectors and license plate readers," in *Proceedings of the Vehicle Navigation and Information Systems Conference*, vol. 2, pp. 257–267, IEEE, October 1991.

[5] R. L. Cheu, D. H. Lee, and C. Xie, "An arterial speed estimation model fusing data from stationary and mobile sensors," in *Proceedings of the IEEE Intelligent Transportation Systems Proceedings*, pp. 573–578, August 2001.

[6] D. J. Dailey and F. W. Cathey, "AVL-equipped vehicles as traffic probe sensors," Tech. Rep. WA-RD 534.1, Washington State Department of Transportation, 2002.

[7] R. Li, G. Rose, and M. Sarvi, "Evaluation of speed-based travel time estimation models," *Journal of Transportation Engineering*, vol. 132, no. 7, pp. 540–547, 2006.

[8] J. W. C. Van Lint, "Empirical evaluation of new robust travel time estimation algorithms," *Transportation Research Record*, vol. 2160, no. 1, pp. 50–59, 2010.

[9] D. Ni and H. Wang, "Trajectory reconstruction for travel time estimation," *Journal of Intelligent Transportation Systems*, vol. 12, no. 3, pp. 113–125, 2008.

[10] H. Yang and J. Zhou, "Optimal traffic counting locations for origin-destination matrix estimation," *Transportation Research, Part B: Methodological*, vol. 32B, no. 2, pp. 109–126, 1997.

[11] L. Bianco, G. Confessore, and P. Reverberi, "A network based model for traffic sensor location with implications on O/D matrix estimates," *Transportation Science*, vol. 35, no. 1, pp. 50–60, 2001.

[12] M. Gentili and P. B. Mirchandani, "Locating active sensors on traffic networks," *Annals of Operations Research*, vol. 136, no. 1, pp. 229–257, 2005.

[13] A. Ehlert, M. G. H. Bell, and S. Grosso, "The optimisation of traffic count locations in road networks," *Transportation Research Part B: Methodological*, vol. 40, no. 6, pp. 460–479, 2006.

[14] X. Fei, H. S. Mahmassani, and S. M. Eisenman, "Sensor coverage and location for real-time traffic prediction in large-scale networks," *Transportation Research Record: Journal of the Transportation Research Board*, vol. 2039, no. 1, pp. 1–15, 2007.

[15] S. M. Eisenman, X. Fei, X. Zhou, and H. S. Mahmassani, "Number and location of sensors for real-time network traffic estimation and prediction: sensitivity analysis," *Transportation Research Record*, vol. 1964, no. 1, pp. 253–259, 2006.

[16] E. Castillo, J. M. Menéndez, and P. Jiménez, "Trip matrix and path flow reconstruction and estimation based on plate scanning and link observations," *Transportation Research Part B: Methodological*, vol. 42, no. 5, pp. 455–481, 2008.

[17] R. Mínguez, S. Sánchez-Cambronero, E. Castillo, and P. Jiménez, "Optimal traffic plate scanning location for OD trip matrix and route estimation in road networks," *Transportation Research Part B: Methodological*, vol. 44, no. 2, pp. 282–298, 2010.

[18] S.-R. Hu, S. Peeta, and C.-H. Chu, "Identification of vehicle sensor locations for link-based network traffic applications," *Transportation Research Part B: Methodological*, vol. 43, no. 8-9, pp. 873–894, 2009.

[19] F. Viti, M. Rinaldi, F. Corman, and C. M. Tampère, "Assessing partial observability in network sensor location problems," *Transportation Research Part B: Methodological*, vol. 70, pp. 65–89, 2014.

[20] N. Zhu, Y. Liu, S. Ma, and Z. He, "Mobile traffic sensor routing in dynamic transportation systems," *IEEE Transactions on Intelligent Transportation Systems Magazine*, vol. 15, no. 5, pp. 2273–2285, 2014.

[21] H. X. Liu and A. Danczyk, "Optimal sensor locations for freeway bottleneck identification," *Computer-Aided Civil and Infrastructure Engineering*, vol. 24, no. 8, pp. 535–550, 2009.

[22] Y. Liu, N. Zhu, S. Ma, and N. Jia, "Traffic sensor location approach for flow inference," *IET Intelligent Transport Systems*, vol. 9, no. 2, pp. 184–192, 2015.

[23] J. Kim, B. Park, J. Lee, and J. Won, "Determining optimal sensor locations in freeway using genetic algorithm-based optimization," *Engineering Applications of Artificial Intelligence*, vol. 24, no. 2, pp. 318–324, 2011.

[24] J. Kianfar and P. Edara, "Optimizing freeway traffic sensor locations by clustering global-positioning-system-derived speed patterns," *IEEE Transactions on Intelligent Transportation Systems*, vol. 11, no. 3, pp. 738–747, 2010.

[25] J. Kwon, K. Petty, and P. Varaiya, "Probe vehicle runs or loop detectors? Effect of detector spacing and sample size on accuracy of freeway congestion monitoring," *Transportation Research Record*, vol. 2012, pp. 57–63, 2007.

[26] G. B. Thomas, "The relationship between detector location and travel characteristics on arterial streets," *ITE Journal*, vol. 69, no. 10, pp. 36–42, 1999.

[27] X. Ban, L. Chu, R. Herring, and J. D. Margulici, "Sequential modeling framework for optimal sensor placement for multiple intelligent transportation system applications," *Journal of Transportation Engineering*, vol. 137, no. 2, pp. 112–120, 2010.

[28] J. W. C. van Lint, "Online learning solutions for freeway travel time prediction," *IEEE Transactions on Intelligent Transportation Systems*, vol. 9, no. 1, pp. 38–47, 2008.

[29] L. D. Vanajakshi, B. M. Williams, and L. R. Rilett, "Improved flow-based travel time estimation method from point detector data for freeways," *Journal of Transportation Engineering*, vol. 135, no. 1, pp. 26–36, 2009.

[30] L. Li, X. Chen, Z. Li, and L. Zhang, "Freeway travel-time estimation based on temporal-spatial queueing model," *IEEE Transactions on Intelligent Transportation Systems*, vol. 14, no. 3, pp. 1536–1541, 2013.

[31] J. T. Morgan and J. D. C. Little, "Synchronizing traffic signals for maximal bandwidth," *Operations Research*, vol. 12, no. 6, pp. 896–912, 1964.

[32] R. Hall, *Handbook of Transportation Science*, Springer, Berlin, Germany, 1999.

Hindawi Publishing Corporation
Discrete Dynamics in Nature and Society
Volume 2015, Article ID 763565, 10 pages
http://dx.doi.org/10.1155/2015/763565

Research Article

A Segmented Signal Progression Model for the Modern Streetcar System

Baojie Wang,[1,2] Wei Wang,[1,2] Xiaojian Hu,[1,2,3] and Xiaowei Li[1,2]

[1] *Jiangsu Key Laboratory of Urban ITS, Southeast University, China*
[2] *Jiangsu Province Collaborative Innovation Center of Modern Urban Traffic Technologies, China*
[3] *Beijing Key Laboratory for Cooperative Vehicle Infrastructure Systems and Safety Control, China*

Correspondence should be addressed to Xiaojian Hu; huxiaojian@seu.edu.cn

Received 10 November 2014; Revised 22 December 2014; Accepted 20 January 2015

Academic Editor: Gualberto Solís-Perales

This paper is on the purpose of developing a segmented signal progression model for modern streetcar system. The new method is presented with the following features: (1) the control concept is based on the assumption of only one streetcar line operating along an arterial under a constant headway and no bandwidth demand for streetcar system signal progression; (2) the control unit is defined as a coordinated intersection group associated with several streetcar stations, and the control joints must be streetcar stations; (3) the objective function is built to ensure the two-way streetcar arrival times distributing within the available time of streetcar phase; (4) the available time of streetcar phase is determined by timing schemes, intersection structures, track locations, streetcar speeds, and vehicular accelerations; (5) the streetcar running speed is constant separately whether it is in upstream or downstream route; (6) the streetcar dwell time is preset according to historical data distribution or charging demand. The proposed method is experimentally examined in Hexi New City Streetcar Project in Nanjing, China. In the experimental results, the streetcar system operation and the progression impacts are shown to affect transit and vehicular traffic. The proposed model presents promising outcomes through the design of streetcar system segmented signal progression, in terms of ensuring high streetcar system efficiency and minimizing negative impacts on transit and vehicular traffic.

1. Introduction

Modern streetcar system is similar to light rail systems and operates along shared or segregated right-of-way. The main difference between light rail and modern streetcar system is the degree of integration into the urban environment and the scale of the associated infrastructure [1, 2]. Given its potential value as an efficient, energy-saving, environmental, and comfortable urban transit mode, there has been a significant increase in the use of the modern streetcar system in Europe since the late 1990s and is currently fast growing throughout the world. Take China as example; modern streetcar systems in some cities of China, such as Beijing, Shanghai, Tianjin, Suzhou, Shenyang, and Dalian, are already under operation. In addition, more streetcar systems are still under construction in more than 30 other cities. By 2020, China will have built more than 100 modern streetcar lines with the total length of 2,500 kilometers.

Although modern streetcar system is considered as an important mode of urban transit systems in China, it still faces massive challenges in its construction and development due to existing conflicts between the streetcars and other vehicles at the intersection. And these problems are even exacerbated since a growing number of vehicles are on the urban streets, with the rapid urbanization and motorization of China. Table 1 presents a series of evening-peak (16:30–18:30) operating data collected from the Shanghai, Tianjin, and Dalian modern streetcar systems between February 24 and March 2, 2014. In this table, dwell time denotes the time a streetcar spends at the station; intersection delay denotes the streetcar deceleration time, stop time, and acceleration time at the intersection; total delay equals a sum of dwell time and intersection delay. The data involves Zhangjiang Streetcar 1# in Shanghai city (10 km long, 15 stations), Binhai New City Streetcar 1# in Tianjin city (7.9 km long, 14 stations), Streetcar 201# (11.6 km, long 19 stations) and Streetcar 202#

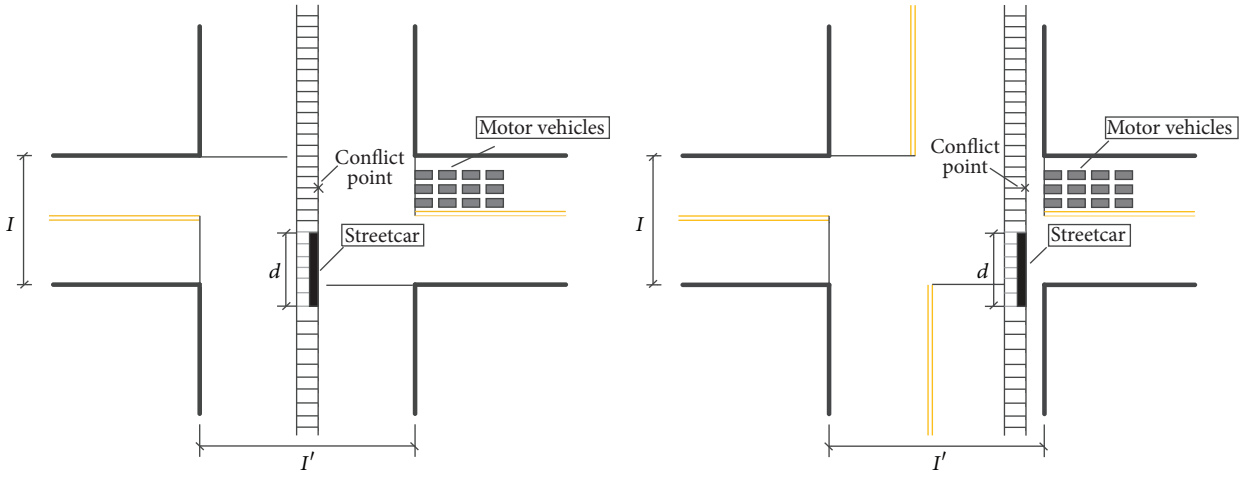

(a) Center lanes (b) Roadside lanes

Figure 1: Track locations of modern streetcar systems.

(12.6 km long, 19 stations) in Dalian city. The data shows a high proportion of delay (23.63%) and stops (38.25%) at the intersection.

Hexi New City Streetcar 1# and Qilin Streetcar 1# in Nanjing city is the first two off-wire modern streetcar systems of Jiangsu province. Furthermore, Hexi New City Streetcar 1# is planned to operate on August 1, which is specially prepared for the Second Summer Youth Olympic Games in Nanjing. Aiming at making Hexi New City Streetcar 1# system more reliable, faster, and cost-effective, Southeast University and Les Information Technology Co., Ltd., are commissioned to study on its priority strategies by Nanjing Department of Transportation. This paper introduces a segmented signal progression methodology for the modern streetcar system in detail.

This paper is organized into six sections. Section one is the introduction which has been discussed above. The next section gives a review of the literature for studies and experiences of streetcar system priority strategies. It is followed by the control framework outlines of the basic control concept, model assumption, design process, and notations adopted. The formulation of the objective function and its constraints are given in the Modeling Methodology. It is followed by the results obtained through microsimulation and the discussion of the results, with preoperating data of Hexi New City Streetcar 1#. In the last section, the major conclusions of the study and the promising directions of the future research are presented.

2. Literature Review

Modern streetcar system is confronted with many challenges, such as poor traveling speeds, unreliability, safety, and difficulties in providing universal access [3]. With the consensus being that Transit Signal Priority (TSP) is identified as a cost-effective way to make on-street transit faster, safer, more reliable, and cost-effective [4], researchers have focused on methodologies of streetcars' signal priority strategy, bunching control, and schedule optimization [5–8]. Some studies have reported the benefits of various practices. The most classic cases of TSP development are in Melbourne, Australia, and Toronto, Canada [3].

In Melbourne, vehicular traffic has impacted streetcar system efficiency to the extent that streetcar speed was in the bottom 20th percentile of system operating speeds for streetcar system services since early this decade. Statistically speaking, the average operating speed of streetcar was merely 15.5 km/h, compared to 16.8 km/h in Brussels, 19.1 km/h in Berlin, and 19.3 km/h in Prague [9]. The major difference in operational terms between Melbourne's streetcar systems and other international systems is that Melbourne's systems do not provide enough priority for streetcars like the overseas examples. Hence, Melbourne launched two projects to improve the streetcar system efficiency. The main policy initiative is called "Think Tram." The other is called the "Route 109" Project. They both carry out a series of infrastructure improvement projects to achieve a high level of streetcar system service. The projects mainly include hardware facility developing and TSP upgrading [10]. Subsequently, a new generation of TSP is under way, which is called Dynamic Signal Priority (DSP) Project. One advantage of this project is the application of conditional priority control. It makes priority more conditional on the degree of traffic congestion experienced. Another is to resolve competing calls for priority (conflicts) in an intelligent manner. It provides priority in a variable manner dependent on a weighting factor given to each priority call. The weighting factor is determined by the degree of lateness of a streetcar [11].

In Toronto, a Transportation Vision of Toronto Official Plan is focused largely on transit infrastructure investment and transit priority control [12]. To translate the vision statements and principles of potential transit priority benefits into reality and quantity, the 504 King streetcar route in heart of Toronto is chosen as a case study. Four priority schemes are modeled in a microsimulation framework, which includes

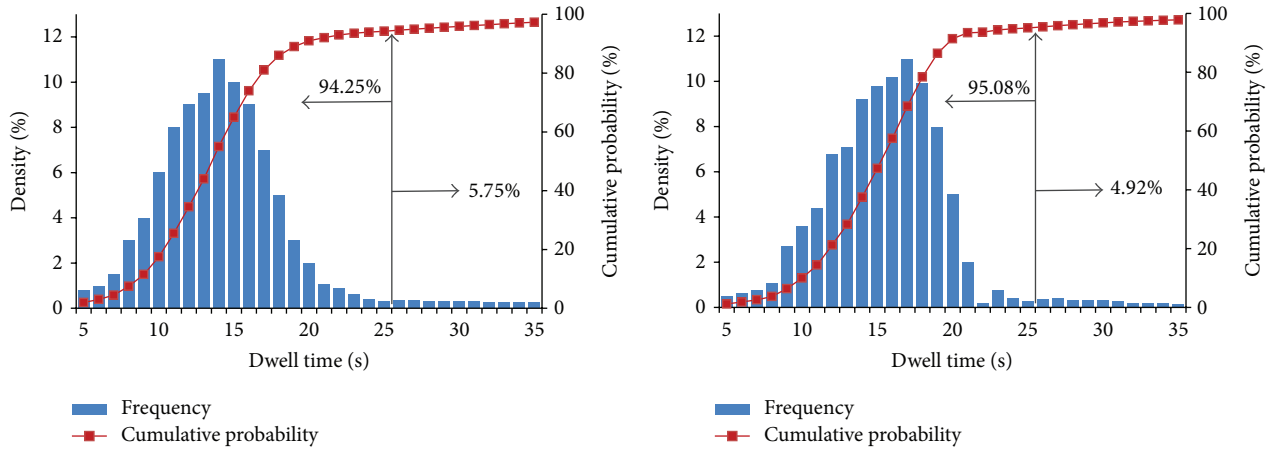

(a) Xuanwumen Station (b) Taiping Beilu Station

Figure 2: Distribution of dwell times.

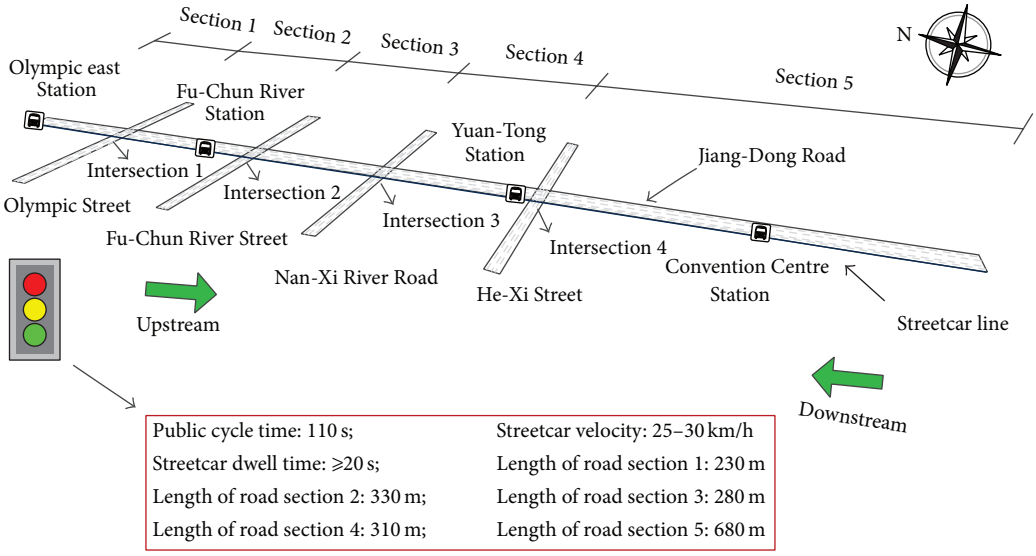

Figure 3: Basic layouts of the section.

unconditional signal priority, turning off signal priority, prohibiting all left turns, and finally prohibiting traffic from King Street. The results show that potentially transforming the arterial into a transit mall accessible only to streetcar systems is recommended [13]. Proof-of-Payment and Multiple-Unit streetcar systems operations are investigated by a microscopic traffic simulation model of the 504 King and the 512 St. Clair streetcar routes in Toronto. They display a better performance than Pay-on-Entry and Single-Unit on headway variability, capacity, and operating speed for streetcar systems [14]. The City of Toronto and Toronto Transit Commission confirm the studies and implement an aggressive plan to ensure streetcar system priority. The plan includes Dedicated Right-of-Way, Active Transit Signal Priority, Multiple-Unit Operation, and Proof-of-Payment [15].

In other cities like San Diego and Shanghai, streetcar systems are allocated with median streetcar-only lanes in the segment and provided with passive priority at the intersection. The priority systems share the following features: the lines are set with near-side stations; the signal timing is fixed; the streetcar dwells in station only if its phase is green [16]. The priority systems in the two cities rely on operators' subjective judgments and transfer the intersection delay to the station dwell time.

The studies and practices in Melbourne, Toronto, San Diego, and Shanghai indicate that there are two measures mainly utilized to achieve streetcar system high efficiency. One is the infrastructure development to separate streetcars and motor vehicles to a maximal extent possible. The other is the advancement of TSP algorithms (Figure 1). With these steps, all of the four cities have increased the efficiency of streetcar operations. Particularly in Melbourne and Toronto, they have proved to gain significant progresses of a reduction

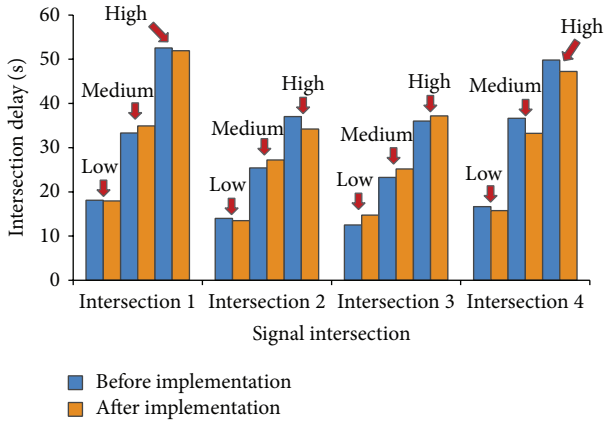

Figure 4: Average vehicular delay at intersections under different level of demand.

(6%–10%) in streetcar travel times [11]. Despite the promising progresses in previous studies, there is still insufficient research on freshly hatched modern streetcar systems. For example, Hexi New City Streetcar 1#, in the City of Nanjing, is a significant project during the Second Summer Youth Olympic Games. It is allocated with up to date infrastructure, 100% modern low-floor vehicles, and dedicated right-of-way along the whole route, except intersections. Nevertheless, there is a lack of adequate historic data supplies to support the design of TSP schemes for it, according to the previous methodologies. Now that it is hard to develop an active signal priority strategy, the pressing matter of the moment is to set up a background signal progression scheme for the system. Additionally, there is not enough research on the background signal progression for modern streetcar system. The objective of the study is to propose and demonstrate a methodology of segmented signal progression for the modern streetcar system.

3. The Control Framework

3.1. Basic Control Concept

3.1.1. Unnecessary to Provide Bandwidth for Streetcar System. Modern streetcar system is an important auxiliary and extension for subway in China. Based on the experience of the completion of some projects in Shanghai, Shenyang, Zhuhai, Shenzhen, Suzhou, and Nanjing, the system costs nearly 25,000,000 USD per kilometer, which is a higher cost compared to other on-street transit systems' cost. Hence, partly for the cost concern, an arterial usually lays only one streetcar line in China. Moreover, it rarely occurs that two or more streetcars arrive at intersection at the same time. Therefore there is no need to provide maximized bandwidth for streetcar systems.

3.1.2. Dividing the Arterial into Several Control Units. The uncertainty of streetcar dwell time is a major cause which troubles the signal progression implementation for modern streetcar system. Specifically, if the arrival time of the streetcar is within a set time period, the streetcar can enjoy progression which has already been set up. And if not, the streetcar cannot enjoy that progression. The arrival time of the streetcar depends on its running speed and dwell time at each station. While the running speed can be guaranteed with streetcar-only lanes, the dwell time is the main factor affecting the actual arrival time of the streetcar deviating from specific time at the intersection. Moreover, the more the number of the stations is, the greater the uncertainties of dwell time will be. And uncertainties of dwell time at each station will be added up to aggravate the arrival time fluctuation. Hence, the arterial for the signal progression implementation should be divided into several control units. The endpoint of each control unit is set up to be an error calibration place for the next control unit.

3.2. Model Assumption. The assumptions of the models in this study are given as follows.

(1) There is only one modern streetcar line operating along an arterial and no other streetcar lines go across it.

(2) All of the intersections are controlled by traffic signals.

(3) Modern streetcar systems are provided with dedicated right-of-way in the segment between two intersections.

(4) There never exists such a situation that two or more vehicles from the same direction arrive at one intersection at the same time.

(5) Streetcar dwell time, like dwell time of on-street transit, follows a certain distribution function.

(6) Dwell time for passenger service or streetcar charging is within passengers' toleration time.

(7) Deceleration and acceleration times are seen as a part of streetcar running time.

(8) For simplicity of elaboration, the start of signal progression time for the segment is set to zero.

By all the assumptions above, the effective construction of a segmented signal progression model for the modern streetcar system can be achieved. And it is allowed to be formulated in a statistical framework.

3.3. Design Process. The specific steps are summarized as below.

(1) Determining the control unit: the control unit usually contains several coordinated intersections associated with no more than 5 streetcar stations. The control joints must be stations. The specific number of intersections and stations is up to managers, depending on their control demand.

(2) Outlining the background signal timing schemes: the background signal timing schemes are set up with Webster method based on vehicular traffic characteristics. Public cycle time of the control unit

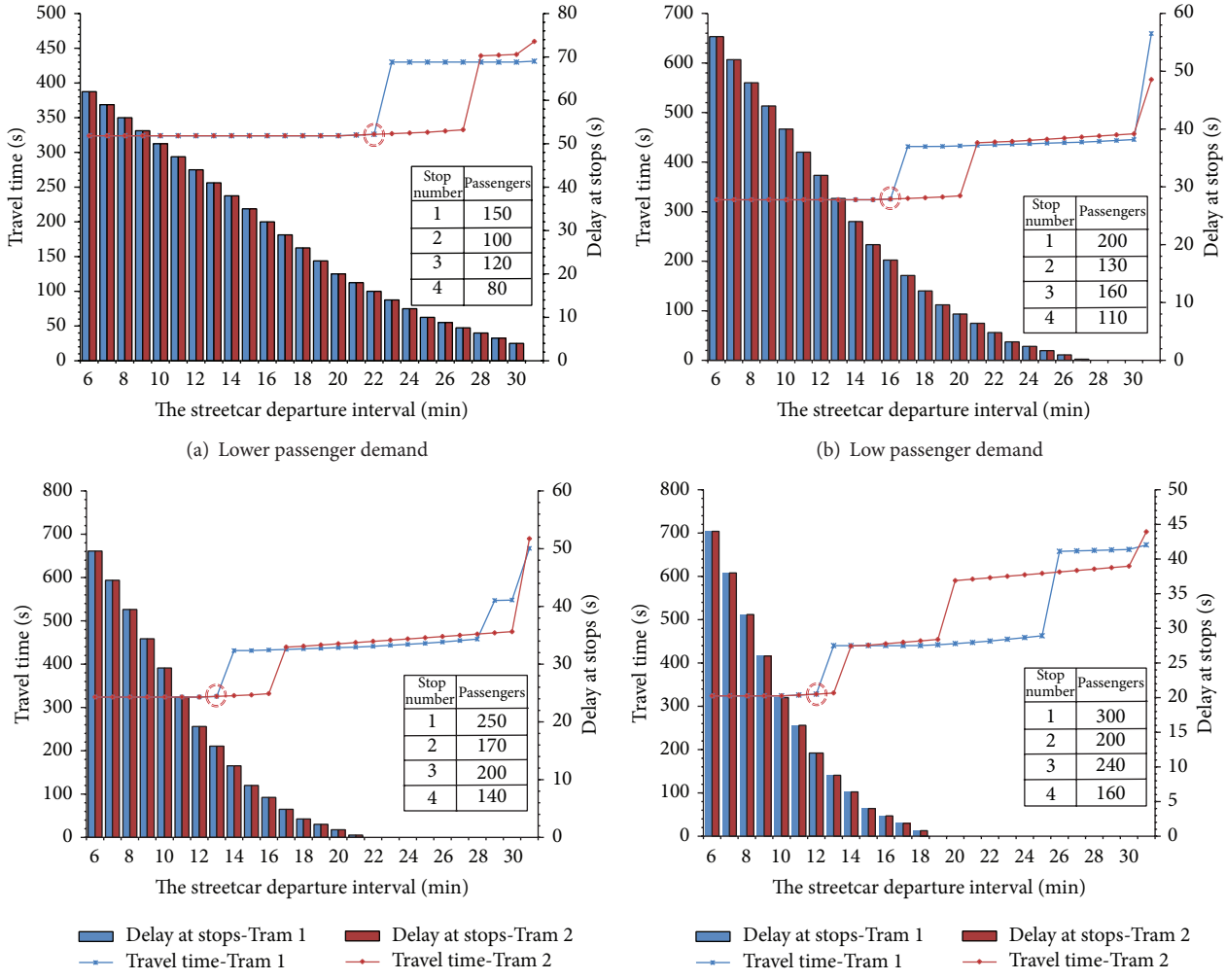

FIGURE 5: Impacts of streetcar departure intervals on streetcar system progression.

is determined by a key intersection, whose traffic demand is the largest or whose position is the most critical.

(3) Building signal progression models: two series of models for upstream and downstream streetcar routes are built separately, which keep a streetcar passing through each intersection at an ideal time.

(4) Defining the constraints: set up constraints for the models, including the signal cycle time constraint, streetcar running speed constraint, available passage time constraint, and dwell time constraint.

(5) Searching for the optimal offsets: search for optimal offsets which satisfy the two-way signal progressions for the streetcar system.

3.4. Notations. The notations used in the model are described below.

T: Public cycle time of the control unit (s)

G_{allow}: Available time for streetcar passage during the streetcar phase (s)

Y: Yellow time (s)

L_i: Length of route section i (m)

A_j: Time of an upstream streetcar arriving at intersection j (s)

$\overline{A}_j$: Time of a downstream streetcar arriving at intersection j (s)

W_i: Dwell time of an upstream streetcar at station i (s)

$\overline{W}_i$: Dwell time of a downstream streetcar at station i (s)

V_{up}: Velocity of upstream streetcars (km/h)

V_{down}: Velocity of downstream streetcars (km/h)

$t_{j,\text{allow}/2}$: The median of available time for the upstream streetcar passage during a streetcar phase at intersection j (s)

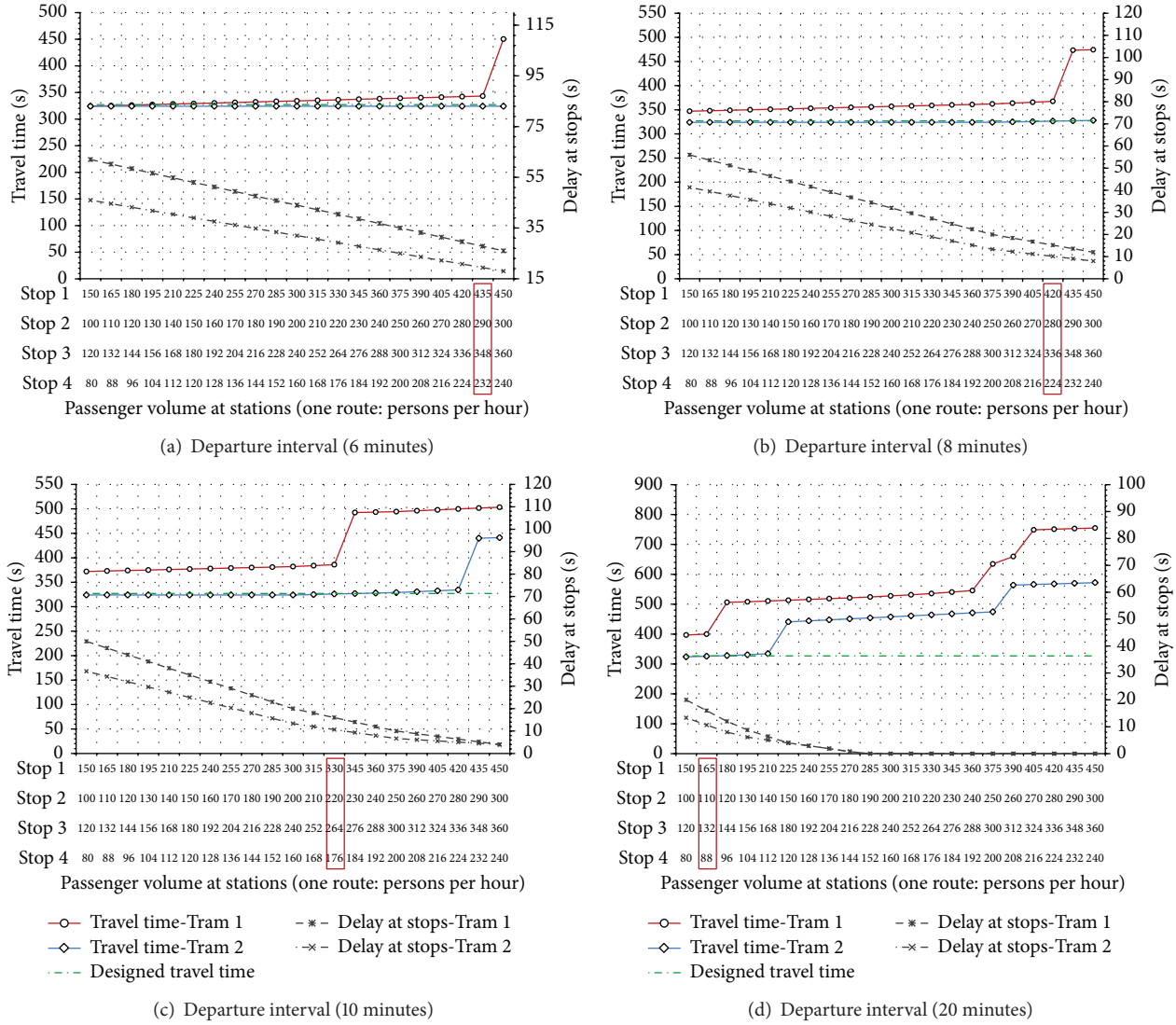

(a) Departure interval (6 minutes)

(b) Departure interval (8 minutes)

(c) Departure interval (10 minutes)

(d) Departure interval (20 minutes)

Figure 6: Impacts of passenger flows on streetcars progression.

$\overline{t}_{j,\text{allow}/2}$: The median of available time for the downstream streetcar passage during a streetcar phase at intersection j (s)

E_j: Offset between intersection $j+1$ and intersection j belonging to upstream route (s)

$\overline{E}_j$: Offset between intersection $j+1$ and intersection j belonging to downstream route (s).

4. Modeling Methodology

4.1. Objective Function

4.1.1. Offsets Calculation for Upstream Streetcar Route. Streetcar running speed in this direction is set up constantly along the segment. The arrival time at each intersection of an upstream streetcar is calculated as follows:

$$A_j = \sum_{i=1}^{k} W_i + \frac{3.6 \times \sum_{i=1}^{j} L_i}{V_{\text{up}}}, \tag{1}$$

where k is the number of stations belonging to 1 to j road sections and $k \in [1, 2, \ldots, n-1]$; n is the number of stations belonging to the control unit; j is an integer variable and $j \in [1, 2, \ldots, m-1]$; m is the number of road sections belonging to the control unit.

In order to make the arrival time of the streetcar at each intersection exactly equal to the median of the available time for streetcar passage, the arrival time is expressed as

$$A_j = t_{j,\text{allow}/2}. \tag{2}$$

Subsequently, the relative offset of two adjacent intersections for upstream streetcar route is deduced as

$$E_j = A_{j+1} - A_j. \tag{3}$$

4.1.2. Offsets Calculation for Downstream Streetcar Route. Repeat the work above for streetcar attached to the other direction. The arrival time at each intersection of a downstream streetcar is calculated as

$$\overline{A}_j = \sum_{i=k+1}^{n} \overline{W}_i + \frac{3.6 \times \sum_{i=j+1}^{m} L_i}{V_{\text{down}}}. \tag{4}$$

Aiming to make the streetcar arrive at each intersection in the median of the available passage time, arrival time in this direction is obtained and expressed as

$$\overline{A}_j = \overline{t}_{j,\text{allow}/2}. \tag{5}$$

Naturally, the relative offset of the two adjacent intersections in this direction is stated as

$$\overline{E}_j = \overline{A}_j - \overline{A}_{j+1}. \tag{6}$$

4.1.3. Offsets Optimization for Two-Way Progressions of Streetcar System. Ideally, a time when both upstream and downstream streetcars arrive at the intersection is expected, which is the median of the available time for streetcar passage in the streetcar phase. If not met, a situation is pursued, when the two-way streetcar arrival times, both, surround the median of available passage time as far as possible. The objective function for the optimal situation is calculated as

$$\text{Minimize} \quad \sum_{j=1}^{m-2} \left| E_j \% T + \overline{E}_j \% T - T \right|, \tag{7}$$

where $E_j\%T$ and $\overline{E}_j\%T$ indicate modular arithmetic.

4.2. Constraints

4.2.1. Cycle Time Constraint. The background signal timing scheme is developed by Webster method. The public cycle time of the segment is determined by the key intersection, whose traffic demand is the largest or whose position is the most critical. It makes little difference in traffic capacity at the intersection when the public cycle time hovers ±5%. If $T_{\min}$ denotes $0.95T$ and $T_{\max}$ denotes $1.05T$, the cycle time constraint is stated as

$$T_{\min} \le T \le T_{\max}. \tag{8}$$

4.2.2. Streetcar Running Speed Constraint. For control convenience and operation comfortableness, the running speed of the streetcar is set as a constant speed in its whole route or at least in its control unit. However, it is unnecessary for upstream and downstream streetcar running speeds to be equal to each other. In this paper, the streetcar running speed is stated as

$$V_{\min} \le V_{\text{up}} \le V_{\max}, \tag{9a}$$

$$\overline{V}_{\min} \le V_{\text{down}} \le \overline{V}_{\max}. \tag{9b}$$

4.2.3. Available Passage Time Constraint at the Intersection. Vehicle length of modern streetcar is almost more than 20 m. A longer vehicle length means a longer running time for the same journey. If a streetcar enters intersection at the end of the streetcar phase, a conflict with other vehicles from the next phase will occur. Subsequently, a clearance time needs to be considered. So, the streetcar phase should be divided into available passage time and streetcar clearance time to avoid such time conflict. Modern streetcar track locations generally consist of center lanes and roadside lanes, shown as Figure 2. In the two situations, both available passage time and clearance time are different.

If a modern streetcar system is allocated with central lanes, for a given intersection j, the time for a streetcar to pass through the intersection can be calculated as

$$t_{\text{str}} = \frac{3.6 \times (d + I/2)}{v_{\text{str}}}, \tag{10}$$

where, v_{str} is the velocity of the streetcar; d is the vehicle length of the streetcar; I is the intersection width along the track.

Time for a vehicular traffic to arrive at the conflict point can be calculated as

$$t_{\text{veh}} = \sqrt{\frac{2I'}{a_{\text{veh}}}}, \tag{11}$$

where, a_{veh} is the acceleration of the vehicular traffic; I' is the intersection width across the track.

In conclusion, the available passage time for streetcars on central lanes can be shown as follows:

$$G_{\text{allow}} = G + Y - \left(t_{\text{str}} - t_{\text{veh}}\right), \tag{12}$$

where G is green time of the streetcar phase.

As to modern streetcar systems on roadside lanes, the time for vehicular traffic to arrive at the conflict point is regarded as zero. The available passage time can be calculated as

$$G_{\text{allow}} = G + Y - t_{\text{str}}. \tag{13}$$

4.2.4. Dwell Time Constraint. Wire-free operation comes to be an important trend for modern streetcar systems. Nice in France has operated two short off-wire segments (435 and 483 m) since 2007. Seville of Spain has taken a 450 m off-wire segment since 2010. Zaragoza began operating with a 2,000 m off-wire segment starting in 2012. Lots of other systems with wire-free operation lines are now under construction, including the First-Hill line in Seattle and several other cities in Europe [2]. Particularly in Nanjing, two modern streetcar systems of Hexi New City Streetcar 1# and Qilin Streetcar 1# are both equipped with off-wire vehicles. However, a wire-free line still needs power and corresponding distribution at certain locations for charging purposes. Therefore, the primary dwell time constraint is needed to meet the charging demand.

The dwell time is mainly for passengers' boarding and alighting, which is usually random. Some studies suggest that

Table 1: Average operating data of Shanghai, Tianjin, and Dalian streetcar systems.

Measure	Value	Measure	Value
Average dwell time	17.49 s	Average intersection delay	21.31 s
Average operating speed	17.28 km/h	Average running speed	31.47 km/h
Proportion of dwell time	35.15%	Proportion of intersection delay	64.85%

Table 2: Signal progression parameters based on the proposed model.

Signal intersection	Cycle time (s)	Offset (s)	Minimum dwell time	Streetcar running speed (ideal value)
Intersection 1	110	0	25 s	25–30 (27) km/h
Intersection 2	110	55		
Intersection 3	110	110		
Intersection 4	110	170		

the dwell time follow a certain distribution upon most occasions, such as normal distribution, lognormal distribution, and Wakeby distribution [17–19]. A peak exists in dwell time distribution, and the probability tends to be zero on both ends. A large-scale survey in Nanjing City was conducted by School of Transportation Southeast University between May 27 and June 28, 2013. In this survey, we observed the dwell time for passengers' boarding and alighting at twelve stations and then we discovered a common property, which is that 95.33% dwell times are less than 25 s. Hence, 25 s is taken as the second dwell time constraint for passenger service. Distributions of the dwell times related to Xuanwumen Station and Taiping Beilu Station are illustrated in Figure 2.

5. Evaluation and Analysis

The VISSIM simulation software is further used to evaluate the operational effects of the proposed model. The experimental section is based on the Hexi New City Streetcar 1#.

5.1. Experimental Section. The experimental section is a part of Hexi New City Streetcar 1# line. It begins from Olympic East Station and ends at Yellow River Station. The section is 1.83 kilometers long, associated with four stations and four signalized intersections, shown as Figure 3. The direction from Olympic East Station to Convention Centre Station is defined as the upstream route with a name of Tram 1, while the direction from Yellow River Station to Olympic East Station is defined as the downstream route named Tram 2.

5.2. Experimental Results and Analysis. In this section, signal lights at intersections are coordinated and controllable with the same cycle time. Since there is a heavy vehicular traffic in Jiang-Dong Road, so, in the direction of Jiang-Dong Road, green time is relatively longer for vehicles passing through the road; thus green time takes up a significant portion of the cycle. And it is long enough to ensure the streetcar passing through the intersection. Furthermore, all turning traffic along Jiang-Dong Road will be forbidden, during a phase with streetcar traveling. As a result, the current background signal timing scheme fits streetcar system well.

Hexi New City Streetcar 1# is lacking in statistical data of dwell time, for sake of not being operated until August 1. However, it is clear that 25 seconds are guaranteed for streetcar charging at each station. Therefore, 25 seconds is the only constraint for dwell time. Table 2 shows the cycle time, offsets, and running speed for the streetcar system progression of this studied section, resulting from the proposed model.

5.3. Simulation Based on Analysis. Data is collected on weekdays under fine weather conditions between May 12 and May 30, 2014. Measures of effectiveness including the streetcar travel time, average vehicular delay at the intersection, and average streetcar delay at the station are employed and obtained from VISSIM. Hence, average streetcar delay at the station means a period from the finish time of passenger service to the deserved departure time of streetcar leaving from the station, when passenger service time is less than 25 seconds. Each simulation runs for two hours and an average value of the 10 times' simulation is adopted.

5.3.1. Impact of Streetcar System Progression on Vehicular Traffic. To investigate the impact of the streetcar system progression generated by the proposed model on vehicular traffic, a comparison of vehicular efficiency before and after the project implementation is made.

Figure 4 shows the simulation results for low, medium, and high volume cases. For each case, average delay at the intersection is used to measure the vehicular efficiency. Take the medium volume scenario as example; the average intersection delay before the project implementation is 33.3 s, 25.4 s, 23.3 s, and 36.6 s from intersection 1 to intersection 4, while it is 34.9 s, 26.7 s, 24.2 s, and 33.3 s after the project implementation. The biggest percentage increase in delay of the intersections under the three volume scenarios is 5.12%. It can be concluded that the streetcar system progression has a negligible effect on the delay of vehicular traffic in the three volume cases. That is because of the methodology having no impact on the original timing scheme.

5.3.2. Impact of Streetcar Departure Intervals on Streetcar System Progression. Under a given passenger demand, shorter departure intervals mean less boarding passengers

and shorter dwell time at the station, while longer departure intervals imply more boarding passengers and longer dwell time. Supposing that the deserved dwell time for passenger service was less than 25 seconds, streetcar delay at the station occurs. However, if the necessary dwell time was much longer than 25 seconds, streetcars cannot enjoy the progression either. Based on Figure 5, it can be concluded that average streetcar delay at the station decreases with the increase of passenger demand and unreliable probability of streetcar travel time. Optimal departure intervals (22 minutes per hour for lower passenger demand, 16 minutes per hour for low passenger demand, 13 minutes per hour for high passenger demand, and 12 minutes per hour for higher passenger demand) decrease from lower passenger demand scenario to higher passenger demand scenario.

5.3.3. Impact of Passenger Volumes on Streetcar System Progression. The impact of passenger volumes on streetcar system progression is shown in Figure 6. Passenger volume determines the dwell time of streetcar at stops, and also the dwell time is the chief factor affecting the application of streetcar progression. When passengers' boarding and alighting time is less than 25 s, the streetcar can enjoy progression, but the delay of streetcar at stops occurs; when passengers' boarding and alighting time is more than 25 s, the streetcar cannot enjoy progression. The simulation analyzes streetcar's delay and travel time at stops under different passenger volumes when the departure interval time is 6 minutes, 8 minutes, 10 minutes, and 20 minutes, respectively. It can be shown that each passenger volume corresponds to an optimal departure interval, and the departure interval decreases with the increase of passenger volumes. If passenger volumes are around this optimal passenger volume, streetcar experiences an ideal travel time with a minimum delay at stops. It also proves that the optimal passenger demand decreases with the increase of streetcar departure interval. For example, in Figure 6, passengers with the volumes 435, 290, 348, and 232 at stops 1, 2, 3, and 4 correspondingly seem to be the optimal passenger demand when the departure interval is 6 minutes in the streetcar system, while passengers with the volumes 165, 110, 132, and 88 at stops 1, 2, 3, and 4 correspondingly are the optimal passenger volume when the departure interval is 20 minutes.

6. Conclusion

The proposed model in this study provides effective coordinated priority for streetcars. Two features stand out with it. Firstly, it does not adopt the concept of maximized bandwidth, because there seldom exists a situation where a queue of streetcars passes through the intersection. Secondly, it presets a dwell time, during which streetcar charging (such as 25 seconds at least) and passenger services (in 95% occasions, passenger service time is less than 25 seconds) are satisfied. Furthermore, it has the potential to be used in setting up a background signal progression scheme for the freshly hatched modern streetcar system.

In addition, a big concern for traffic and transit officials is the negative impacts of streetcar system progression on transit and vehicular traffic. Worries are unnecessary, due to the little differences from the original signal timing scheme. It practically indicates little change in the traffic capacity. Besides, analysis shows that the vehicular traffic delays in three volume scenarios, caused by streetcar system progression, are all very small. It can be negligible when compared to the benefits it brings to streetcar systems.

Also, the performance of the streetcar system progression is validated by the case study results. Two conclusions are drawn. One is that each passenger demand is matched with an optimal departure interval. And it decreases with the increase of passenger demand. The other is that the average streetcar delay at the station gets significant, in cases where departure intervals are much shorter than the optimal for a given passenger demand. Likewise, streetcars deviate from the signal progression, when departure intervals are much longer.

In the future, modern streetcar dwell times associated with passenger boarding and alighting characteristics at the station are recommended to be analyzed based on large amounts of statistical data. More extensive numerical experiments and field tests are required to assess the effectiveness and reliability of the proposed model, under various traffic volumes, streetcar passenger demands, streetcar schedules, and so forth. Further priority strategies for modern streetcar system, such as Green Extension, Red Truncation, Phase Insertion, and Phase Rotation, need to be developed, which help to reply stochastic impacts of streetcar running speed and dwell time causing streetcars to deviate from the progression.

Conflict of Interests

The authors declare that there is no conflict of interests regarding the publication of this paper.

Acknowledgments

This study is performed as a part of Transit Signal Priority Project in Hexi New City of Nanjing, which is sponsored by Nanjing Department of Transportation. The study is supported by the National High-Tech Research and Development Program of China (no. 2014AA110303). The authors would like to thank Beijing Key Laboratory for Cooperative Vehicle Infrastructure Systems and Safety Control and the senior students from Transportation School of Southeast University for their assistance in data collection.

References

[1] Transportation Research Board, *Transit Capacity and Quality of Service Manual*, Transportation Research Board of the National Academies, Washington, DC, USA, 3rd edition, 2013.

[2] American Public Transportation Association, *Modern Streetcar Vehicle Guideline*, American Public Transportation Association, Washington, DC, USA, 2013.

[3] G. Currie and A. Shalaby, "Success and challenges in modernizing streetcar systems: experiences in Melbourne, Australia and Toronto, Canada," *Transportation Research Record: Journal of the Transportation Research Board*, no. 2006, pp. 31–39, 2007.

[4] H. R. Smith, B. Hemily, and M. Ivanovic, *Transit Signal Priority (TSP): A Planning and Implementation Handbook*, Intelligent Transportation Society of America, Washington, DC, USA, 2005.

[5] K. Ling and A. Shalaby, "A reinforcement learning approach to streetcar bunching control," *Journal of Intelligent Transportation Systems*, vol. 9, no. 2, pp. 59–68, 2005.

[6] D. Luckerath, O. Ullrich, and E. Speckenmeyer, "Modeling time table based tram traffic," *Journal on Developments and Trends in Modelling and Simulation*, vol. 22, no. 2, pp. 61–68, 2012.

[7] O. Ullrich, S. Franz, E. Speckenmeyer, and D. Luckerath, "Simulation and optimization of Cologne' s tram schedule," *Journal on Developments and Trends in Modelling and Simulation*, vol. 22, no. 2, pp. 69–76, 2012.

[8] T. Nagatani, "Dynamical model for retrieval of tram schedule," *Physica A: Statistical Mechanics and its Applications*, vol. 377, no. 2, pp. 661–671, 2007.

[9] G. Currie, *Melbourne Public Transportation Investment: The Why, the What and the Way Forward*, Monash University, Melbourne, Australia, 2005.

[10] D. Cliché and S. Reid, "Growing patronage—think tram?" in *Proceedings of the International Conference on Competition and Ownership in Land Passenger Transport*, University of Sydney, 2007.

[11] G. Currie and A. Shalaby, "Active transit signal priority for streetcars: experience in Melbourne, Australia, and Toronto, Canada," *Transportation Research Record*, no. 2042, pp. 41–49, 2008.

[12] *A Transportation Vision for the City of Toronto Official Plan*, Urban Development Services, Toronto, Canada, 2001.

[13] A. Shalaby, B. Abdulhai, and J. Lee, "Assessment of streetcar transit priority options using microsimulation modelling," *Canadian Journal of Civil Engineering*, vol. 30, no. 6, pp. 1000–1009, 2003.

[14] A. Shalaby, A. Georgi, K. Ling, J. Sinikas, and A. Salzberg, "Evaluation of proof-of-payment and multiple-unit operation in difference streetcar route configurations," in *Proceedings of the 86th Annual Meeting of the Transportation Research Board*, Washington, DC, USA, 2007.

[15] G. Gormick, *The Streetcar Renaissance: Its Background and Benefits. A Research Report for the St. Clair Avenue Transit Improvements Environmental Assessment Study*, 2004.

[16] M. Li, G. Y. Wu, Y. Li, F. Bu, and W.-B. Zhang, "Active signal priority for light rail transit at grade crossings," *Transportation Research Record*, no. 2035, pp. 141–149, 2007.

[17] S. Guo, Y. Wei, W. Shi, and Y. Xue, "Statistical analysis of buses'stopping time," *Journal of Guangxi Normal University: Natural Science Edition*, vol. 24, no. 2, pp. 5–9, 2006.

[18] F. Li, Z. Duan, and D. Yang, "Dwell time estimation models for bus rapid transit stations," *Journal of Modern Transportation*, vol. 20, no. 3, pp. 168–177, 2012.

[19] S. Rashidi and P. Ranjitkar, "Approximation and short-term prediction of bus dwell time using AVL data," *Journal of the Eastern Asia Society for Transportation Studies*, vol. 10, pp. 1281–1291, 2013.

Hindawi Publishing Corporation
Discrete Dynamics in Nature and Society
Volume 2015, Article ID 429219, 11 pages
http://dx.doi.org/10.1155/2015/429219

Research Article

Timetable Design for Urban Rail Line with Capacity Constraints

Yu-Ting Zhu,[1,2] Bao-Hua Mao,[1,2] Lu Liu,[1] and Ming-Gao Li[1]

[1] *MOE Key Laboratory for Urban Transportation Complex Systems Theory and Technology, Beijing Jiaotong University, Beijing 100044, China*
[2] *School of Traffic and Transportation, Beijing Jiaotong University, Beijing 100044, China*

Correspondence should be addressed to Bao-Hua Mao; bhmao@china.com

Received 26 December 2014; Accepted 4 March 2015

Academic Editor: Juan R. Torregrosa

To design an efficient and economical timetable for a heavily congested urban rail corridor, a scheduling model is proposed in this paper. The objective of the proposed model is to find the departure time of trains at the start terminal to minimize the system cost, which includes passenger waiting cost and operating cost. To evaluate the performance of the timetable, a simulation model is developed to simulate the detailed movements of passengers and trains with strict constraints of station and train capacities. It assumes that passengers who arrive early will have more chances to access a station and board a train. The accessing and boarding processes of passengers are all based on a first-come-first-serve basis. When a station is full, passengers unable to access must wait outside until the number of waiting passengers at platform falls below a given value. When a train is full, passengers unable to board must wait at the platform for the next train to arrive. Then, based on the simulation results, a two-stage genetic algorithm is introduced to find the best timetable. Finally, a numerical example is given to demonstrate the effectiveness of the proposed model and solution method.

1. Introduction

As the economy develops rapidly, deepening urbanization and the increasing urban population lead to a large demand for urban rail transit in many cities. In 2013, over 3.2 billion and 2.5 billion passenger rides were delivered by the Beijing and Shanghai subway systems, respectively; the average passenger rides on weekdays are more than 10 million and 7 million, respectively [1]. With such high demand, making urban rail transit more efficient has become a primary task for many cities. To improve the service quality of urban rail transit, a variety of operation strategies have been proposed, such as adjusting the speed of trains [2] and optimizing train formation [3]. Of all these strategies, timetable design has been accepted as the most straightforward and effective solution [4].

Timetable design problem (TDP) aims at determining a preoperational schedule for a set of trains and follows some train operational requirements [5]. The most popular technique to design timetable is to use mathematical programming, which is initialized by Amit and Goldfarb [6] in 1971 for railway transportation and developed by a large number of researches (such as Carey and Crawford [7], Castillo et al. [8, 9], and Castillo et al. [10]).

Although there are some differences between urban public transportation and railway transportation, the mathematical programming method has still been introduced to create efficient timetables for urban public transportation to reduce passenger waiting time. Cury et al. [11], Furth and Wilson [12], Wang et al. [13], and Barrena et al. [14] proposed optimization models to design a timetable for a single line. With the expansion of subway networks, some researchers have attempted to set up a timetable for multiple services in a connected transit network (de Palma and Lindsey [15], Caprara et al. [16], Liebchen [17], Wong et al. [18], and Aksu and Akyol [19]). However, most of them assumed that the capacity of the trains is always sufficient to receive all passengers who want to enter the train and the capacity of the stations is large enough to receive all passengers who need to be evacuated. Moreover, the average waiting time of passengers is always simplified as half of the transportation headway. In fact, infinite capacity is unrealistic and

the average waiting time of passengers may be longer when capacity constraints are considered.

In order to provide a more efficient timetable for passengers, vehicle capacity has been widely considered. Ceder [20] first addressed the importance of ridership information and stated that service frequency should correspond to temporal passenger demand. One important target of this research is to avoid overcrowding (in an average sense) on the vehicles. For a further study, Ceder [21] proposed a scheduling model to replace constant headway. In this model, the ridership of each vehicle is under an ideal value. These models, however, are not suitable for a public service with high frequency [22]. Koutsopoulos et al. [23] proposed a model to find optimal headway by minimizing social cost. In their model, vehicle capacity is indirectly incorporated in the inconvenience cost due to crowding on the vehicles, and the inconvenience cost will increase as the volume to capacity ratio increases. However, as this setup will only increase the inconvenience cost when the transit vehicle is more congested, it still allows the capacity to be exceeded. Different from the three studies above, the capacity constraints are strictly enforced in the optimization models formulated in Sun et al. [4], Niu and Zhou [24], Albrecht [25], Chen [26], and Hassannayebi et al. [27]. In their models, all passengers boarding a vehicle obey the first-come-first-serve (FCFS) principle and when a vehicle is full, passengers unable to board must wait for the next vehicle to arrive. Thus, the waiting time of a passenger is the sum of time waiting for the first coming service and for the next one as a result of previous boarding failure.

Although there is a comprehensive body of literature on TDP, few studies have drawn attention to the limitation of station capacity; also, the outside-station waiting time (OSWT) caused by being unable to get into a crowding station has always been neglected. In fact, waiting outside the station is a common phenomenon in overcrowded urban rail transit systems, such as subway systems in China. In order to provide a safe and efficient movement in stations, especially in an underground station with more enclosed and very limited internal space, operators will routinely restrict the number of passengers in stations. That is to say, some passengers will be required to wait outside the station when the number of passengers in stations exceeds the safe-value. For example, in Beijing, 63 urban rail stations mainly along Line 1, Line 5, Line 6, Line 13, Batong Line, and Changping Line instituted these restrictions since July 8, 2014, during a.m. peak hours. And OSWT in some stations, such as ShaHe, an intermediate station of Changping Line, is more than 20 minutes.

In addition, many studies in the area of TDP aim to minimize the waiting time of passengers [24–27]. This single-sided approach, however, results in timetables with high operational costs since timetables that offer the minimum waiting time for passengers usually require a high-frequency service even for transit lines with low demand. It should be noted that, although studies such as the work in [24] do not take operational interests into account explicitly, some constraints are considered to restrict the operational costs within reasonable values. A more realistic approach, which is also followed in this paper, is to minimize an objective function that consists of both the operational and passenger waiting costs, such as the approach proposed by [19].

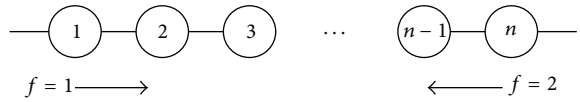

Figure 1: The representation of an urban transit rail line.

This paper fully considers the constraints of station and train capacities. Thus, the passenger waiting time can be divided into three parts, namely, (1) initial platform waiting time (IPWT), time spent waiting on the platform for the first coming train; (2) extra platform waiting time (EPWT), waiting time spent by left-behind passengers, who fail to board the first coming train due to the limitation of train capacity; and (3) OSWT, waiting time spent outside the station. Then, an optimization model is proposed to create an efficient and economical timetable. The contributions of this paper are summarized as follows.

(i) A simulation model is developed to simulate the movements of passengers and trains with constraints of capacities, such as train maximum capacity and station safety capacity.

(ii) The total waiting time of passengers, which includes IPWT, EPWT, and OSWT, is measured based on the outputs of the simulation model.

(iii) An optimization model is proposed to minimize the operational and passenger waiting costs; a two-stage simulation-based genetic algorithm is developed to solve the model.

The remainder of the paper is as follows. Section 2 describes the timetable design problem of urban rail line in detail. The simulation model of an urban rail line is presented in Section 3. Based on the simulation model in Section 3, a two-stage simulation-based optimization approach is proposed in Section 4. In Section 5, a numerical experiment is performed to show the application of the proposed model and solution algorithm. The final section concludes the paper and discusses future research issues.

2. Timetable Design Problem

2.1. Problem Description. This paper focuses on the TDP of an urban rail line with n stations, as shown in Figure 1. The stations are numbered consecutively with the index values $1, 2, \ldots, n$, where stations 1 and n denote the start terminal and the return terminal, respectively. Each train departs from station 1, makes a U-turn at station n, comes back to station 1 after a given recovery time at return terminal n, and then prepares for a new departure. To simplify, all trains are assumed to have the same travel time between two consecutive stations and the same dwelling time at each station. Thus, the TDP in this paper aims at determining a departure schedule for trains at the start terminal.

Let $[0, T]$ denote the study period; that is, 0 and T represent the start and end of the study hours. To simplify

the problem, the paper divides the continuous study period $[0, T]$ equally into a number of equal-length time intervals. Then, the study period $[0, T]$ can be represented as a set of discrete time points of the form $\Gamma = \{0, \delta, 2\delta, \ldots, m\delta\}$, where δ denotes the time interval which is equal to T/m and m is a positive integer. To simplify the presentation, we ignore δ and simply write Γ as $\{0, 1, 2, \ldots, m\}$. We also assume that all times (section running times of trains, etc.) are multiples of δ. For example, a travel time of five units means, $5 \times \delta$ seconds.

Other assumptions made throughout the paper are explained as follows.

Assumption 1. The distribution of passenger demand is given and is steady during the study period.

Assumption 2. Whether a station is under an overcrowding situation is decided by the number of waiting passengers in station. That is, passengers cannot enter a station when the number of waiting passengers at station is larger than the safe-value. In fact, alighting passengers will also lead to a crowding situation at station. However, it is difficult for operators to forecast the number of alighting passengers of each train. For simplification, we only forecast the maximum possible number of alighting passengers. Then, the safe capacity for waiting passengers is equal to design capacity minus this maximum number.

Assumption 3. In general, passengers who arrive early will have more chances to access a station or board a train. In order to facilitate simplification, the paper assumes that all passengers accessing a station or boarding a train obey the FCFS principle. The passengers who fail to access an overcrowding station or fail to board a full train must wait for the next chance.

Assumption 4. The proposed model focuses on reducing passenger waiting time. The accessing walking time of passengers at a station is not considered in this model. Here, we assume that the accessing walking time of passenger is assumed to be fixed and equal to 0.

The following notations and parameters are used throughout this paper.

Sets are as follows:

Γ: set of time intervals,

N: set of stations,

R: set of trains.

Indices are as follows:

u, v: index of stations,

j: index of passengers,

r: index of trains,

t: index of modeling time intervals, $t \in \Gamma$,

f: index of travel direction; let $f = 1$ when a train travels from start terminal to return terminal and $f = 2$ for the opposite direction.

Parameters are as follows:

λ_u^t: number of passengers who arrive at station u at time t,

ρ_{uv}: passenger destination probability, the probability of potential destination station v from origin station u,

q_u: total number of passengers who arrive at station u during the study period,

d_u: dwelling time at station u,

$s_{u,u+1}$: running time between stations u and $u + 1$

e_1, e_n: recovery times at start terminal and return terminal,

$r_{\max}$: maximum number of trains

K: prespecified fleet size,

m: number of time intervals,

φ: train operating cost per vehicle per unit time,

η: waiting time cost per passenger per unit time,

$H_{\max}$: maximum service headway,

$H_{\min}$: minimum service headway,

CT: maximum capacity of trains,

CS_u: design capacity of station u,

$LA_u^{\max}$: maximum possible number of passengers alighting at station u during study period,

γ_u: maximum capacity for waiting passengers at station u, $\gamma_u = \mathrm{CS}_u - LA_u^{\max}$,

θ_u: threshold which is used to judge whether passengers can access the overcrowding station u. Passengers waiting outside the station can access station u if the number of passengers in station u is less than $\theta_u \cdot \gamma_u$; otherwise, they cannot access this station,

$w_{u,t}$: let $w_{u,t} = 1$ if passenger can access the station u at time t, and 0 otherwise.

Intermediate variables in simulation modelare as follows:

b_r^t: number of boarded passengers on train r at time t,

LO_u^t: number of passengers waiting outside station u at time t,

$LP_{u,f}^t$: number of passengers waiting at time t on the platform of station u to board on train in direction f,

LA_u^t: number of passengers alighting at station u at time t,

$TD_{u,f}^r$: departure time of train r at station u in direction f,

$TA_{u,f}^r$: arrival time of train r at station u in direction f,

$TR_t^{u,j}$: departure time of the first train for the direction of the jth passenger who accesses the station u at time t,

TF_r: time by the end of the recovery operation after the train r returns to the start terminal,

PA_u^j: arrival time of the jth passenger at station u,

PC_u^j: accessing time of the jth passenger at station u,

PB_u^j: boarding time of the jth passenger at station u,

NF_t: number of idle train unit at time t; initialize $NF_0 = K$,

$\sigma_{u,t}$: let $\sigma_{u,t} = 1$ if station u is under an overcrowding situation at time t and 0 otherwise.

Decision variable is as follows:

x_t: let $x_t = 1$ if a train departs from start terminal at time t and 0 otherwise.

2.2. Model Formulation. The TDP in this paper aims at determining the departure time of each service at start terminal. The objective is to minimize the total cost of the transit system C, which is the sum of the operating cost C^o and the passenger waiting cost C^w. Thus, the problem can then be formulated as follows:

$$\text{Min } C = C^o + C^w, \tag{1}$$

$$C^o = \varphi \cdot \left(2 \cdot \left(\sum_{u=1}^{n-1} s_{u,u+1} + \sum_{u=1}^{n} d_u\right) + e_1 + e_n\right) \cdot \sum_{t \in \Gamma} x_t, \tag{2}$$

$$C^w = \eta \cdot \sum_{u \in N} \sum_{j \in [1, q_u]} \left(\left(TR^{u,j}_{PC^j_u} - PC^j_u\right) + \alpha \cdot \left(PB^j_u - TR^{u,j}_{PC^j_u}\right) + \beta \cdot \left(PC^j_u - PA^j_u\right)\right), \tag{3}$$

subject to

$$\sum_{t \in [t_1, t_2]} x_t \le 1, \quad t_2 = t_1 + \frac{H_{\min}}{\delta} - 1, \ \forall t_1, t_2 \in \Gamma, \tag{4}$$

$$\sum_{t \in [t_1, t_2]} x_t \ge 1, \quad t_2 = t_1 + \frac{H_{\max}}{\delta} - 1, \ \forall t_1, t_2 \in \Gamma, \tag{5}$$

$$x_m = 1, \tag{6}$$

$$b^t_r \le \text{CT}, \quad \forall t \in \Gamma, \ \forall r \in R, \tag{7}$$

$$\sum_{f=\{1,2\}} LP^t_{u,f} + LA^t_u \le \text{CS}_u, \quad \forall t \in \Gamma, \ \forall u \in N, \tag{8}$$

$$w_{u,t} = \begin{cases} 1 & \text{if } \sigma_{u,t} = 0 \text{ or } \sum_{f=\{1,2\}} LP^t_{u,f} < \theta_u \cdot \gamma_u \\ 0 & \text{else,} \end{cases}, \tag{9}$$

$$NF_t \ge 0, \quad \forall t \in \Gamma, \tag{10}$$

$$LP^t_{u,f} = 0, \quad t = TD^{r_{\max}}_{u,f}, \ \forall u \in N. \tag{11}$$

In this formulation, the objective function (1) minimizes the total cost of transit system. Equation (2) calculates the total operation cost C^o, which is the sum of the operating cost of all departure trains during the study period. Equation (3) calculates the total waiting cost of passengers C^w, which is the product of the number of passengers and their waiting time. In general, total waiting time of a passenger can be simply calculated by $PB^j_u - PA^j_u$. However, passengers may have different feelings for different kinds of waiting time [28], especially for OSWT, since passengers may need to brave the scorching sun or biting wind. Therefore, EPWT and OSWT may be presented at a higher rank. Here, two magnification factors α and β ($\alpha, \beta \geqslant 1$) are introduced to describe this higher rank.

Constraint (4) ensures that the headway between two successive trains should meet the safety requirement. Constraint (5) ensures that the headway between two successive trains should not be too long or else passenger will have to wait long time. Constraint (6) predefines the last service of the urban rail line. Constraints (7) and (8) correspond to the limited capacity, ensuring that occupancy of trains and stations is not more than capacity. Note that it is difficult for operators to forecast the number of alighting passengers of each train. Thus, a simplified constraint, $\sum_{f=\{1,2\}} LP^t_{u,f} + LA^{\max}_u < \text{CS}_u$, is proposed to replace the original constraint (8) based on Assumption 2. Constraint (9) guarantees that the accessing process occurs only when the station is under an undersaturated situation ($\sigma_{u,t} = 0$) or the number of passengers at the station is less than threshold ($\theta_u \cdot \gamma_u$). Constraint (10) guarantees that there exist available train units to depart from the start terminal at scheduled departure times. Constraint (11) ensures that the train supply could meet the total passenger demands during the study period.

For our case, the movement of passengers is restricted by a series of constraints, and it is difficult to use mathematical modeling approach to describe the detailed movement of passengers or calculate passenger waiting time. As mentioned in [13], minimizing passenger waiting time is a nonlinear nonconvex objective function and it is computationally expensive to evaluate. Here, due to the nonlinear nature of the optimization problem, an alternative approach, simulation modeling, is proposed to evaluate solutions.

3. Simulation Model

In this section, a simulation model of urban rail line is presented to evaluate the performance of timetables. It is characterized by a discrete-event and synchronous simulation to model dynamic processes. The simulation process is illustrated in Figure 2.

As shown in Figure 2, six main events are defined in the simulation model. They can be divided into two kinds, namely, passenger dynamic event and train operation dynamic event. The details of the events are described as follows.

(1) Events concern the passenger dynamics: four main events are defined to describe passenger dynamics. The flowcharts of system events and the changes in variables related to passenger arrival, accessing, boarding, and alighting are shown in Figures 3, 4, 5, and 6, respectively. Every time a new passenger arrives at the station, he or she accesses the station based on the FCFS rule. If the number of passengers in station is more than the safe-value, the passengers are required to stay outside the station and wait for permission to access the station (Figure 4). In station, passengers stay in a queue at the platform to board incoming trains.

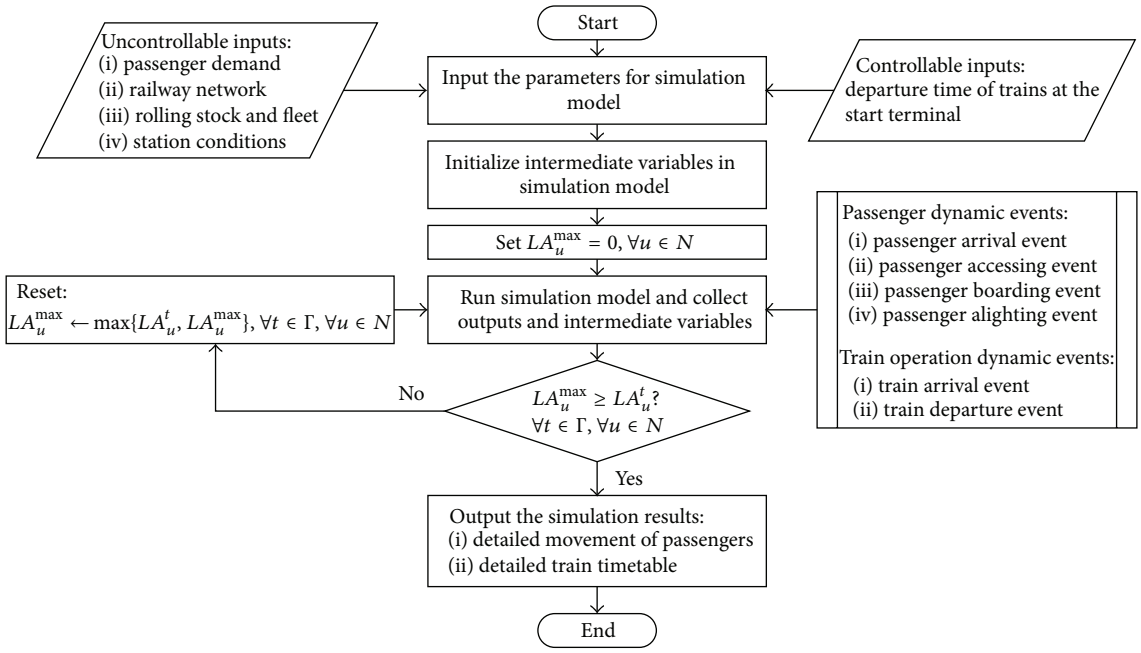

Figure 2: Framework of simulation model.

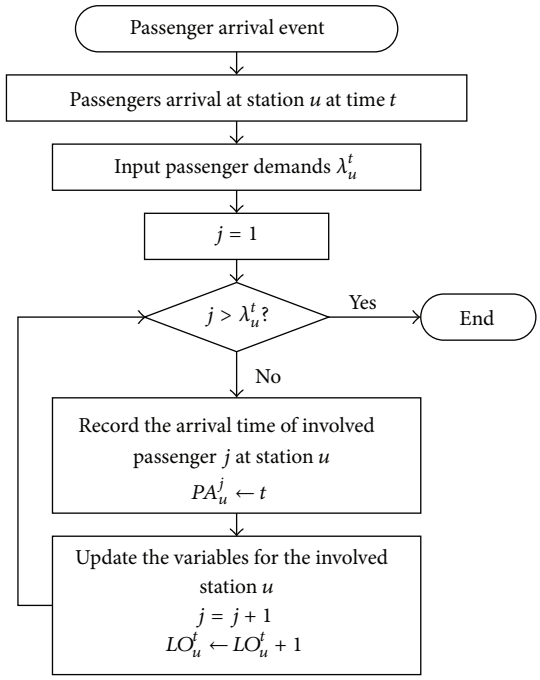

Figure 3: Flowchart of passenger arrival event.

The boarding processes of passengers also obey the FCFS rule. The passengers who cannot board a full train should wait for the next incoming train at the platform (Figure 5). The variables in order to handle the logics and constraints, such as the length of queues ($LP_{u,f}^t$ and LO_u^t) and the load of trains (b_r^t), are updated at the time events. The arrival time (PA_u^j), accessing time (PC_u^j), and boarding time (PB_u^j) are recorded for calculating the waiting time of passengers.

(2) Events concern the train dynamics: two main events are defined to describe passenger dynamics, namely, train arrival event (Figure 7) and departure event (Figure 8). Every time when a train needs to depart from the start terminal, the number of idle train units (NF_t) should be checked. If there exist available train units, the train can depart punctually and the number of idle train units decreases ($NF_t \leftarrow NF_t - 1$); otherwise, the train cannot depart according to the given schedule, which means the given timetable is infeasible (Figure 8). After the train has departed from the start terminal, the details of train timetable including arrival time and departure time at each station are recorded at time events. When the train returns to the start terminal, the number of idle train units increases ($NF_t \leftarrow NF_t + 1$) after a recovery time.

Note that the maximum number of alighting passengers ($LA_u^{\max}$) is an important factor, which determines the maximum capacity for waiting passengers (γ_u). However, it is hard to forecast before the simulation. Thus, a feedback is designed to adjust the value of $LA_u^{\max}$ to ensure that the number of passengers in station is always under its design capacity.

4. Simulation-Based Optimization Approach

The TDP in this paper belongs to the NP-hard class (see [29]), which is difficult to solve by gradient-based methods or commercial optimization solvers. Therefore, an artificial intelligence algorithm is needed to solve the model to ensure that an optimal solution can be obtained within a reasonable amount of time.

The genetic algorithm (GA) is a stochastic search method that is inspired by the natural evolution of species. Due to its

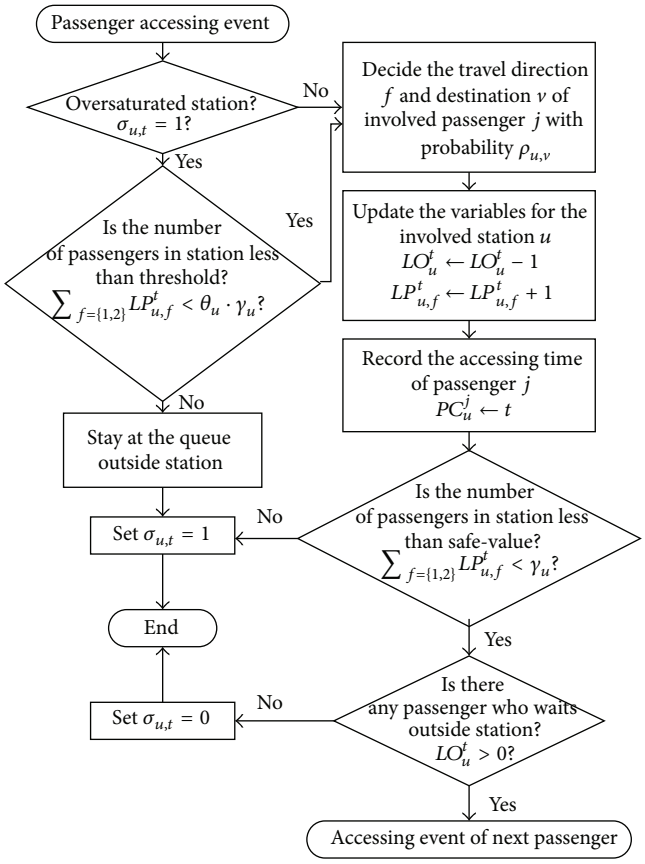

Figure 4: Flowchart of passenger accessing event.

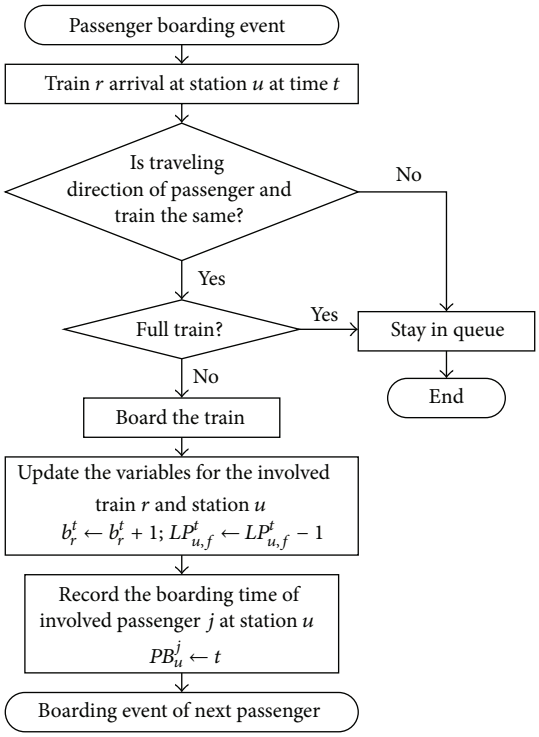

Figure 5: Flowchart of passenger boarding event.

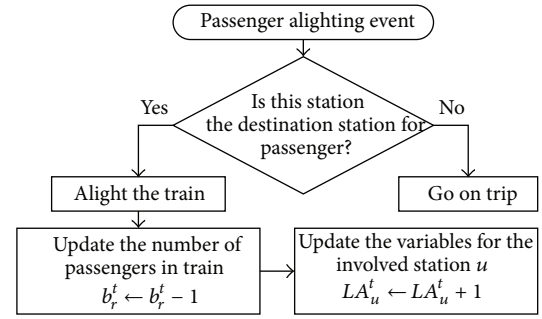

Figure 6: Flowchart of passenger alighting event.

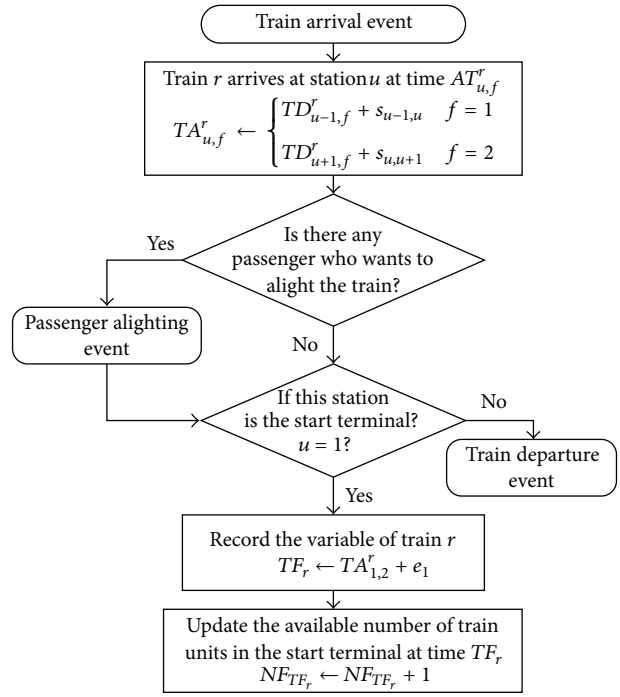

Figure 7: Flowchart of train arrival event.

extensive generality, strong robustness, high efficiency, and practical applicability, GA has become increasingly popular in solving complex optimization problems since the seminal work of Holland [30]. In particular, it has been successfully applied to the research on transportation systems [5, 12, 14, 19, 20, 22]. In this paper, we apply GA to solve the proposed model.

4.1. Solution Representation. As the decision variable x_t is a binary variable, a solution $X = (x_1, x_2, \ldots, x_m)$ can be used as a chromosome in GA directly. It is obvious that the proposed chromosome structure can represent every possible solution, and the number of departing trains changes from 0 to m. However, due to the constraints in the optimization model, most of the solutions are infeasible. For example, a solution with a gap or closeness between departures may not satisfy constraint (4) or (5). Thus, it is time-consuming to initialize a certain amount of feasible chromosomes randomly. In this paper, a preprocessing stage is proposed to

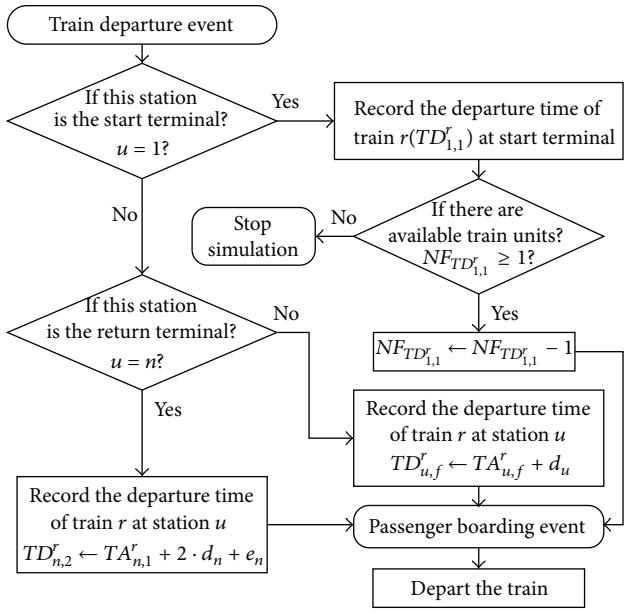

Figure 8: Flowchart of train departure event.

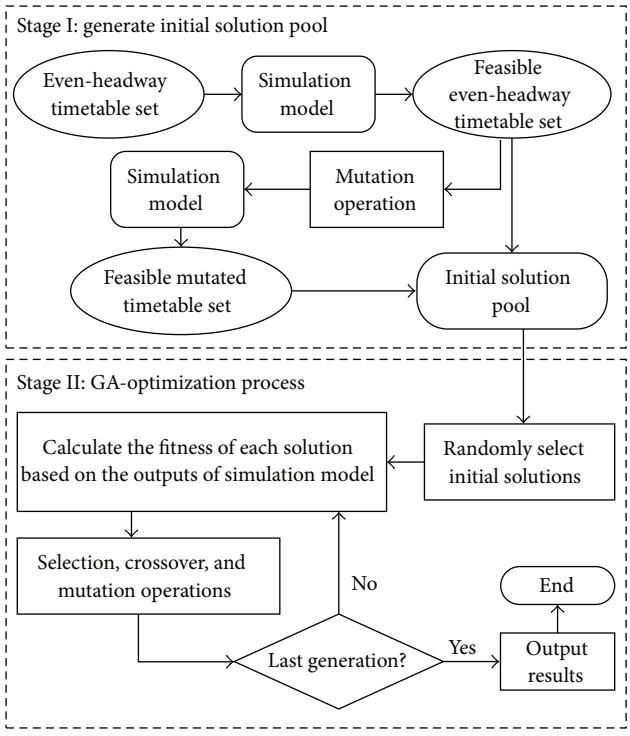

Figure 9: Optimization procedure integrating simulation and GA.

reduce the time spent to generate initial chromosomes. The detailed procedure of the two-stage simulation-based GA-optimization framework is demonstrated in Figure 9.

4.2. The First Stage: Generate Initial Solution Pool. An initial solution pool with *pool-size* chromosomes is generated in this stage. It is conceivable that even-headway timetables are

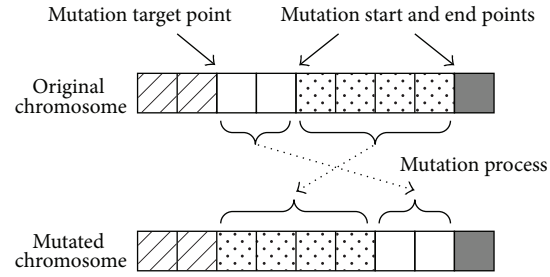

Figure 10: Mutation operation I.

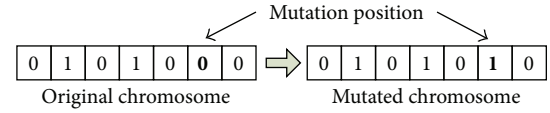

Figure 11: Mutation operation II.

solutions for the optimization model. Thus, the scheduled services that run with an even-headway are in question first, and the simulation experiments will be conducted to determine the feasible even-headway timetables. In this paper, a timetable is feasible if it satisfies all constraints (4)–(11). Then, add feasible even-timetables to the initial solution pool. Finally, a mutation operation is introduced to enrich the initial solution pool.

Mutation Operation. In order to guarantee the diversity and availability of the mutated timetable, two mutation principles are proposed as shown in Figures 10 and 11, respectively. The algorithm of mutation is described as follows. (1) Randomly select a chromosome from feasible even-headway timetable set as the parent for mutation. (2) Randomly generate a real number $a \in [0, 1]$. If $a < 0.5$, obtain a mutated chromosome based on mutation operator I; otherwise, obtain a mutated chromosome based on mutation operator II.

4.3. The Second Stage: GA-Optimization Process. The procedure for GA includes the following. (1) Initialize a population with *pop-size* chromosomes, which are selected from the initial solution pool randomly. (2) Calculate evaluation function value $\text{Eval}(X_i)$ of chromosome i in the population based on the output of the simulation model. Here, we use objective function (1) as the evaluation function. The best individual is the chromosome with the minimum value of $\text{Eval}(X)$. (3) Obtain fine chromosomes via selection, crossover, and mutation operations. (4) Terminate when the maximum number of generations is reached. The flowchart of GA is demonstrated in Figure 9.

Mutation Operation. Different from the mutation operation in the first stage, mutation operation in this stage occurs with a certain probability P_m. Randomly select a chromosome and generate a real number $a \in [0, 1]$ randomly. If $a < P_m$, a mutated chromosome is obtained based on mutation operator I or mutation operator II. And then take it to replace

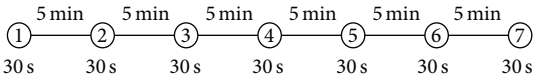

Figure 12: An urban rail line with 7 stations.

the original one if it is feasible; otherwise, keep the original one.

Other detailed steps or approaches of GA, such as selection and crossover processes, are similar to the standard GA, and interested readers are referred to the related references (e.g., Gen and Cheng [31]).

5. Numerical Example

5.1. Input of Date and Parameter Settings. In order to show applications of the proposed model and solution algorithm, an urban rail line with seven stations, which is shown in Figure 12, is adopted. The stations are numbered consecutively with notations 1, 2, 3, 4, 5, 6, and 7, where stations 1 and 7 denote the start terminal and the return terminal, respectively. All the stations have an island platform. The section running time between two successive stations and dwelling time of each station are fixed at 5 min and 30 s, respectively. The recovery time at the start terminal and the return terminal is taken as 90 s; that is, $e_1 = e_7 = 90$ s. The design capacity (CS_u) and control threshold (θ_u) of the station u ($u \in N$) are taken as 1800 and 0.7.

In this example, we aim to determine the departure time of each service at station 1 during the morning peak period [7:00, 8:30]. For the convenience of the expression of passenger demand, we use "second" as a basic unit to describe the study period. That is, 0 denotes the time 7:00, 3600 denotes the time 8:00, and the representations of other times can be deduced by analogy. Then, after determining the length of modeling time interval δ, the passenger demand of station u at the tth time interval (i.e., time period $(\delta(t-1), \delta t]$) can be calculated by

$$\lambda_u^t = \psi_u \cdot \int_{\delta(t-1)}^{\delta t} \frac{1}{\sqrt{2\pi}\sigma_u} \cdot \exp\left(-\frac{(\tau - \mu_u)^2}{2\sigma_u^2}\right) d\tau, \quad (12)$$

where ψ_u, μ_u, and σ_u are characteristic parameters of station u, and the values of them are shown in Table 1. Here, we give an example of how to calculate. If we let $\delta = 180$ s, the passenger demand of station 1 at the first time interval (i.e., time period $(0, 180]$) will be 443 passengers, which can be obtained by the formula above with the value of ψ_u, μ_u, and σ_u ($\psi_u = 19800$, $\mu_u = 1680$, and $\sigma_u = 2700$) in Table 1.

Another important parameter related to demand, passenger destination probability ρ_{uv}, is depicted in Table 2. As we can see, 10% of the passengers enter the urban rail transit system from station 3 and then travel to station 1.

Other necessary parameters used in the simulation model and GA are summarized in Table 3. P_c and P_m denote the crossover and mutation rate, respectively.

All experiments in this paper are tested on a personal computer with an Inter Celeron G1620 2.7 GHz and 2 GB RAM. The simulation-based optimization model is coded in MATLAB 7.11.

Table 1: Value of demand related parameters.

	u						
	1	2	3	4	5	6	7
ψ_u	19800	18000	12600	3000	18000	15600	10200
μ_u	1680	1680	1800	900	1800	2100	1800
σ_u	2700	2700	2100	4200	3300	3600	3600

Table 2: Passenger destination probability ρ_{uv}.

From		To v						
		1	2	3	4	5	6	7
u	1	—	0.05	0.05	0.05	0.2	0.4	0.25
	2	0.05	—	0.05	0.1	0.2	0.3	0.3
	3	0.1	0.05	—	0.05	0.1	0.35	0.35
	4	0.05	0.1	0.05	—	0.25	0.2	0.35
	5	0.1	0.1	0.05	0.05	—	0.3	0.4
	6	0.05	0.05	0.05	0.05	0.4	—	0.4
	7	0.2	0.2	0.05	0.15	0.2	0.2	—

5.2. Optimization Results with Different Time Intervals. In this section, we solve the optimization problem with different time intervals, namely, $\delta = 5$ s, 10 s, and 30 s. The optimization process of GA is shown in Figure 13, and the comparison between different optimal results is shown in Table 4. Several conclusions are put forward here.

(1) The objective value is obtained using numerical calculation of the operation cost and passenger waiting cost in the system. By optimizing the objective, the scheduled timetable makes a balance between operators and passengers. Figure 13 shows that the proposed two-stage GA in this paper is convergent and the optimal objective can be obtained before 70 generations.

(2) The objective value C and the CPU time are different with different time intervals. And the shorter the time interval δ is, the better the objective value can be obtained and the longer the CPU time will be needed. As shown in Table 4, the best found value 15503.92 USD is obtained with the minimum time interval ($\delta = 5$ s) with the longest CPU time 5834.57 s. Table 5 gives the departure time of trains at the start terminal with the best found value.

(3) In order to show the superiority of the model, the optimal results are also compared with the best even-headway timetable (shown in Table 4). The results show that the proposed optimization model can not only reduce passenger waiting cost but also reduce operational cost, and the total cost of the transportation system has been reduced by almost 15%, which clearly demonstrates the effectiveness of the proposed optimization model. The main reason of this result is that, comparing with even-headway timetable, the proposed optimization model is more flexible that it can adjust the departure time of each train, and the headways between any two consecutive departures vary more appropriately based

Table 3: Parameters used in numerical example.

Parameters	K	H_{max}	H_{min}	CT	φ	η	α	β	*Pop-size*	*Pool-size*	Max-generation	P_c	P_m
Value	40	15 min	120 s	1680	640 USD/h	1 USD/h	1	1	40	260	Up to 70	0.9	0.2

Table 4: Comparison between different optimal results.

δ (s)	C^w (USD)	C^o (USD)	C (USD)	CPU (s)
$\delta = 5$	2810.59	12693.33	15503.92 (85.2%)	5834.57
$\delta = 10$	2841.84	12693.33	15535.17 (85.4%)	2768.51
$\delta = 30$	3136.25	12693.33	15829.58 (87.0%)	929.09
Even-headway	3259.35	14933.33	18192.69 (100%)	281.36

Table 5: Best solution: departure times of trains at the start terminal.

Train	Departure time
1	7:04:55
2	7:09:30
3	7:14:20
4	7:18:20
5	7:21:40
6	7:25:10
7	7:29:10
8	7:33:10
9	7:37:10
10	7:41:30
11	7:47:30
12	7:51:30
13	7:56:35
14	8:02:25
15	8:08:50
16	8:16:45
17	8:30:00

on the time-varying demand. As we can see in Table 5, the headways in the optimal timetable range from 200 s to 795 s.

5.3. Analysis of the Impact of Station Capacity. Station capacity is an important constraint in our model. In order to analyze the impact of station capacity CS_u, sensitivity analysis is conducted with $\delta = 30$ s against $CS_u = 1000, 1100, \ldots, 1700, 1800$. The results are shown in Figure 14.

As we can see, when $CS_u \leq 1400$ pax, a decreasing trend in system cost can be observed with the growth of station capacity. The total system cost improved from 29777.60 USD to 15837.34 USD when the capacities of stations increase from 1000 pax to 1400 pax. When $CS_u > 1400$ pax, however, the system cost remains at a relatively stable value (about 15854 USD). This is mainly because the larger the station capacity is, the fewer the passengers will need to wait outside station and the less the outside waiting time a passenger will have. Also, fewer trains used to quicken the decreasing of the number of waiting passengers at platform are needed. Just as shown in Figure 14, the operational cost decreases nearly monotonically from 17920.00 USD to 12693.33 USD (i.e., the number of departure trains decreases from 24 to 17) with the increase of station capacity. Then, the system cost will decrease. However, when a particular value ($CS_u = 1400$ pax in this example) is reached, the total waiting time of passenger outside station will become rather small, which is difficult to have influence on the optimal result. Thus, the system cost will not change evidently.

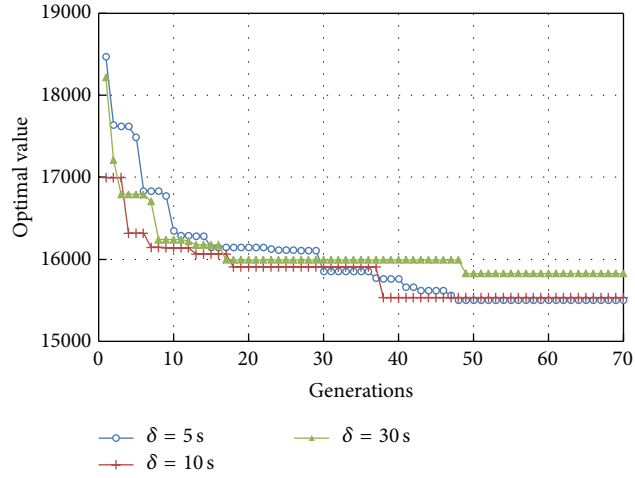

Figure 13: Optimization process of GA.

These results indicate that a limited station capacity will have a great influence on the service quality and operation plan of urban rail transit. And the smaller the station capacity is the higher system cost will be. However, on the other side, a too large capacity for a station will contribute little to the improving of transportation system but may bring a high infrastructure cost. Therefore, it is necessary to preestimate the system cost in the operation stage before building the station.

6. Conclusions

In this paper, we present a scheduling approach for a heavily congested urban rail line. It aims to create an efficient timetable with minimal passenger waiting cost and operational cost. In order to evaluate the performance of the created timetable, a simulation model is proposed with strict constraints on train and station capacities. Then, based on the simulation results, a two-stage GA is designed to find the best timetable. Finally, the feasibility of the solution method is demonstrated through a numerical example.

Although only a small case is discussed in this paper, it is shown that the strict constraint of station capacity is essential for TDP; the timetable designed by the proposed model will have a better balance between passengers and operators.

In addition, the passenger demand in our work is assumed to be steady. However, in real work, timetables will

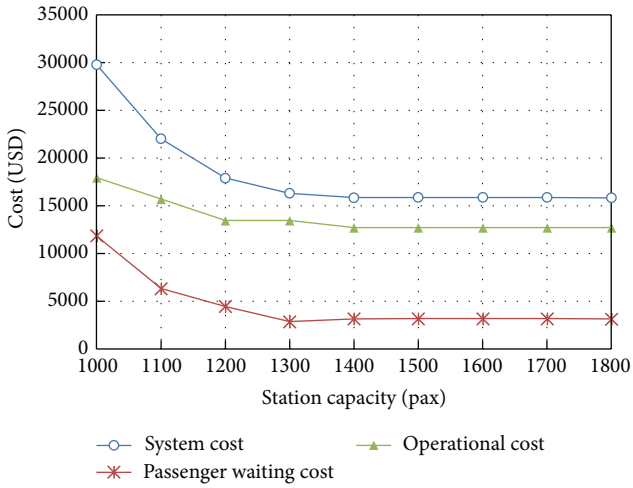

FIGURE 14: Optimal values with different station capacities.

have a feedback on the distribution of passenger demand. In our future research, we will try to create a new timetable considering this feedback.

Conflict of Interests

The authors declare that there is no conflict of interests regarding the publication of this paper.

Acknowledgments

This research was funded by the Nation Basic Research Program of China (no. 2012CB725406) and the National Natural Science Foundation of China (nos. 71131001 and 71201007). The authors also thank the anonymous reviewers and the editor for their suggestions to improve this paper.

References

[1] Research Group of Annual Report of China Urban Mass Transit, *2013 Annual Report of China Urban Mass Transit*, Beijing Jiaotong University Press, Beijing, China, 2014.

[2] X. Feng, B. Mao, X. Feng, and J. Feng, "Study on the maximum operation speeds of metro trains for energy saving as well as transport efficiency improvement," *Energy*, vol. 36, no. 11, pp. 6577–6582, 2011.

[3] X. Feng, H. Liu, H. Zhang, B. Wang, and Q. Sun, "Rational formations of a metro train improve its efficiencies of both traction energy utilization and passenger transport," *Mathematical Problems in Engineering*, vol. 2013, Article ID 643274, 7 pages, 2013.

[4] L. Sun, J. G. Jin, D.-H. Lee, K. W. Axhausen, and A. Erath, "Demand-driven timetable design for metro services," *Transportation Research Part C: Emerging Technologies*, vol. 46, pp. 284–299, 2014.

[5] L. Kang, J. Wu, H. Sun, X. Zhu, and B. Wang, "A practical model for last train rescheduling with train delay in urban railway transit networks," *Omega*, vol. 50, pp. 29–42, 2015.

[6] I. Amit and D. Goldfarb, "The timetable problem for railways," *Developments in Operations Research*, vol. 2, pp. 379–387, 1971.

[7] M. Carey and I. Crawford, "Scheduling trains on a network of busy complex stations," *Transportation Research Part B: Methodological*, vol. 41, no. 2, pp. 159–178, 2007.

[8] E. Castillo, I. Gallego, J. M. Ureña, and J. M. Coronado, "Timetabling optimization of a single railway track line with sensitivity analysis," *TOP*, vol. 17, no. 2, pp. 256–287, 2009.

[9] E. Castillo, I. Gallego, J. M. Ureña, and J. M. Coronado, "Timetabling optimization of a mixed double- and single-tracked railway network," *Applied Mathematical Modelling*, vol. 35, no. 2, pp. 859–878, 2011.

[10] E. Castillo, I. Gallego, S. Sánchez-Cambronero et al., "An alternate double-single track proposal for high-speed peripheral railway lines," *Computer-Aided Civil and Infrastructure Engineering*, vol. 30, no. 3, pp. 181–201, 2015.

[11] J. E. Cury, F. A. C. Gomide, and M. J. Mendes, "A methodology for generation of optimal schedules for an underground railway system," *IEEE Transactions on Automatic Control*, vol. 25, no. 2, pp. 217–222, 1980.

[12] P. G. Furth and N. H. M. Wilson, "Setting frequencies on bus routes: theory and practice," *Transportation Research Record*, vol. 818, pp. 1–7, 1981.

[13] Y. Wang, B. de Schutter, T. van den Boom, B. Ning, and T. Tang, "Real-time scheduling for single lines in urban rail transit systems," in *Proceedings of the IEEE International Conference on Intelligent Rail Transportation (ICIRT '13)*, pp. 1–6, Beijing, China, September 2013.

[14] E. Barrena, D. Canca, L. C. Coelho, and G. Laporte, "Single-line rail rapid transit timetabling under dynamic passenger demand," *Transportation Research Part B: Methodological*, vol. 70, pp. 134–150, 2014.

[15] A. de Palma and R. Lindsey, "Optimal timetables for public transportation," *Transportation Research Part B: Methodological*, vol. 35, no. 8, pp. 789–813, 2001.

[16] A. Caprara, M. Fischetti, and P. Toth, "Modeling and solving the train timetabling problem," *Operations Research*, vol. 50, no. 5, pp. 851–861, 2002.

[17] C. Liebchen, "The first optimized railway timetable in practice," *Transportation Science*, vol. 42, no. 4, pp. 420–435, 2008.

[18] R. C. W. Wong, T. W. Y. Yuen, K. W. Fung, and J. M. Y. Leung, "Optimizing timetable synchronization for rail mass transit," *Transportation Science*, vol. 42, no. 1, pp. 57–69, 2008.

[19] D. T. Aksu and U. Akyol, "Transit coordination using integer-ratio headways," *IEEE Intelligent Transportation Systems Magazine*, vol. 15, no. 4, pp. 1633–1642, 2014.

[20] A. Ceder, "Bus frequency determination using passenger count data," *Transportation Research Part A: General*, vol. 18, no. 5-6, pp. 439–453, 1984.

[21] A. Ceder, "Bus timetables with even passenger loads as opposed to even headways," *Transportation Research Record*, vol. 1760, no. 1, pp. 3–9, 2001.

[22] A. Ceder, *Public Transit Planning and Operation: Theory, Modeling and Practice*, Butterworth-Heinemann, 2007.

[23] H. N. Koutsopoulos, A. Odoni, and N. H. M. Wilson, "Determination of headways as a function of time varying characteristics on a transit network," in *Computer Scheduling of Public Transport*, vol. 2, pp. 391–413, 1985.

[24] H. Niu and X. Zhou, "Optimizing urban rail timetable under time-dependent demand and oversaturated conditions," *Transportation Research Part C: Emerging Technologies*, vol. 36, pp. 212–230, 2013.

[25] T. Albrecht, "Automated timetable design for demand-oriented service on suburban railways," *Public Transport*, vol. 1, no. 1, pp. 5–20, 2009.

[26] Q. Chen, "Global optimization for bus line timetable setting problem," *Discrete Dynamics in Nature and Society*, vol. 2014, Article ID 636937, 9 pages, 2014.

[27] E. Hassannayebi, A. Sajedinejad, and S. Mardani, "Urban rail transit planning using a two-stage simulation-based optimization approach," *Simulation Modelling Practice and Theory*, vol. 49, pp. 151–166, 2014.

[28] X.-M. Chen, Q.-X. Liu, and G. Du, "Estimation of travel time values for urban public transport passengers based on SP survey," *Journal of Transportation Systems Engineering and Information Technology*, vol. 11, no. 4, pp. 77–84, 2011.

[29] O. J. Ibarra-Rojas and Y. A. Rios-Solis, "Synchronization of bus timetabling," *Transportation Research Part B: Methodological*, vol. 46, no. 5, pp. 599–614, 2012.

[30] J. H. Holland, *Adaptation in Natural and Artificial Systems*, University of Michigan Press, Ann Arbor, Mich, USA, 1975.

[31] M. Gen and R. W. Cheng, *Genetic Algorithms and Engineering Optimization*, John Wiley & Sons, 2000.

Hindawi Publishing Corporation
Discrete Dynamics in Nature and Society
Volume 2015, Article ID 284906, 11 pages
http://dx.doi.org/10.1155/2015/284906

Research Article

Big Data-Driven Based Real-Time Traffic Flow State Identification and Prediction

Hua-pu Lu, Zhi-yuan Sun, and Wen-cong Qu

Institute of Transportation Engineering, Tsinghua University, Beijing 100084, China

Correspondence should be addressed to Zhi-yuan Sun; sun-zy12@mails.tsinghua.edu.cn

Received 17 July 2014; Accepted 11 September 2014

Academic Editor: Wei Guan

With the rapid development of urban informatization, the era of big data is coming. To satisfy the demand of traffic congestion early warning, this paper studies the method of real-time traffic flow state identification and prediction based on big data-driven theory. Traffic big data holds several characteristics, such as temporal correlation, spatial correlation, historical correlation, and multistate. Traffic flow state quantification, the basis of traffic flow state identification, is achieved by a SAGA-FCM (simulated annealing genetic algorithm based fuzzy *c*-means) based traffic clustering model. Considering simple calculation and predictive accuracy, a bilevel optimization model for regional traffic flow correlation analysis is established to predict traffic flow parameters based on temporal-spatial-historical correlation. A two-stage model for correction coefficients optimization is put forward to simplify the bilevel optimization model. The first stage model is built to calculate the number of temporal-spatial-historical correlation variables. The second stage model is present to calculate basic model formulation of regional traffic flow correlation. A case study based on a real-world road network in Beijing, China, is implemented to test the efficiency and applicability of the proposed modeling and computing methods.

1. Introduction

Real-time traffic flow state identification and prediction is one of the critical components of intelligent transportation system. It is of practical significance to identify and predict traffic flow state quickly, precisely and timely. As the first problem that needs to be solved, traffic flow state can be measured by level of service (LOS), which is first introduced in the 1965 Highway Capacity Manual (HCM 1965) [1]. The latest version of Highway Capacity Manual (HCM 2010) [2] divided LOS into six levels. Sasaki and Iida [3] divided LOS into three levels. China GB 50220-1995 [4] divided LOS into four levels. Existing studies of LOS evaluation can be classified into four categories in transportation literature: subjective evaluation based models [5], statistical analysis based models [6], artificial intelligence based models [7], traffic flow theory based models [8, 9].

Many previous research works concerning traffic flow state identification especially for Beijing have been carried out. Guan and He [10] analyzed the statistical features of speed distribution at different density and divided traffic flow state into four levels based on flow-rate-density plane. Liao et al. [11] studied traffic state identification based on perceptual experiment. Xia et al. [12] built traffic state rapid identification model based on fuzzy theory. Qu et al. [13] determined the relation between traffic state and travel speed. Moreover, Beijing Traffic Management Bureau built Beijing Regional Traffic Conditions and LOS Evaluation System mainly based on fixed detectors [14], and Beijing Municipal Commission of Transport built Traffic Performance Index System mainly based on floating car data [15].

Real-time traffic flow prediction aims at evaluating anticipated traffic flow state at a future time. Many studies focused on traffic flow state and parameters prediction. Liu et al. [16] analyzed multidimensional parameters and developed the traffic prediction models of different dimensions based on the support vector machine. Dong et al. [17] proposed a preselection space time model to estimate the traffic condition at poor-data-detector, especially nondetector locations. Canaud et al. [18] presented a probability hypothesis density filtering based model for real-time traffic flow state prediction. Pan et al. [19] put forward a modified stochastic

cell transmission model to support short-term traffic flow state prediction. Antoniou et al. [20] proposed an approach for local traffic flow state estimation and prediction based on data-driven computational approaches. Zhang et al. [21] designed a traffic flow state estimator based on extended-Kalman-filter method.

Traffic big data, massive and multisource, brings both opportunities and challenges to effective traffic management and control. During data processing, traffic big data meets the same difficulties with the general big data, such as capture, storage, search, sharing, analytics, and visualization. The differences between traffic big data and traditional data in the field of traffic flow state identification and prediction are obvious. For traffic flow state identification, the advantage of traffic big data is mainly manifested in the full coverage. That is, traffic big data can represent traffic flow characteristics as much as possible. However, the difficulties of data processing are enhanced with the increasing of the size of data. Therefore, big data-driven methods should have a stronger capacity of data processing. For traffic flow state prediction, the advantage of traffic big data is mainly manifested in the multisource. That is, the traffic big data has a higher accuracy to describe the relationships between traffic flow state of section s at time t and the others. However, the relationships are not easy to be found. So, big data-driven methods should have a clearer description of physical significance of traffic flow. Traffic big data can improve the efficiency of real-time traffic flow state identification and prediction. However, it may face more challenges.

Taking into account all the present researches in this field, there is still a lack of consideration of traffic big data. Further researches remain to be conducted on the direction of traffic flow state analysis. In this paper, the method of real-time traffic flow state identification and prediction, which perceives ability to handle big data, is put forward in detail. The remainder of this paper is organized as follows. Section 2 presents the basic characteristics of traffic big data. In Section 3, the methodology of real-time traffic flow state identification and prediction is proposed. A case study based on a real-world road network is carried out in Section 4 to demonstrate the performance and applicability of the proposed method. Finally, conclusions are drowned in Section 5.

2. Traffic Big Data Analysis

2.1. Temporal Correlation. By laying fixed and mobile traffic flow detectors, dynamic traffic data of a section can be obtained. Dynamic traffic flow data V are time-series data, which continuously change over time t with a certain trend; namely,

$$V_t = T\left(V_{t-1}, V_{t-2}, \ldots\right), \tag{1}$$

where V_t is the traffic flow parameter at time t, representing flow q_t, speed v_t, or occupancy ρ_t. T is a function that describes trends of traffic flow time-series data.

2.2. Spatial Correlation. A regional transportation network consists of multiple intersections and roads. It exists a spatial association between traffic flow data of neighboring junctions or sections and that of target junctions or sections; namely,

$$V_{s,t} = S\left(V_{1,t}, V_{2,t}, \ldots\right), \tag{2}$$

where $V_{s,t}$ is the traffic flow parameter of section s at time t, representing flow $q_{s,t}$, speed $v_{s,t}$, or occupancy $\rho_{s,t}$. S defines the relationship between the data of upstream and downstream sections.

2.3. Historical Correlation. For different weekdays or weekends, trip distribution of inhabitants in the same period shows similar characteristics. The law of traffic flow cycle is especially evident. Correlation between dynamic traffic flow data and historical data is as follows:

$$V_{D,t} = H\left(V_{D-1,t}, V_{D-2,t}, \ldots\right), \tag{3}$$

where $V_{D,t}$ is the traffic flow parameter on day D at time t, representing flow $q_{D,t}$, speed $v_{D,t}$, or occupancy $\rho_{D,t}$. H defines the relationship between the data of different workdays or holidays at the same time.

2.4. Multistate. Traffic flow state can be determined by the traffic flow parameters. The correspondence between traffic flow states and traffic flow parameters is as follows:

$$A = \mathrm{MS}\left(v, q, \rho\right), \tag{4}$$

where A is LOS. v, q, and ρ are the traffic flow parameters. MS defines the relationship between traffic flow states and traffic flow parameters.

3. Methodology

3.1. Overall Framework. The overall traffic flow state identification and prediction framework is outlined in Figure 1.

(a) SAGA-FCM Based Traffic Clustering Model. As a random social phenomenon, traffic flow state holds fuzzy characteristics. For example, "congested" and "uncongested" are the fuzzy descriptions of traffic flow. It is difficult to describe these states quantitatively. Since membership function can be used to explain the fuzzy phenomenon, fuzzy c-means algorithm (FCM) is designed to evaluate traffic flow state [22]. However, FCM is sensitive to its initial clustering center and it is easy to fall into the local optimum, especially for big data [23]. SAGA-FCM algorithm integrates the strong local search ability of simulated annealing algorithm (SA) and the strong global search ability of genetic algorithm (GA) to overcome the drawbacks of traditional FCM algorithm [24].

(b) DFT Based Historical Data Fusion Model. Road traffic flow state information is periodic [25]. Each object to predict can be associated with a set of historical data. Actual intelligent traffic system has accumulated massive historical data. However, it is difficult to achieve the integration of historical data. During the on-going development of traffic prediction

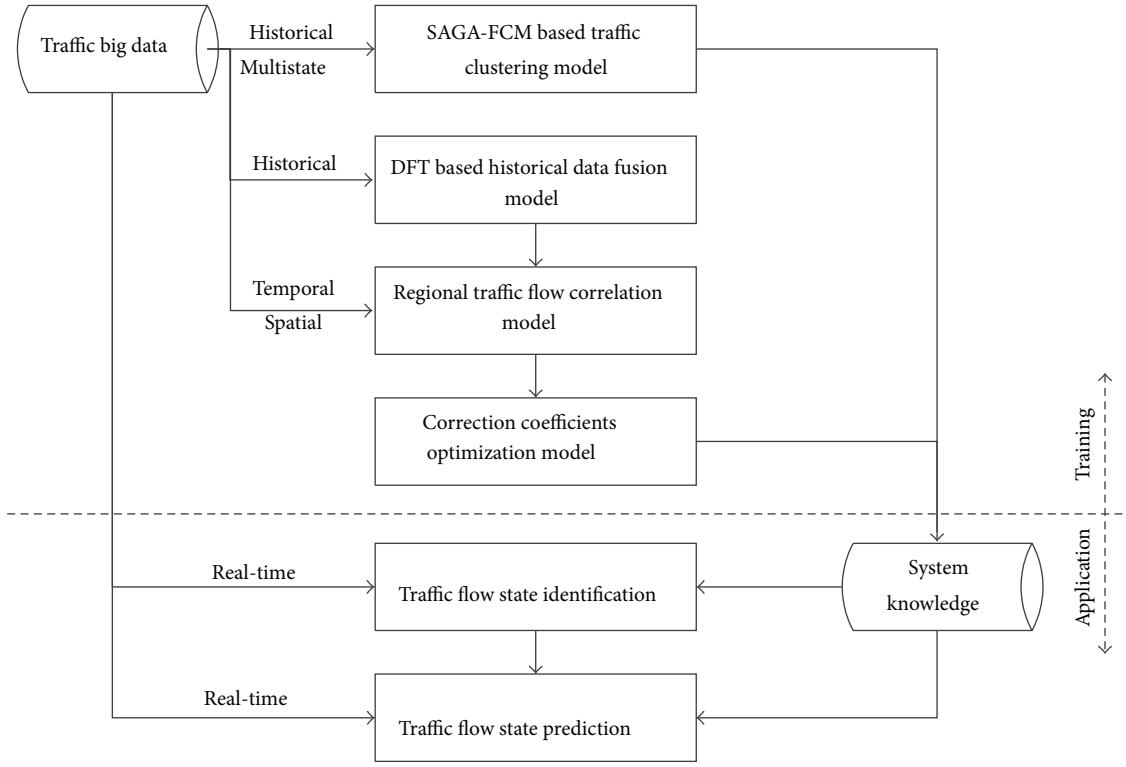

Figure 1: Overall traffic flow state identification and prediction framework.

system in Beijing, discrete Fourier transform (DFT) is found effective in achieving the average of historical data and noise elimination [26]. Traffic parameters are discrete time series sequence; therefore DTF is applied to integrate massive historical data [27].

(c) Regional Traffic Flow Correlation Model. Temporal correlation, spatial correlation and historical correlation are the characteristics of traffic big data. Based on this principle, regional traffic flow correlation model can be established to predict traffic flow parameters. Taking simple calculation and predictive accuracy into consideration, a bi-level optimization model is proposed to simplify the regional traffic flow correlation model.

(d) Correction Coefficients Optimization Model. Considering the amount of temporal, spatial, and historical variables, each of which corresponds to an unknown parameter, the model is too difficult to calibrate. Therefore, a two-stage model for correction coefficients optimization is put forward to reduce the number of variables and ensure accuracy simultaneously.

3.2. SAGA-FCM Based Traffic Clustering Model

3.2.1. Basic Traffic Clustering Model. Based on HCM 2010 [2], LOS (A) can be divided into six types, as $A = [A_1, A_2, \ldots, A_6]$. Considering the monotonicity between traffic flow parameters and LOS, speed (v) and occupancy (ρ) are chosen as clustering parameters. Therefore, data sample used for traffic clustering model can be written as $X = \{x_1, x_2, \ldots, x_n\}$, $x_j = (v_j, \rho_j)$. Since traditional FCM algorithm is put forward to find an optimal classification, the objective function is expressed as

$$\begin{aligned} \min \quad & J_b(U, a) = \sum_{i=1}^{6}\sum_{j=1}^{n}\left(\mu_{ij}\right)^b\left(d_{ij}\right)^2 \\ \text{s.t.} \quad & \sum_{i=1}^{6}\mu_{ij} = 1, \quad 0 \le \mu_{ij} \le 1 \\ & i = 1, 2, \ldots, 6, \quad j = 1, 2, \ldots, n, \end{aligned} \tag{5}$$

where U is membership matrix, $U = [\mu_i(x_j)]_{6\times n}$. a is the set of clustering centers, $a = \{a_1, a_2, \ldots, a_6\}$, $a_i = (v_i, \rho_i)$. d_{ij} is the Euclidean distance that measures distance between data sample (x_j) and clustering center (a_i), $d_{ij} = d(x_j - a_i) = \|x_j - a_i\|$. b is weighted parameter, $b \in [1, +\infty)$. $\mu_i(x_j)$ is the degree of membership of which the sample data x_j belongs to LOS A_i, shorten for μ_{ij}.

a_i can be calculated by the flowing formulation

$$\begin{aligned} & a_i = \frac{\sum_{j=1}^{n}\left(\mu_{ij}\right)^b x_j}{\sum_{j=1}^{n}\left(\mu_{ij}\right)^b}, \\ & \text{s.t.} \quad \sum_{i=1}^{6}\mu_{ij} = 1, \quad 0 \le \mu_{ij} \le 1, \ 0 \le \sum_{j=1}^{n}\mu_{ij} \le 1 \\ & \qquad i = 1, 2, \ldots, 6, \quad j = 1, 2, \ldots, n. \end{aligned} \tag{6}$$

μ_{ij} can be calculated by the flowing formulation

$$\mu_{ij} = \begin{cases} \dfrac{1}{\sum_{k=1}^{6} \left(d_{ij}/d_{kj}\right)^{2/(b-1)}}, & d_{ij} > 0, \\ 1, & d_{ij} = 0,\ i = j, \\ 0, & d_{ij} = 0,\ i \neq j. \end{cases} \tag{7}$$

Modification of the clustering centers and degrees of membership is the core of FCM. When the algorithm is convergent, clustering centers a_i can be found, and degrees of membership μ_{ij} can be calculated. Therefore, fuzzy clustering result can be achieved.

3.2.2. SAGA-FCM Based Solution Algorithm. SAGA-FCM algorithm is used to improve the clustering quality of FCM. The process of SAGA-FCM algorithm can be summarized as in the following steps [28].

Step 1 (parameters initialization). Population size (*sizepop*), maximum genetic evolution algebra (*MAXGEN*), crossing probability (P_c), gene variation probability (P_m), original temperature (T_0), cooling coefficient (l), and final temperature (T_{end}).

Step 2 (clustering centers initialization). Randomly selecting six clustering centers (a), designing the original sequence (*chrom*), calculating degrees of membership (μ_{ij}), and fitness value of each individual (f_i).

Step 3 (genetic evolution algebra initialization). $gen = 0$.

Step 4 (genetic operations). Selection, crossover, and mutation of original sequence (*chrom*), achieving new clustering centers (a), calculating degrees of membership (μ'_{ij}), and fitness value of each individual (f'_i).

Step 5 (fitness value judgment). If $f'_i > f_i$, replace all of the old individual with the new individual; otherwise, replace the old individual with the new individual by probability ($P = \exp(f_i - f'_i)T$).

Step 6 (*MAXGEN* judgment). If $gen < MAXGEN$, $gen = gen + 1$, turn to Step 4; otherwise, turn to Step 7.

Step 7 (temperature judgment). If $T_i < T_{\text{end}}$, the new solution is outputted, and that is the most optimized assembly sequence; otherwise, $T_{i+1} = lT_i$, turning to Step 3.

3.2.3. Calculation of LOS. Based on SAGA-FCM algorithm, six clustering centers (a) can be found. Thus, μ_{ij} is calculated by formulation (7). Combining the numerical magnitude of μ_{ij}, the LOS of $x_j(A(x_j))$ is achieved:

$$\begin{aligned} &A\left(x_j\right) = A_k \\ &\text{s.t.} \quad \mu_{kj} > \mu_{ij}, \quad k \neq i, \end{aligned} \tag{8}$$

where $A(x_j)$ is the LOS of x_j.

3.3. DFT Based Historical Data Fusion Model. Given a discrete temporal series $\{x(0), x(1), \ldots, x(N-1)\}$, the length of which is N, its discrete Fourier transform with M sampling points can be calculated:

$$X(k) = \frac{1}{N} \times \sum_{n=0}^{N-1} x(n) \times e^{-j(2k\pi/N)n}, \quad (k = 0, 1, \ldots, M-1). \tag{9}$$

The corresponding inverse Fourier transform formulation is

$$x(n) = \sum_{k=0}^{M-1} X(k) \times e^{j(2k\pi/N)n}, \quad (k = 0, 1, \ldots, M-1). \tag{10}$$

Normally, take $M = N$. To facilitate the program, the natural logarithm complex power form above is converted to trigonometric form:

$$\begin{aligned} x(i) = a_0 + \sum_{f=1}^{N-1} &\left(\alpha_n \cos\left(\frac{2\pi}{N} f_i\right) + \beta_n \sin\left(\frac{2\pi}{N} f_i\right)\right) \\ &\times \left(f_i = e^{j(2k\pi/N)i} \ \ (i = 0, 1, \ldots, N-1)\right). \end{aligned} \tag{11}$$

Suppose that the traffic flow varies in one week cycle, which includes 7 days with different characteristics. Each day contains 288 pieces of data with a time interval of 5 minutes. Apply DFT to average massive historical data and to eliminate noise, so as to achieve the integration of historical data. Consider

$$V_D^H = \left\{V_{D,1}^H, \ldots, V_{D,t}^H, \ldots, V_{D,288}^H\right\}, \tag{12}$$

where V_D^H is the collection of historical data on day D, $D = [1, 2, \ldots, 7]$. $V_{D,t}^H$ is the traffic data on day D at time t, $V_{D,t}^H = [q_{D,t}^H, v_{D,t}^H, \rho_{D,t}^H]^T$, $t = [1, 2, \ldots, 288]$.

For example, the process of DFT of traffic volume (q) can be summarized as in the following steps.

Step 1. Enter the discrete temporal series $\{q(0), q(1), \ldots, q(287)\}$.

Step 2. Apply DFT and acquire Fourier coefficients sequence $\{\alpha_1, \beta_1, \alpha_2, \beta_2, \ldots, \alpha_{287}, \beta_{287}\}$.

Step 3. Filter Fourier coefficients series to excise all coefficients less than the specified amplitude threshold of coefficient. Record the rest of the coefficients. The value of the threshold needs to be chosen by analyzing the historical data.

Step 4. Restore data at any point in the sequence $q(i)$.

3.4. Regional Traffic Flow Correlation Model

3.4.1. Basic Model Formulation. The basic assumption of the regional traffic flow correlation model is that traffic flow has a strong temporal-spatial-historical correlation, namely:

(i) in the temporal series, the traffic flow of the last moment can be regarded as the continuation of the current traffic flow;

(ii) in the spatial series, downstream sections of the traffic flow can be seen as a continuation of the upstream traffic flow;

(iii) in the historical series, traffic demand characteristics determine that traffic flow characteristics of the same day in the same period are similar.

Basic form of regional traffic flow correlation model is expressed as

$$\begin{aligned} &V_s(t) = \gamma_T V_T(t) + \gamma_S V_S(t) + \gamma_H V_H(t) \\ &\text{s.t.} \quad \gamma_T + \gamma_S + \gamma_H = 1, \quad \gamma_T, \gamma_S, \gamma_H \geq 0, \end{aligned} \tag{13}$$

where $V_s(t)$ is the traffic flow parameter of section s at time t, representing flow $q_s(t)$, speed $v_s(t)$, or occupancy $\rho_s(t)$. $V_T(t)$, $V_S(t)$, and $V_H(t)$ are the estimated value of $V_s(t)$. $V_T(t)$ is calculated by temporal correlation analysis. $V_S(t)$ is calculated by spatial correlation analysis. $V_H(t)$ is calculated by historical correlation analysis. γ_T, γ_S, and γ_H are coefficients of these three variables.

According to formulation (1), T is generally achieved by regression analysis model. Thus, $V_T(t)$ is created by the following equation:

$$\begin{aligned} &V_T(t) = \theta_1 V_s(t-1) + \theta_2 V_s(t-2) + \cdots \\ &\text{s.t.} \quad \sum \theta = 1, \quad \theta \geq 0, \end{aligned} \tag{14}$$

where $V_s(t-d)$ is the traffic flow parameter of section s at time $t-d$. d is time delay, $d \geq 0$. $\theta_1, \theta_2, \ldots$ are regression coefficients.

According to formulation (2), S is generally achieved by neighbor regression model. Thus, $V_S(t)$ is created by the following equation:

$$\begin{aligned} &V_S(t) = \lambda_1 V_1(t-1) + \lambda_2 V_2(t-2) + \cdots \\ &\text{s.t.} \quad \sum \lambda = 1, \quad \lambda \geq 0, \end{aligned} \tag{15}$$

where $V_j(t-d)$ is the traffic flow parameter of section j at time $t-d$. $\lambda_1, \lambda_2, \ldots$ are regression coefficients.

According to formulations (12), (13), (14), and (15), simplified equation is achieved:

$$\begin{aligned} &V_s(t) = \sum \sum \omega_{jd} V_j(t-d) \\ &\text{s.t.} \quad \sum \omega = 1, \quad \omega > 0, \ \eta \in N^*, \end{aligned} \tag{16}$$

where ω_{jd} is regression coefficient of $V_j(t-d)$. η is the number of ω_{jd}.

3.4.2. Effectiveness Proof of Proposed Formulation. The general form of formula (16) is

$$\begin{aligned} &Y = \sum_{i=1}^{n} w_i Y_i \\ &\text{s.t.} \quad \sum_{i=1}^{n} w_i = 1, \quad w_i \geq 0, \end{aligned} \tag{17}$$

where Y is the state of physical system with the measurement of multisensors. Y_i is the measured value of ith sensor, and they are independent. w_i is a weighting factor.

The total mean square error δ^2 is a multivariate quadratic function of w_i:

$$\delta^2 = \sum_{i=1}^{n} {w_i}^2 \delta_i^2, \tag{18}$$

where δ_i is the mean square error of Y_i.

According to extreme value theorem of multivariate quadratic function, weighting factor can be calculated as follows:

$$w_i = \frac{1}{{\delta_i}^2 \sum_{i=1}^{n} \left(1/\delta_i^2\right)}. \tag{19}$$

Assume that the detection accuracy varies with sensors, the mean square error of the measurements from the least accurate sensor is $\delta_{\min}^2$ and that from the most accurate sensor is $\delta_{\max}^2$. Then,

$$\begin{aligned} \text{esp}[Y] &= \left[\frac{1}{\delta_{\max}^2} + \frac{1}{\delta_{\min}^2} + \sum_{i=1}^{n-2} \frac{1}{\delta_i^2} \right]^{-1} \\ &< \left[\frac{1}{\delta_{\min}^2} + \sum_{i=1}^{n-2} \frac{1}{\delta_i^2} \right]^{-1} < \delta_{\min}^2. \end{aligned} \tag{20}$$

The formula above shows that the measurement accuracy of the system can be improved by multisensor measurement and that participation of an inaccurate sensor also helps improve the accuracy of the system.

3.4.3. Bilevel Optimization Model. For big date-driven analysis, the speed and accuracy of data processing are both important. The number of unknown parameters in formulation (16) is large and uncontrolled. Therefore, taking simple calculation and predictive accuracy into consideration, a bilevel optimization model is proposed.

The upper level model is formulated to optimize the speed of date processing by minimizing the number of temporal-spatial-historical correlation variables. The upper level formulation is

$$\begin{aligned} &\min \quad \eta \\ &\text{s.t.} \quad \eta \in N^*. \end{aligned} \tag{21}$$

The lower level model is articulated in accordance with predictive accuracy. Therefore, the lower level formulation is proposed in order to minimize predictive encoding. The lower level formulation is

$$\begin{aligned} &\min \quad \left| V_s(t) - \widehat{V}_s(t) \right| \\ &\text{s.t.} \quad V_s(t) = \sum \sum \omega_{jd} V_j(t-d), \quad \sum \omega = 1, \ \omega \geq 0, \end{aligned} \tag{22}$$

where $\widehat{V}_s(t)$ is actual value of $V_s(t)$.

In the bilevel optimization model, the purpose of objective function is to achieve a best combination, which holds both fast calculation speed and high prediction accuracy.

3.5. Correction Coefficients Optimization Model. The more the temporal-spatial-historical correlation variables are, the slower the program calculates and the higher the accuracy is. The bilevel optimization model above is difficult to solve. To put it in another way, we can define a threshold of computing speed and therefore derive the maximum of acceptable number of temporal-spatial-historical correlation variables. In addition, we can put forward a new variable which can be calculated to replace the variable ω_{jd}. Since the alternative process will bring some errors, which are likely to be systematic, a linear correction method is put forward. Therefore, the correction coefficients optimization model is a two-stage model.

3.5.1. The First Stage Model. The first stage model is mainly used to determine the number of unknown parameters η. It can be determined through the following steps.

Step 1 (determination of the range of η). The number of unknown parameters should not exceed a threshold value. After several data tests, it is found that when η is less than 4, the correlation coefficients are not very different from relatively high values; when η is more than 8, the rapid decay of the correlation coefficients is observed with relatively low values. Therefore η ranges from $[4, 8]$.

Step 2 (calculation of the correlation coefficients). Calculate the correlation coefficients (r_{jd}) between the studied section s and the related section j, solve the max correlation coefficient (r_j) corresponding to each section j, and determine the corresponding time delay (d); namely, $r_j = \max r_{jd}$. r_{jd} can be solved by

$$r_{jd} = \left(\sum_{t=1}^{n-d} V_s(t) V_j(t-d) - \frac{1}{n-d} \sum_{t=1}^{n-d} V_s(t) \sum_{t=1}^{n-d} V_j(t-d) \right) \times \left(\left[\sum_{t=1}^{n-d} V_s^2(t) - \frac{1}{n-d} \left(\sum_{t=1}^{n-d} V_s(t) \right)^2 \right] \times \left[\sum_{t=1}^{n-d} V_j^2(t-d) - \frac{1}{n-d} \left(\sum_{t=1}^{n-d} V_j(t-d) \right)^2 \right] \right)^{-1/2}$$

$$\text{s.t} \quad d \geq 0. \tag{23}$$

Step 3 (selection of the relative section). Sort r_j in ascending order, and take the first η section as a range of temporal and spatial correlation.

3.5.2. The Second Stage Model. The second stage model is mainly used to reduce parameters and determines the base model. Through the first stage model, the number of unknown parameters is reduced. But the model is still difficult to solve and can be further simplified.

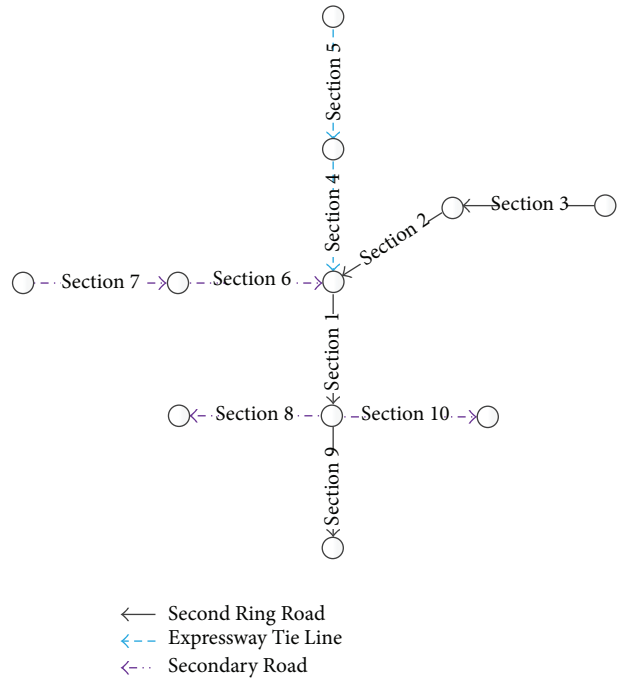

Figure 2: Spatial location of research object.

Step 1 (calculation of the normalization factor). Take normalized r_j as the parameters of $V_j(t-d)$:

$$\omega_j = \frac{r_j}{\sum_{j=1}^{\eta} r_j}, \quad \sum_{j=1}^{\eta} \omega_j = 1, \quad \omega_j > 0. \tag{24}$$

Step 2 (solving the system error). Introduce the correction parameters φ and ε to calibrate, in order to reduce the system error caused by parameter substitution:

$$\begin{aligned} &\min \quad \left| V_s(t) - \widehat{V}_s(t) \right| \\ &\text{s.t.} \quad V_s(t) = \varphi \sum_{j=1}^{\eta} \omega_j V_j(t-d) + \varepsilon. \end{aligned} \tag{25}$$

4. Case Study

4.1. Data Characteristics. Taking a section of the Second Ring Road (Section 1, as shown in Figure 2) and its surrounding roads in Beijing, China, as the object of study, it verifies the effectiveness and feasibility of the proposed method. Basic traffic flow data are detected by microwave detectors.

As shown in Figure 2, Section 1, Section 2, Section 3, and Section 9 are all Second Ring Road. Section 4 and Section 5 are Expressway Tie Line. Section 6, Section 7, Section 8, and Section 10 are Secondary Road. Section $2, 3, \ldots, 10$ are the temporal-spatial correlated sections of Section 1.

For traffic flow state identification, it needs enough data to divide LOS. The historical data of Section 1 (one week, five minutes for the interval) are used to build SAGA-FCM based traffic clustering model. The amount of data is large enough to represent nearly all the traffic flow characteristics.

Table 1: Clustering centers.

LOS	Speed (km/h)	Occupancy (%)
A	68.1	2.1
B	58.3	3.1
C	51.2	11.4
D	46.0	14.9
E	38.0	20.5
F	23.4	35.1

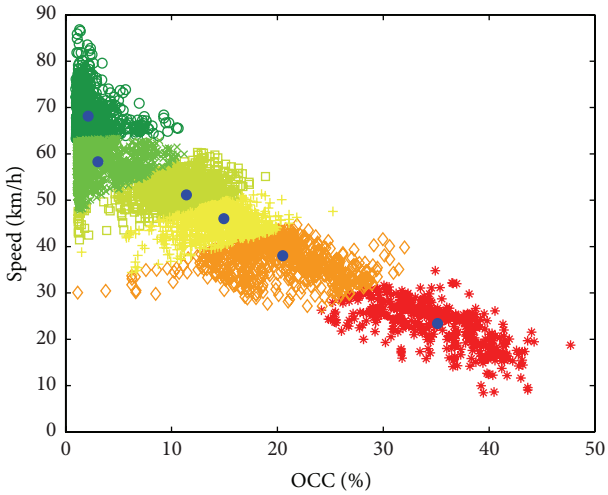

Figure 3: Traffic flow state evaluation result.

For traffic flow prediction, it needs enough data to describe the temporal-spatial-historical correlation characteristic, that is, to build correction coefficients optimization model. The historical data of Section 1 (one week, five minutes for the interval) are used for temporal-spatial correlation analysis. The historical data of Section $1, 2, \ldots, 10$ (one week, five minutes for the interval) are used for temporal-spatial-historical correlation analysis. The historical data of Section 1 (one month, five minutes for the interval) are used for historical correlation analysis.

4.2. Traffic Flow State Identification

4.2.1. Offline Training. The main task of offline training is to establish the evaluation method of traffic flow state. Case study of traffic flow state identification is done based on the two clustering methods (FCM and SAGA-FCM). The value of objective function calculated by SAGA-FCM is better than the one by FCM. Different traffic flow states are respected by different colors. As shown in Figure 3, traffic flow state is divided into six levels, as A to F. Clustering centers are shown in Table 1.

4.2.2. Online Application. The main task of online application is to realize traffic flow state identification. Traffic flow state identification result is shown in Figure 4.

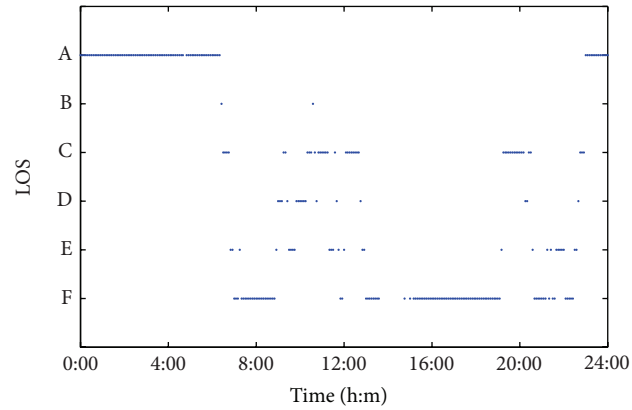

Figure 4: Traffic flow state identification.

Table 2: Temporal-spatial-historical correlation coefficients.

j	d (min)	r_{jd}	ω_j
9	0	0.9970	0.2677
1 (temporal correlation)	5	0.9797	0.2630
1 (historical correlation)	0	0.9167	0.2461
2	0	0.8312	0.2232

4.3. Traffic Flow State Prediction

4.3.1. Offline Training. The offline training mainly summarizes the prior knowledge based on historical data.

(1) Parameter Initialization. Choose 9 of the upstream and downstream sections of Section 1 based on their attributes and transport network characteristics. Let $\eta \in [4, 8]$.

(2) Search of Temporal-Spatial-Historical Correlative Sections. Calculate the correlation coefficient between Section 1 and its relative sections, time series data, and historical trend data. The top 6 of the calculation result are shown in Figure 5, where the abscissa is the time delay d and the vertical axis is the value of the correlation coefficient r_{jd}.

Compare r_{jd}, decide the value of corresponding d, and then get r_j. According to the distribution characteristics of r_j, let $\eta = 4$. The search results of temporal-spatial-historical correlative sections are Section 9, Section 1 (time series data), Section 1 (historical trend data), and Section 2.

Results of temporal-spatial-historical correlation coefficients are shown in Table 2.

(3) Calculation of Normalization Parameter. Calculate the normalization parameters ω_j, as shown in Table 2.

(4) Solving Correction Parameters. Apply regression analysis to solve correction parameters φ and ε:

$$v_1(t) = 1.029 \times \left[0.2677 \cdot v_9(t) + 0.2630 \cdot v_1(t-5) + 0.2461 \cdot v_1^H(t) + 0.2232 \cdot v_2(t)\right] + 1.8173, \quad (26)$$

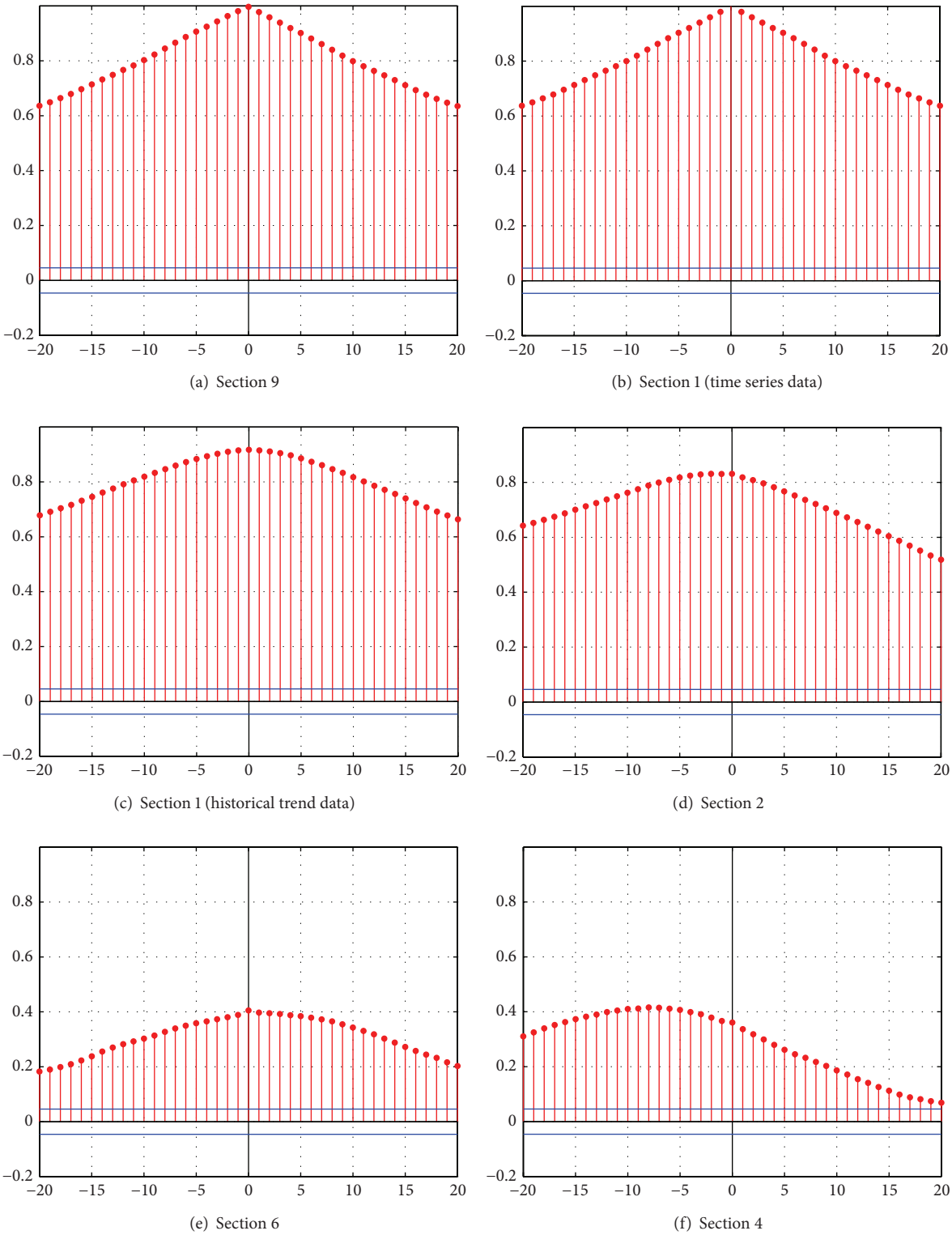

(a) Section 9

(b) Section 1 (time series data)

(c) Section 1 (historical trend data)

(d) Section 2

(e) Section 6

(f) Section 4

Figure 5: Temporal-spatial-historical correlation analysis based speed.

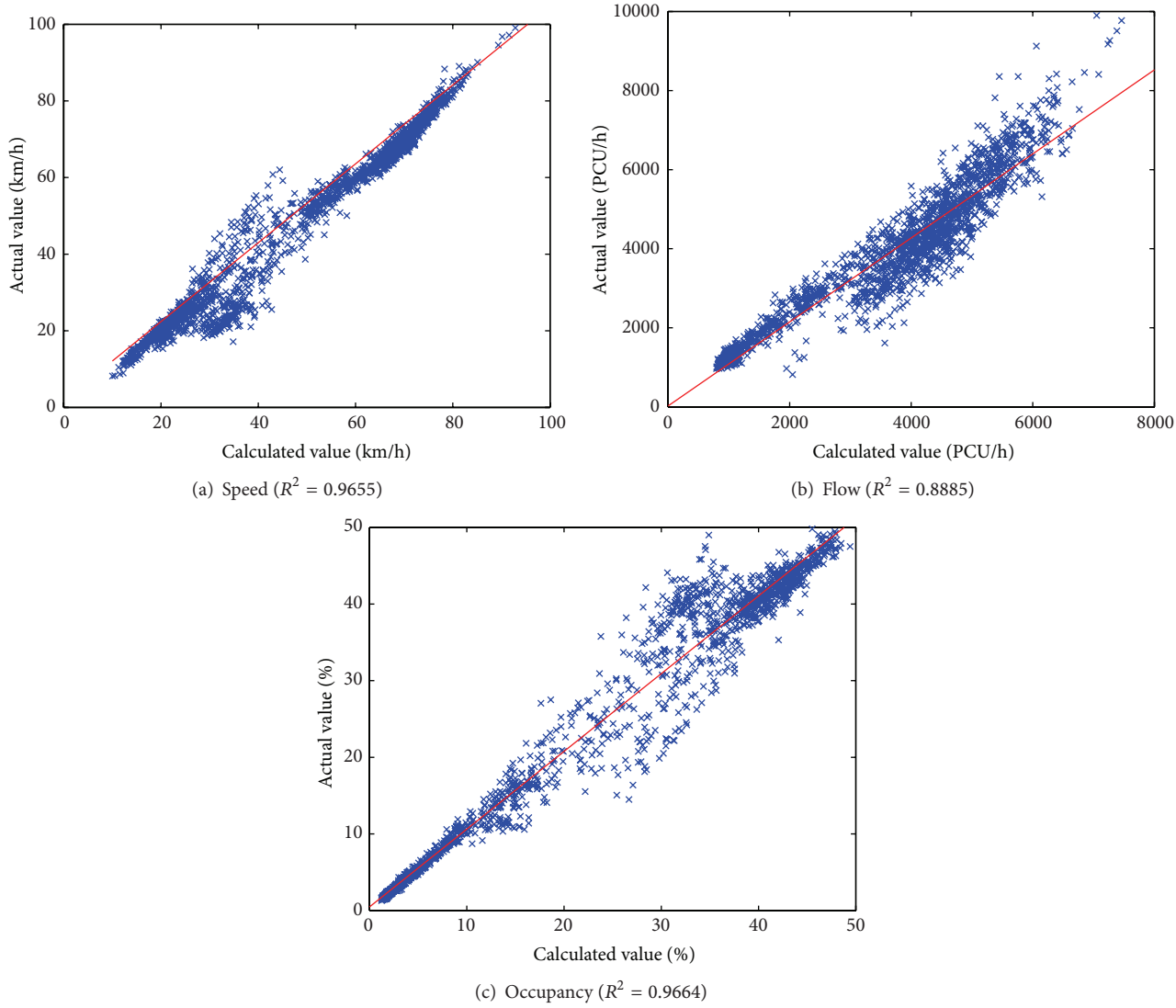

(a) Speed ($R^2 = 0.9655$)

(b) Flow ($R^2 = 0.8885$)

(c) Occupancy ($R^2 = 0.9664$)

Figure 6: Fitting curve.

where $v_j(t)$ is the velocity of section j at time t and $v_1^H(t)$ is the historical relative data of Section 1.

Apply the same method to analyze flow and occupancy:

$$q_1(t) = 1.0629 \times [0.2246 \cdot q_9(t) + 0.2151 \cdot q_1(t-5) + 0.2145 \cdot q_1^H(t-5) + 0.1787 \cdot q_2(t) + 0.1670 \cdot q_6(t-10)] + 22.652, \quad (27)$$

$$\rho_1(t) = 1.0148 \times [0.2791 \cdot \rho_9(t) + 0.2747 \cdot \rho_1(t-5) + 0.2294 \cdot \rho_2(t) + 0.2168 \cdot \rho_1^H(t)] + 0.4793, \quad (28)$$

where $q_j(t)$ is the flow of Section j at time t, $q_1^H(t)$ is the historical relative data of Section 1, $\rho_j(t)$ is the occupancy of Section j at time t, and $\rho_1^H(t)$ is the historical relative data of Section 1.

Fitting curve is shown in Figure 6.

4.3.2. Online Application. Online calculations mainly deal with real-time data based on prior knowledge. Figure 7 shows the predicted results. The prediction errors of speed, flow, and occupancy are controlled around 10%. Traffic state deviation is shown in Table 3. Two-level-deviation and Three-level-deviation are considered as errors, which are controlled in 10%.

5. Conclusions

In the era of big data, real-time traffic flow state identification, and prediction may face many challenges. This difficulty is decided by the characteristics of big data. This paper uses speed and occupancy to build the traffic flow state clustering

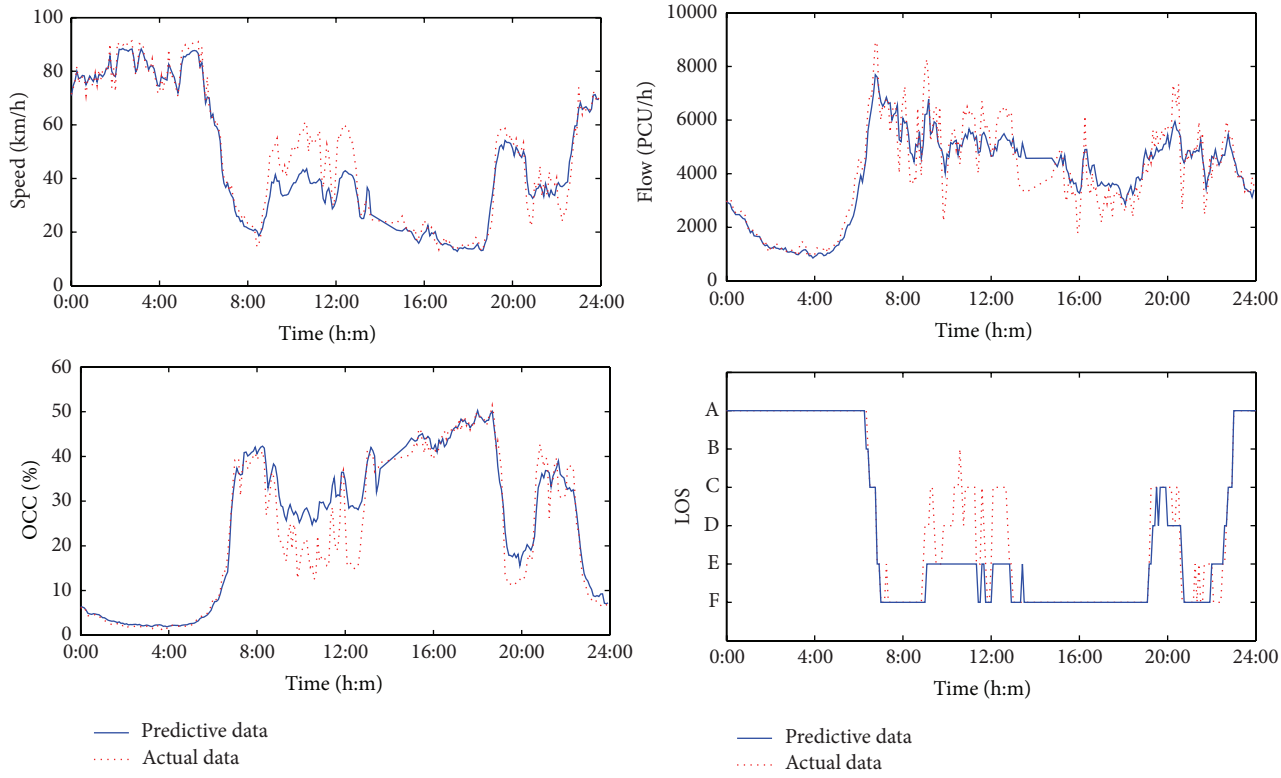

Figure 7: Modification effective analysis.

Table 3: Comparative analysis.

Deviation	Non-level-deviation	One-level-deviation	Two-level-deviation	Three-level-deviation
Accuracy	75.37%	15.80%	8.46%	0.37%

model. And real-time traffic flow state identification is based on speed and occupancy. Traditional fuzzy c-mean clustering does not meet the requirements of big data analysis. To improve the feasibility of traffic flow state clustering, this paper uses the simulated annealing genetic algorithm based fuzzy c-means (SAGA-FCM). Case study shows that the value of objective function calculated based on SAGA-FCM is better.

Traffic flow big data strongly shows temporal, spatial, and historical correlations. The regional traffic flow correlation model is established for real-time traffic flow prediction. The characteristics of big data make it difficult to resolve the model. In order to reduce parameters and ensure calculation speed and calculation accuracy, the correction coefficients optimization model, which can be divided into two stages, is put forward. Effectiveness of the method has been validated by the case study.

The core of this paper is to present a traffic temporal-spatial-historical correlation model, which comprehensively considers the temporal, spatial, and historical correlations of traffic flow big data. Compared with the model based on a single nature, the accuracy of proposed model is relatively high. Besides, this model quantitatively solves, from the perspective of spatiotemporal correlation analysis, the weight selection problem of different analytical methods in the traditional combined model. The traffic temporal-spatial-historical correlation model can be applied in other researches such as identification and correction of abnormal data and traffic congestion mechanism analysis.

Conflict of Interests

The authors declare that there is no conflict of interests regarding the publication of this paper.

Acknowledgments

The authors are grateful to the editor and anonymous reviewers for their valuable suggestions. This research was funded by Beijing Science and Technology Plan (no. Z121100000312101).

References

[1] Transportation Research Board, *1965 Highway Capacity Manual*, Transportation Research Board of the National Academies, Washington, D C, USA, 1965.

[2] Transportation Research Board, *Highway Capacity Manual 2010*, Transportation Research Board of the National Academies, Washington, DC, USA, 2010.

[3] T. Sasaki and Y. Iida, *Traffic Engineering*, Ohmsha, Tokyo, Japan, 1992.

[4] "Code for transport planning on urban road," GB 50220-1995, CN-GB, Beijing, China, 1995.

[5] K. Choocharukul, K. C. Sinha, and F. L. Mannering, "User perceptions and engineering definitions of highway level of service: an exploratory statistical comparison," *Transportation Research Part A: Policy and Practice*, vol. 38, no. 9-10, pp. 677–689, 2004.

[6] C. C. Xu, P. Liu, W. Wang, and Z. B. Li, "Evaluation of the impacts of traffic states on crash risks on freeways," *Accident Analysis and Prevention*, vol. 47, pp. 162–171, 2012.

[7] L. Wang, Y. Z. Fan, and H. Zhang, "A new traffic state evaluation approach based on probe vehicle and multi-classification fuzzy pattern recognition," *Journal of Highway and Transportation Research and Development*, vol. 24, no. 9, pp. 92–95, 2007.

[8] B. S. Kerner, "Three-phase traffic theory and highway capacity," *Physica A*, vol. 333, no. 1–4, pp. 379–440, 2004.

[9] H. Li, J. Lu, G. Jiang, and Y. Ma, "Traffic incident detection algorithm for expressway," *Journal of Southeast University*, vol. 43, no. 3, pp. 649–653, 2013.

[10] W. Guan and S. Y. He, "Phase identification of urban freeway traffic based on statistical properties," *Journal of Transportation Systems Engineering and Information Technology*, vol. 7, no. 5, pp. 42–50, 2007.

[11] Y. Q. Liao, L. M. Jia, C. X. Li, H. H. Dong, and Y. Qin, "A perceptual experiment study on level of service for regional road traffic," *Journal of Beijing Jiaotong University*, vol. 7, no. 5, pp. 42–50, 2007.

[12] J. Xia, W. Huang, and J. Guo, "A clustering approach to online freeway traffic state identification using ITS data," *KSCE Journal of Civil Engineering*, vol. 16, no. 3, pp. 426–432, 2012.

[13] Z. W. Qu, Q. Wei, Y. M. Bie, H. Zhu, and D. H. Wang, "Method for traffic state identification based on fixed detector," *Journal of Central South University (Science and Technology)*, vol. 44, no. 1, pp. 403–410, 2013.

[14] X. L. Sun, H. H. Dong, M. Guo, S. W. Lin, J. Qiao, and P. Zheng, "The design and implementation of Beijing regional traffic conditions and LOS evaluation system, road traffic safety," *Road Traffic & Safety*, vol. 10, no. 4, pp. 36–40, 2010.

[15] Y. S. Quan, J. F. Guo, J. Z. Guan, L. Yu, and H. M. Wen, "Research on traffic congestion evaluation and empirical analysis of Beijing," in *Proceedings of the 3rd China Annual Conference on ITS*, pp. 1–6, 2007.

[16] X.-L. Liu, P. Jia, S.-H. Wu, and B. Yu, "Short-term traffic flow forecasting based on multi-dimensional parameters," *Journal of Transportation Systems Engineering and Information Technology*, vol. 11, no. 4, pp. 140–146, 2011.

[17] H.-H. Dong, X.-L. Sun, L.-M. Jia, H.-J. Li, and Y. Qin, "Traffic condition estimation with pre-selection space time model," *Journal of Central South University of Technology*, vol. 19, no. 1, pp. 206–212, 2012.

[18] M. Canaud, L. Mihaylova, J. Sau, and N.-E. El Faouzi, "Probability hypothesis density filtering for real-time traffic state estimation and prediction," *Networks and Heterogeneous Media*, vol. 8, no. 3, pp. 825–842, 2013.

[19] T. L. Pan, A. Sumalee, R. X. Zhong, and N. Indra-Payoong, "Short-term traffic state prediction based on temporal-spatial correlation," *IEEE Transactions on Intelligent Transportation Systems*, vol. 14, no. 3, pp. 1242–1254, 2013.

[20] C. Antoniou, H. N. Koutsopoulos, and G. Yannis, "Dynamic data-driven local traffic state estimation and prediction," *Transportation Research Part C: Emerging Technologies*, vol. 34, pp. 89–107, 2013.

[21] S. Zhang, Z. X. Huang, and A. W. Kuang, "Estimation of real-time traffic state of city expressway under incomplete information," *Systems Engineering*, vol. 31, no. 5, pp. 16–21, 2013.

[22] Y. Guo, X. Zhang, B. Dong, and L. Wu, "Traffic state of rapid identification and transitions shift method based on fuzzy theory," *Journal of Central South University (Science and Technology)*, vol. 44, no. 1, pp. 1–5, 2013.

[23] H. B. Shan, S. X. Li, D. G. Gong, and P. Lou, "Genetic simulated annealing algorithm-based assembly sequence planning," in *Proceedings of the International Technology and Innovation Conference (ITIC '06)*, pp. 1573–1579, November 2006.

[24] K.-L. Zhou and S.-L. Yang, "An improved fuzzy C-Means algorithm for power load characteristics classification," *Power System Protection and Control*, vol. 40, no. 22, pp. 58–63, 2012.

[25] D. W. Xu, L. M. Jia, and X. L. Sun, "Design method of road traffic information template," *Journal of Highway and Transportation Research and Development*, vol. 30, no. 12, pp. 132–137, 2013.

[26] L. G. Sun, R. M. Li, S. Dong, and H. P. Lu, "Study on short-term traffic flow combined forecast method," *Journal Wuhan University of Technology (Transportation Science & Engineering)*, vol. 34, no. 5, pp. 874–876, 2010.

[27] H. P. Lu, Y. G. Sui, M. Guo, and R. M. Li, *Urban Mixed Traffic Flow Analysis Model and Method*, China Railway Publishing House, Beijing, China, 2009.

[28] F. Shi, H. Wang, L. Yu, and F. Hu, *Thirty Cases Analysis of Intelligence Algorithm Based on Matlab*, Beihang University Press, Beijng, China, 2010.

Hindawi Publishing Corporation
Discrete Dynamics in Nature and Society
Volume 2015, Article ID 365367, 10 pages
http://dx.doi.org/10.1155/2015/365367

Research Article

The Optimization of Transportation Costs in Logistics Enterprises with Time-Window Constraints

Qingyou Yan and Qian Zhang

School of Economics and Management, North China Electric Power University, Beijing 102206, China

Correspondence should be addressed to Qian Zhang; zhangqian881111@163.com

Received 25 November 2014; Revised 26 March 2015; Accepted 27 March 2015

Academic Editor: Delfim F. M. Torres

This paper presents a model for solving a multiobjective vehicle routing problem with soft time-window constraints that specify the earliest and latest arrival times of customers. If a customer is serviced before the earliest specified arrival time, extra inventory costs are incurred. If the customer is serviced after the latest arrival time, penalty costs must be paid. Both the total transportation cost and the required fleet size are minimized in this model, which also accounts for the given capacity limitations of each vehicle. The total transportation cost consists of direct transportation costs, extra inventory costs, and penalty costs. This multiobjective optimization is solved by using a modified genetic algorithm approach. The output of the algorithm is a set of optimal solutions that represent the trade-off between total transportation cost and the fleet size required to service customers. The influential impact of these two factors is analyzed through the use of a case study.

1. Introduction

In a competitive environment, obtaining the maximum profit plays a key role in the success of an enterprise. Logistics costs make up a large portion of the total costs of enterprises but can be reduced through supply chain optimization. Analysis of the logistics costs of enterprises reveals that transportation costs are an important part of the costs of logistics enterprises. Therefore, it is very important to study how transportation costs can be optimized in logistics enterprises.

The transportation costs of logistics enterprises are influenced by the fixed costs and variable costs involved in the transportation process. However, transportation costs are more closely related to time-window constraints, which are governed by customers' arrival times. Logistics enterprises must pay penalties when time-window constraints are violated, and this causes increases in transportation costs.

Many past studies have been dedicated to determining how to achieve the lowest possible transportation cost. For example, McCann [1] addressed two interrelated questions: the optimum size of a vehicle or vessel and the structure of transportation costs with respect to haulage distance. C. Pilot and S. Pilot [2] focused on minimizing the total costs involved in a transportation problem. Jha et al. [3] considered a joint-location inventory problem and minimized the transportation cost involved in a joint inventory location model by using a modified adaptive different evolution algorithm. Chanas and Kuchta [4] proposed what they see as an optimal solution to the transportation problem, which makes use of fuzzy cost coefficients and an algorithm determining the nature of the solution.

As exploration of transportation problems has developed, multiobjective transportation cost problems have emerged. For instance, Prakash et al. [5] drew attention to a cost-time trade-off bulk transportation problem, which they solve by using Pareto optimal solutions. Ojha et al. [6] formulated a multiobjective transportation solution, with fuzzy relations under fuzzy logic. The objectives of their model are the minimization of the total transportation cost and total time for transportation required for the system.

The conditions that force each vehicle to start with each customer at a period specified by that customer are called time-window constraints. Existing literature on transportation problems with time-window constraints has mainly concentrated on vehicle routing problems. Vehicle routing problems, with different variations and generalizations, have been studied for several decades, since the pioneering work of Dantzig and Ramser [7] on a truck dispatching problem.

Alvarenga et al. [8] proposed a robust heuristic approach to vehicle routing problems with time windows (VRPTW), using travel distance as the main objective through an efficient genetic algorithm and a set partitioning formulation.

Ghoseiri and Ghannadpour [9] presented a new model and solution for multiobjective VRPTW using goal programming and genetic algorithm, in which decision makers specify optimistic aspiration levels to objectives and deviations from those aspirations are minimized. They used a direct interpretation of VRPTW as a multiobjective problem, in which both total required fleet size and total traveling distance were minimized, while capacity and time-window constraints were secured.

Al-Khayyal and Hwang [10] formulated a model for finding the minimum-cost route in a network for a heterogeneous fleet of ships engaged in the pickup and delivery of several liquid bulk products. They showed that the model can be reformulated as an equivalent mixed-integer linear program with a special structure.

Yu et al. [11] proposed a hybrid approach, which consists of ant colony optimization (ACO) and Tabu search, to solve VRPTW.

Chiang and Hsu [12] proposed their own approach to solve a multiobjective vehicle routing problem with time windows. The objectives were to simultaneously minimize the number of vehicles and the total distance. Their approach was based on an evolutionary algorithm and it aims to find a set of Pareto optimal solutions.

Because of the many applications of different vehicle routing problems, a wide variety of researchers have focused on developing solutions to them. Useful techniques for solving general vehicle routing problems can be found in [13–15].

Our analysis of the works described above has shown that existing literature based on accurate algorithms and heuristic algorithms aims to achieve the lowest transportation cost possible. To our knowledge, no study has considered the time-window constraints in the transportation cost model. Time-window constraints increase transportation costs in logistics enterprises, and so it is necessary for logistics enterprises to take the time-window constraints into consideration when making decisions.

This paper presents a biobjective transportation cost model with time-window constraints, which is modeled through modified genetic algorithm. In our study, the simultaneous minimization of fleet size and total transportation cost are considered objective functions.

The model is formulated under the following assumptions:

(1) Time-window constraints are soft, and the time windows specified by customers are elastic.

(2) The service time for a vehicle at its destination is equal to zero.

(3) A route is defined as starting from a depot, going through a number of customers, and ending at the depot. Every customer on the route must be visited only once by one of the vehicles.

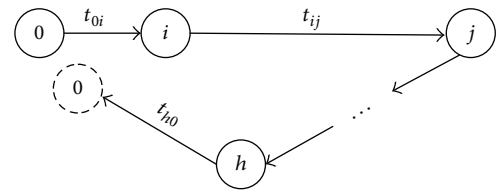

Figure 1: A network representation of the transportation process.

2. Model Formulation

This paper assumes that a logistics enterprise is the single supplier in a transportation process. The logistics enterprise distributes goods to customers according to the number of orders. The customer number for a route is uncertain, and the vehicle route must be determined in order to optimize transportation cost.

The system of logistics enterprise transportation can be regarded as a simple network. In this network, the start node and end node are both the central depot of the logistics enterprise. Each arc of the network represents the transportation relationship between customers. The number of the arc represents the travel time between the two customers. Let us assume there are $N+1$ customers, $C = \{0, 1, 2, \ldots, N\}$, and for simplicity denote the depot as customer 0. Figure 1 presents a network representation of the transportation process.

The transportation cost model in this paper takes time-window constraints into consideration. Any customer i must be serviced within a predefined time interval $[ES_i, LF_i]$, limited by an earliest arrival time ES_i, and a latest arrival time LF_i. Vehicles arriving later than the latest arrival time are penalized, while those arriving earlier than the earliest arrival time have to pay for the inventory cost involved.

In order to formulate the model, the notations in it are defined as follows:

K: the maximum possible size of the fleet,

C_k: the transportation cost per unit mass or volume of vehicle k,

$C = \{0, 1, 2, \ldots, N\}$: the customer set,

(i, j): the transportation process from customer i to customer j,

t_{ij}: the travel time between customer i and customer j,

m_i: the demand of customer i,

Q_k: the limited capacity of vehicle k,

$$x_{ijk}: \begin{cases} 1, & \text{vehicle } k \text{ drives from customer } i \\ & \text{to customer } j \\ 0, & \text{otherwise,} \end{cases}$$

r_k: the maximum route time allowed for vehicle k,

$[ES_i, LF_i]$: the predefined time interval that customer i must be serviced within, with ES_i being the earliest arrival time of customer i, and LF_i being the latest arrival time of customer i,

d_1: the inventory cost that the logistics enterprise has to pay if a vehicle arrives one day earlier than the earliest arrival time,

d_2: the penalty cost that the logistics enterprise has to pay if a vehicle arrives one day later than the latest arrival time,

e_{ik}: the arrival time in advance for vehicle k at node i,

f_{ik}: the delayed arrival time for vehicle k at node i,

T_{ik}: the real arrival time for vehicle k at node i.

There are two objectives in the transportation cost model. One is to minimize the transportation cost, and the other is to minimize the fleet size used to serve the customers. The model has four constraints. This paper observes vehicle capacity constraints and time-window constraints. In it, each customer is served exactly once and each vehicle starts its journey from a depot and ends at the depot.

The transportation cost model in this paper can be written as

$$\begin{aligned}\text{Min} \sum_{i=1}^{N} m_i \sum_{j=0, i\neq j}^{N} \sum_{k=1}^{K} x_{ijk} \times C_k + \sum_{i=1}^{N} \sum_{k=1}^{K} e_{ik} \times d_1 \\ + \sum_{i=1}^{N} \sum_{k=1}^{K} f_{ik} \times d_2, \qquad (1)\end{aligned}$$

$$\text{Min} \sum_{k=1}^{K} \sum_{j=1}^{N} x_{0jk},$$

subject to

$$\sum_{j=1, j\neq i}^{N} x_{ijk} = \sum_{j=1, j\neq i}^{N} x_{jik} \leq 1 \qquad (2)$$

$$\text{for } i = \{0, 1, \ldots, N\}, \ k = \{1, 2, \ldots, K\},$$

$$\sum_{k=1}^{K} \sum_{j=0, j\neq i}^{N} x_{ijk} = 1 \quad \text{for } i = \{1, 2, \ldots, N\}, \qquad (3)$$

$$\sum_{k=1}^{K} \sum_{i=0, i\neq j}^{N} x_{ijk} = 1 \quad \text{for } j = \{1, 2, \ldots, N\}, \qquad (4)$$

$$\sum_{i=1}^{N} m_i \sum_{j=0, j\neq i}^{N} x_{ijk} \leq Q_k \quad \text{for } k = \{1, 2, \ldots, K\}, \qquad (5)$$

$$\sum_{i=0}^{N} \sum_{j=0, j\neq i}^{N} x_{ijk} t_{ij} \leq r_k \quad \text{for } k = \{1, 2, \ldots, k\}, \qquad (6)$$

$$\text{ES}_0 = \text{LF}_0 = 0, \qquad (7)$$

$$\sum_{k=1}^{K} \sum_{i=0, i\neq j}^{N} x_{ijk} \left(T_{ik} + t_{ij}\right) = T_{jk} \quad \text{for } j = \{i, \ldots, N\}, \qquad (8)$$

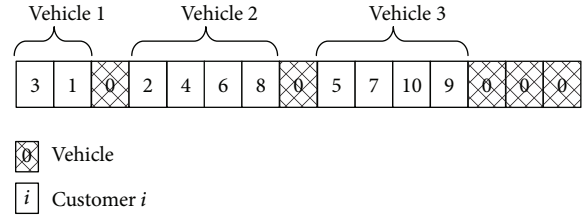

Figure 2: Representation of the individual integer code.

$$\text{ES}_i \leq \sum_{k=1}^{K} T_{ik} + e_i - f_i \leq \text{LF}_i, \qquad (9)$$

$$e_i \times f_i = 0. \qquad (10)$$

Constraint (2) specifies that every route starts and ends at the central depot. Constraints (3) and (4) define that every customer node is visited only once by one vehicle. Constraint (5) is the capacity constraint. Constraint (6) is the maximum travel time constraint. Constraints (7)–(10) define the time windows.

3. Modified Genetic Algorithm

As mentioned before, Ghoseiri and Ghannadpour [9] studied a vehicle routing problem with time windows and presented a genetic algorithm (GA) to solve it. In this section, we modify the presented GA to be used in the multiobjective optimization model above, by further considering the total transportation cost and time-window constraints. The specific content is described below.

A GA starts with a set of chromosomes referred to as the initial population. Each chromosome represents a solution to the problem, and the initial population is randomly generated. A selection mechanism is then used to select prospective parents based on their fitness, computed by the evaluation function. The selected parent chromosomes are then recombined via the crossover operator to create a potential new population. The next step is to mutate a small number of newly obtained chromosomes, in order to introduce a level of randomness that prevents the GA from converging to a local optimum.

3.1. Chromosome Representation and the Initial Population. To solve a transportation cost model, each individual is usually represented by just one chromosome, which is a chain of integers (as discussed by Ghoseiri and Ghannadpour [9]). In this representation, each vehicle identifier is represented by 0 and is also a separator between two different routes. There are $K - 1$ vehicle identifiers in the chromosome, which can divide the chromosome into K routes. The customer identifiers are represented by i ($i = 1, 2, \ldots, N$), and a string of customer identifiers represents the sequence of deliveries that a vehicle must cover during its route. Figure 2 shows a representation of a possible solution with 10 customers and 6 vehicles. The route of vehicle 1 is $3 \rightarrow 1$, the second route is $2 \rightarrow 4 \rightarrow 6 \rightarrow 8$, and the third is $5 \rightarrow 7 \rightarrow 10 \rightarrow 9$. There are no travel tasks for vehicles 4, 5, and 6.

An initial population is built such that each individual must at least be a feasible candidate solution (i.e., every route in the initial population must be feasible). In this paper, an individual is feasible when the limited capacity of the vehicle and the maximum route time allowed are satisfied. Based on this, the population initialization algorithm can be written as follows.

Step 1. Determine the set of all unscheduled customers $\alpha = \{1, 2, \ldots, N\}$ and the maximal size of fleets K. Denote Z_k and R_k as the rest capacity and travel time of vehicle k ($k = 1, 2, \ldots, K$), respectively. Let β_k be the set consisting of all customers served by vehicle k. Initialize $Z_k = Q_k$, $R_k = r_k$, and $\beta_k = \varnothing$ for all $k = 1, 2, \ldots, K$.

Step 2. Randomly select an unscheduled customer i who has higher demand than others (i.e., $i \in \{r \mid m_r = \max_{r\in\alpha}\{m_r\}\}$). Let c_k ($k = 1, 2, \ldots, K$) be the last customer in the set β_k (if $\beta_k = \varnothing$, then c_k represents the central depot). Then, determine the set χ, which consists of all vehicles whose rest capacities and rest route times are sufficient to serve customer i (i.e., $\chi = \{k | m_i \le Z_k, t_{i_k i} \le R_k, k = 1, 2, \ldots, K\}$). Finally, randomly choose a vehicle $\bar{k}$ from the set χ to serve customer i and update $\beta_{\bar{k}} = \{\beta_{\bar{k}}, i\}$, $\alpha = \alpha \setminus \{i\}$, $Z_{\bar{k}} = Z_{\bar{k}} - m_i$, and $R_{\bar{k}} = R_{\bar{k}} - t_{c_{\bar{k}} i}$.

Step 3. If $\alpha = \varnothing$, go to the next step; otherwise, go to Step 2.

Step 4. Rearrange the sequence of customers in set β_k and randomly generate a feasible travel route for vehicle k, denoted by FR_k, for all $k = 1, 2, \ldots, K$. Finally, a complete individual can be represented as $\{\mathrm{FR}_1, 0, \mathrm{FR}_2, 0, \ldots, \mathrm{FR}_K\}$.

Using the above presentation method, the individual shown in Figure 2 is coded as $\{\{3, 1\}, 0, \{2, 4, 6, 8\}, 0, \{5, 7, 10, 9\}, 0, 0, 0\}$.

3.2. Selection. A feasible solution (i.e., individual solution) for the models is said to dominate another solution if it is not worse with regard to any of the objectives and clearly better with regard to at least one. In the current problem, a feasible solution (C, N) is said to dominate another solution (C', N') if both C and N are smaller than or equal to C' and N', where C and C' denote the total transportation costs and N and N' denote the total number of vehicles. The feasible solution (C, N) is said to be a nondominated solution (or a Pareto solution), if there is no other solution that can dominate it. Based on this nondomination criterion, this paper evaluates and selects the individuals through the following procedure.

Step 1. Calculate the objective function values for all individuals, where the total transportation costs are determined by (11), and total numbers of vehicles are determined directly by decoding the chromosome.

Step 2. Assign a rank value to each individual, depending on its position within the population. The smaller the number of solutions that dominate an individual, the smaller the rank of the individual. If we suppose that, for a given generation t, an individual k is dominated by the number of d_k of individuals in the considered population, its rank will be determined as follows:

$$\mathrm{rank}\,(k, t) = 1 + d_t. \tag{11}$$

It is easy to determine that all nondominated solutions will have a rank equal to 1. Note also that, for a given individual, this metric may vary across generations because of the population distribution changes.

Step 3. Compute the fitness value of an individual k in a population at a generation t by calculating the following (as discussed by Elloumi and Fortemps [16]):

$$f\,(k, t) = \frac{1}{\mathrm{rank}\,(k, t)}. \tag{12}$$

Step 4. Randomly select POP/2 pairs of individuals, by roulette selection, to undergo forthcoming evolutionary operations, where POP denotes the number of individuals within a population. The selection probability of individual k in generation t is given by the following:

$$p\,(k, t) = \frac{f\,(k, t)}{\sum_{l=1}^{\mathrm{POP}} f\,(l, t)}. \tag{13}$$

3.3. Crossover. This paper employs a problem-specific best cost-route crossover (as discussed by Ombuki et al. [13]), with the probability of crossover p_{cross}. This aims to simultaneously minimize the fleet size and the total transportation cost, while also assessing the feasibility of constraints. For any pair of individuals randomly selected through the selection operation above, one is called the "father" and is denoted by $I^F = (\beta_1^F, 0, \beta_2^F, 0, \ldots, \beta_K^F)$. Another is termed the "mother" and is denoted by $I^M = (\beta_1^M, 0, \beta_2^M, 0, \ldots, \beta_K^M)$.

First, a random route from the father is selected. Second, all of the genes in the selected route are removed from the mother, and the remaining chromosome is directly passed on to the son, I^S. Third, each of the removed genes is reinserted into the son's line, based on the minimum cost principle, and the whole offspring I^S is then obtained by the end of this step. We proceed similarly for the daughter, I^D, but replace the father with the mother and vice versa.

The pseudocode for generating the son I^S can be described as shown in Procedure 1.

In Procedure 1, length (I^D) is the number of genes of I^D. $I^D_{i\to j}$ is the chromosome of I^D between position i and position j.

3.4. Mutation. The mutation operator is applied to newly generated individuals with a probability of mutation p_{mut}. First, we randomly choose two positions, q_{mut1} and q_{mut2}, such that $1 \le q_{\mathrm{mut1}} < q_{\mathrm{mut2}} \le N + K - 1$, $q_{\mathrm{mut1}} \ne 0$, and $q_{\mathrm{mut2}} \ne 0$ (recall that N and K are the numbers of customers and vehicles, resp.). Then, we check whether customers in positions q_{mut1} and q_{mut2} can be permuted. In other words, if the change does not result in infeasibility, we can permute the customers. Otherwise, we choose another position, q'_{mut2}.

BEGIN:
(1) Randomly generate a number q_{cross}, such that $1 \le q_{\text{cross}} \le K$ and $\beta^F_{\text{cross}} \neq \varnothing$;
(2) Let $I^D = I^M \setminus \{\beta^F_{\text{cross}}\}$;
(3) Randomly select a gene g^F in β^F_{cross};
(4) **FOR** $i = 1$ TO length(I^D);
(5) Generate the partial schedule $P_i = (I^D_{1\to i-1}, g^F, I^D_{i\to \text{end}})$;
(6) Compute the total transportation cost C_i of P_i. If P_i is infeasible, let C_i = a sufficiently large number;
(7) Let $i^* = \min_i\{r \mid C_r\}$ and reinsert gene g^F in the position i^* of I^D;
(8) Update $I^D = (I^D_{1\to i^*-1}, g^F, I^D_{i^*\to \text{end}})$ and $\beta^F_{\text{cross}} = \beta^F_{\text{cross}} \setminus g^F$; **ENDFOR**
(9) If $\beta^F_{\text{cross}} \neq \varnothing$, return to Step (3); otherwise, terminate the procedure.
END

Procedure 1

BEGIN
Input: all necessary data related to customers and vehicles
GA parameters: POP, p_{cross}, p_{mut}
Generate a new population of individuals
While maximal iteration number is not met DO
Evaluate the individuals
Select the better individuals
Generate the offspring population using evolutionary operators
Output: a set of non-dominated solutions
END

Procedure 2

Table 1: The situation of vehicles in the logistics enterprise S.

Vehicle model	Q_k	C_k	Quantity
a	15 ton/59 m^3	0.2 yuan/kg	2
b	2 ton/15 m^3	0.3 yuan/kg	1
c	25 ton/77 m^3	0.15 yuan/kg	2
d	40 ton/100 m^3	0.1 yuan/kg	2

We repeat the procedure until two customers are permuted or until a certain number of unsuccessful attempts are made.

Finally, the main process of proposed GA can be described as shown in Procedure 2.

4. Experimental Results and Comparisons

A logistics enterprise named S has 10 vehicles, the situation of which is shown in Table 1. S needs to deliver goods to 10 customers. Table 2 shows the travel time for S's logistics enterprise. The positions and demands of the customers can be seen in Figure 3 and Table 3. Table 4 presents the time-windows constraints for each customer. When a vehicle's arrival time is one day earlier than the earliest permitted arrival time, the inventory cost is equal to 0.44 yuan/(ton × day). The penalty cost, when the vehicle's arrival time is one day later than the latest permitted arrival time, is 4,000 yuan/weekday. The maximum travel time for each route is 30 weekdays.

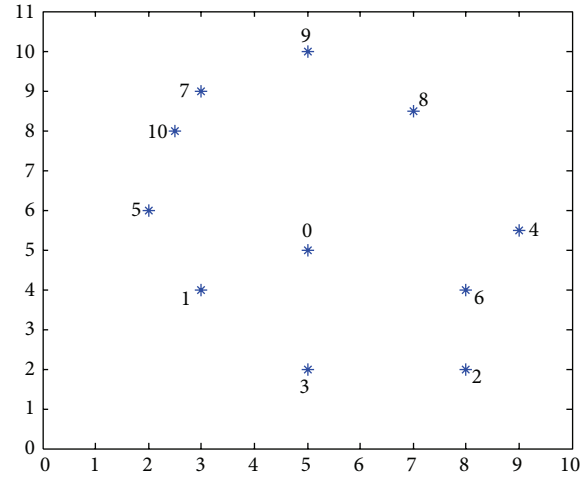

Figure 3: The position relationship of the customers.

In real life, it is important to confirm the trade-off between fleet sizes and total transportation costs of logistics enterprises. These two aspects may positively correlate with each other. In other words, a higher transportation cost may be incurred if more vehicles are involved. At the same time, these two values may conflict with each other. Such situations are difficult to determine when using the classical approach but are easily analyzed with our suggested approach.

Table 2: The travel time of S logistics enterprise (day).

Travel time	0	1	2	3	4	5	6	7	8	9	10
Depot 0	0	2	3	2	3	3	3	4	4	5	3
Customer 1	—	0	3	3	2	2	3	3	5	5	3
Customer 2	—	—	0	4	3	2	1	2	4	3	2
Customer 3	—	—	—	0	4	4	5	5	6	6	4
Customer 4	—	—	—	—	0	2	2	3	5	5	2
Customer 5	—	—	—	—	—	0	2	2	5	5	1
Customer 6	—	—	—	—	—	—	0	1	4	4	1
Customer 7	—	—	—	—	—	—	—	0	5	3	1
Customer 8	—	—	—	—	—	—	—	—	0	5	5
Customer 9	—	—	—	—	—	—	—	—	—	0	4
Customer 10	—	—	—	—	—	—	—	—	—	—	0

Table 3: The demand of customers.

Customer	Demand
Customer 1	3000 kg
Customer 2	10000 kg
Customer 3	5000 kg
Customer 4	2000 kg
Customer 5	2000 kg
Customer 6	10000 kg
Customer 7	8000 kg
Customer 8	5000 kg
Customer 9	7000 kg
Customer 10	20000 kg

Table 4: The time windows constraints of each customer.

Customer	Time windows
Customer 1	[1, 2]
Customer 2	[2, 4]
Customer 3	[3, 5]
Customer 4	[4, 8]
Customer 5	[3, 10]
Customer 6	[11, 15]
Customer 7	[3, 6]
Customer 8	[7, 12]
Customer 9	[4, 10]
Customer 10	[2, 7]

In this paper, the proposed GA is run under the MATLAB development environment and performed on a computer with a 2 GHz Intel dual-core processor with 2 GB RAM, running Windows 7. We tuned the algorithm parameters, including population size, max iteration, mutation rate, and crossover rate, by using crossover values of $\{0.6, 0.7, 0.8, 0.9\}$ and mutation rates of $\{0.1, 0.2, 0.3, 0.4\}$. After many trials, the population size, crossover rate, mutation rate, and max iteration were set to 50, 0.8, 0.4, and 500, respectively. The example case was solved and repeated 30 times, and the average CPU time was 102 seconds. The best results for the GA are listed in Tables 5 and 6.

The results with time-window constraints are shown in Table 5, and the results without time-window constraints are shown in Table 6. Table 5 shows that the transportation cost of a solution is reduced as the number of vehicles is increased. For example, when the fleet size is 2, the total transportation cost is 65,320 yuan, while when the fleet size is 3, the total transportation cost is 34,581 yuan. When the fleet size is increased by 1, the total transportation cost is thus reduced by 47.06% (from 65,320 to 34,581).

Comparing the results of Tables 5 and 6, we can find that the total transportation cost with time-window constraints is higher than the transportation cost without them. In particular, when the fleet size is equal to 2, the gap between the two costs can be as high as 26,520 yuan. Tables 5 and 6 present the different vehicle routes for the two results. This situation can be explained by the real transportation process. In reality, in daily life, some customers determine the goods arrival time interval according to their demand, and this arrival time interval is called a time window. If a customer is serviced before the earliest arrival time, extra inventory costs are incurred. If the customer is serviced after the latest arrival time, penalty costs have to be paid. Therefore, time-window constraints may influence transportation costs and vehicle routes. It must be mentioned that decision-makers may make the wrong decisions when they ignore the effects of time-window constraints, which results in resource wasting and customer dissatisfaction.

The vehicle routes with time-window constraints of different fleet sizes are shown in Figure 4. When the fleet size is equal to 2, there are two routes, when the fleet size is equal to 3, there are three routes, and so on. When the fleet size is increased by 1, the vehicle routes also increase by 1. Note that the results in Table 5 and Figure 4 are clearly comparable, and the decision-maker of S can decide which vehicle route is more preferable, based on specific preferences. For instance, if the decision-maker wants fewer transfers to occur, in order to use vehicle space efficiently, the two-vehicle route may be more reasonable. If the decision maker wants to lower cost, the six-vehicle route may be more reasonable.

The results of this example case allow us to obtain information on the trade-off relationship between fleet size and total transportation cost, as shown in Figure 5. It can be

Table 5: The results with time-window constraints.

Fleet size	Limited capacity	The vehicle route	Total transportation cost
2	[40, 40]	0 → 1 → 5 → 10 → 7 → 9 → 0; 0 → 3 → 2 → 6 → 4 → 8 → 0	65320
3	[40, 40, 25]	0 → 10 → 7 → 9 → 8 → 0; 0 → 2 → 6 → 4 → 5 → 0; 0 → 1 → 3 → 0	34581
4	[40, 40, 25, 25]	0 → 2 → 6 → 8 → 0; 0 → 10 → 7 → 9 → 0; 0 → 1 → 5 → 4 → 0; 0 → 3 → 0	30533
5	[40, 40, 25, 25, 15]	0 → 10 → 7 → 9 → 0; 0 → 2 → 6 → 5 → 0; 0 → 1 → 4 → 0; 0 → 8 → 0; 0 → 3 → 0	29440
6	[40, 40, 15, 15, 25, 25]	0 → 10 → 7 → 9 → 0; 0 → 2 → 6 → 4 → 0; 0 → 8 → 0; 0 → 3 → 0; 0 → 1 → 0; 0 → 5 → 0	29240
7	[40, 40, 25, 25, 15, 15, 2]	0 → 10 → 7 → 9 → 0; 0 → 2 → 6 → 4 → 0; 0 → 8 → 0; 0 → 3 → 0; 0 → 1 → 0; 0 → 5 → 0	29240

Table 6: The results without time-window constraints.

Fleet size	Limited capacity	The vehicle route	Total transportation cost
2	[40, 40]	0 → 2 → 6 → 7 → 9 → 8 → 0; 0 → 10 → 5 → 1 → 3 → 4 → 0	38800
3	[40, 40, 25]	0 → 10 → 7 → 9 → 4 → 0; 0 → 2 → 6 → 8 → 0; 0 → 3 → 1 → 5 → 0	33350
4	[40, 40, 25, 25]	0 → 6 → 2 → 8 → 0; 0 → 10 → 7 → 9 → 0; 0 → 1 → 5 → 4 → 0; 0 → 3 → 0	31000
5	[40, 40, 25, 25, 15]	0 → 10 → 7 → 9 → 0; 0 → 6 → 2 → 5 → 0; 0 → 8 → 0; 0 → 1 → 4 → 0; 0 → 3 → 0	29400
6	[40, 40, 15, 15, 25, 25]	0 → 2 → 6 → 4 → 0; 0 → 10 → 7 → 9 → 0; 0 → 3 → 0; 0 → 8 → 0; 0 → 5 → 0; 0 → 1 → 0	29200
7	[40, 40, 25, 25, 15, 15, 2]	0 → 10 → 7 → 5 → 0; 0 → 6 → 2 → 9 → 0; 0 → 8 → 0; 0 → 3 → 0; 0 → 1 → 0; 0 → 4 → 0	29200

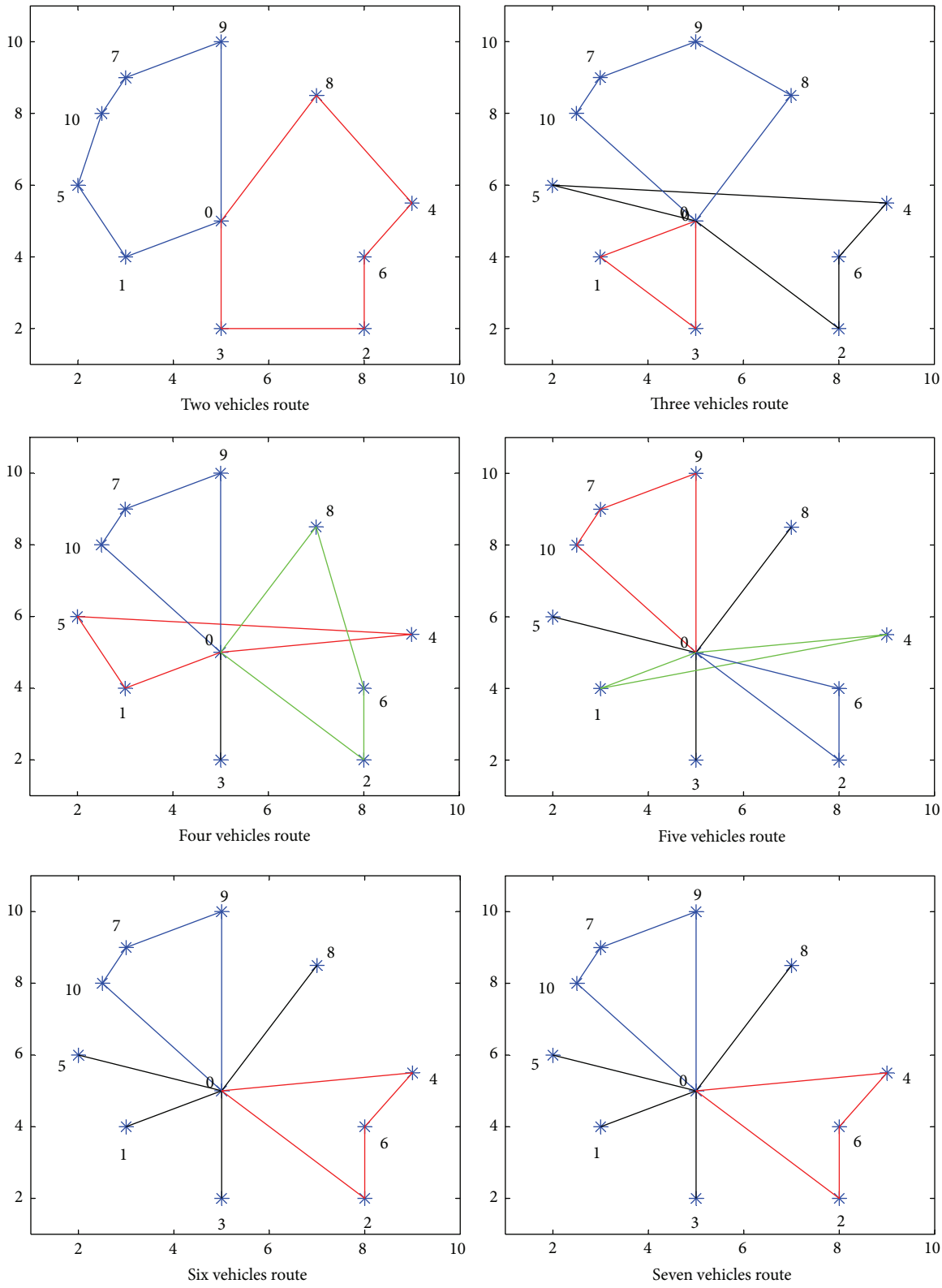

Figure 4: The vehicle routes with time-window constraints of different fleet sizes.

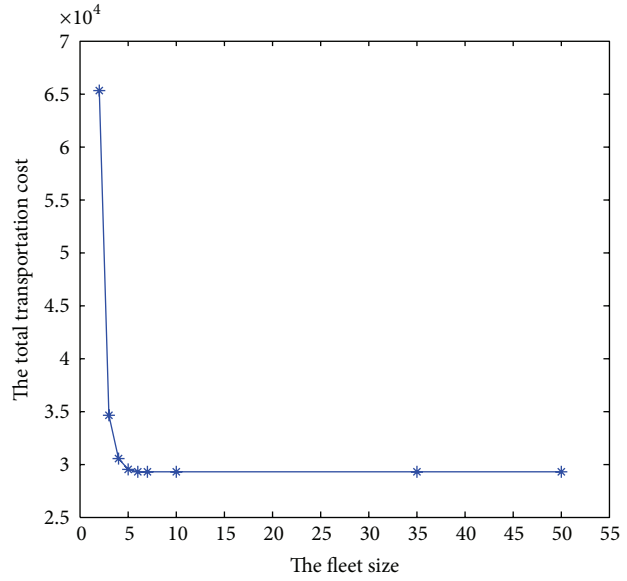

Figure 5: The trade-off relationship between fleet size and total transportation cost.

found that these two objectives conflict with each other, and the total transportation cost is reduced as the fleet size is increased. The reason for this is that the transportation weight is a dominant part of transportation cost. However, transportation cost reduction decreases gradually with the increase of fleet size. When the fleet size is six, the transportation cost is at a minimum and will not change further if the fleet size keeps increasing. This situation may be due to fuel consumption, driver salaries, or vehicle maintenance costs, which increase transportation cost.

Based on these findings, this paper emphasizes that the number of vehicles involves separate objectives, beyond the total cost of traveling. This is because there is a cost associated with having more vehicles, and considering this in different cases is important. In some cases when a vehicle and its associated costs (namely, manpower costs, fuel consumptions cost, etc.) are negligible, the routing plan will be irrational. This model represents a range of possible answers, with different numbers of vehicles and costs, with which a decision-maker can decide which kind of solution is preferable.

5. Conclusion

In this paper, we have considered a transportation cost problem with time-window constraints as a biobjective problem in which the size of a fleet of vehicles and total transportation costs are minimized, while capacity and time-window constraints are not violated. This paper uses a modified algorithm approach to solve this transportation cost problem. The proposed GA employs a string of customer identifiers, which represent the sequence of deliveries that must cover a vehicle during its route. Each vehicle identifier represents a separator between two different routes in the chromosome. A selection mechanism is then used to select prospective parents based on their fitness, as computed by an evaluation function. In this paper, the selected parent chromosomes are then recombined via a crossover operator to create a potential new population. A special mutation is applied to introduce a level of randomness that will preserve the GA from converging to a local optimum.

Finally, the algorithm is applied to solve an enterprise transportation problem for S logistics. In the last part of this paper, we compare two results (results with time-window constraints and results without time-window constraints). Based on the gap between these two situations, we find that the total transportation cost with time-window constraints is higher than the transportation cost without time-window constraints. In addition, time-window constraints also change vehicle routes during transportation.

Through an analysis of the case, we also find that total transportation cost and fleet size conflict with one another and that the total transportation cost is reduced as fleet size is increased. The results with time-window constraints are clearly comparable, and the decision-maker for S can decide which vehicle route is more preferable based on specific preferences. Thus, it is important for logistics enterprises' decision-makers to ensure that the sizes of their fleets of vehicles are appropriate.

Conflict of Interests

The authors declare that there is no conflict of interests regarding the publication of this paper.

Acknowledgments

The authors are indebted to Delfim F. M. Torres (Editor) and the two anonymous referees of the journal for their most helpful comments ever. This research is supported by the project of the production-study-building for joint training of graduate students in Beijing.

References

[1] P. McCann, "A proof of the relationship between optimal vehicle size, haulage length and the structure of distance-transport costs," *Transportation Research Part A: Policy and Practice*, vol. 35, no. 8, pp. 671–693, 2001.

[2] C. Pilot and S. Pilot, "A model for allocated versus actual costs in assignment and transportation problems," *European Journal of Operational Research*, vol. 112, no. 3, pp. 570–581, 1999.

[3] A. Jha, K. Somani, M. K. Tiwari, F. T. S. Chan, and K. J. Fernandes, "Minimizing transportation cost of a joint inventory location model using modified adaptive differential evolution algorithm," *International Journal of Advanced Manufacturing Technology*, vol. 60, no. 1–4, pp. 329–341, 2012.

[4] S. Chanas and D. Kuchta, "A concept of the optimal solution of the transportation problem with fuzzy cost coefficients," *Fuzzy Sets and Systems*, vol. 82, no. 3, pp. 299–305, 1996.

[5] S. Prakash, P. Kumar, B. V. N. S. Prasad, and A. Gupta, "Pareto optimal solutions of a cost-time trade-off bulk transportation problem," *European Journal of Operational Research*, vol. 188, no. 1, pp. 85–100, 2008.

[6] A. Ojha, S. K. Mondal, and M. Maiti, "Transportation policies for single and multi-objective transportation problem using fuzzy logic," *Mathematical and Computer Modelling*, vol. 53, no. 9-10, pp. 1637–1646, 2011.

[7] G. B. Dantzig and R. H. Ramser, "The truck dispatching problem," *Management Science*, vol. 6, no. 1, pp. 80–91, 1959.

[8] G. B. Alvarenga, G. R. Mateus, and G. de Tomi, "A genetic and set partitioning two-phase approach for the vehicle routing problem with time windows," *Computers & Operations Research*, vol. 34, no. 6, pp. 1561–1584, 2007.

[9] K. Ghoseiri and S. F. Ghannadpour, "Multi-objective vehicle routing problem with time windows using goal programming and genetic algorithm," *Applied Soft Computing Journal*, vol. 10, no. 4, pp. 1096–1107, 2010.

[10] F. Al-Khayyal and S.-J. Hwang, "Inventory constrained maritime routing and scheduling for multi-commodity liquid bulk. Part I. Applications and model," *European Journal of Operational Research*, vol. 176, no. 1, pp. 106–130, 2007.

[11] B. Yu, Z. Z. Yang, and B. Z. Yao, "A hybrid algorithm for vehicle routing problem with time windows," *Expert Systems with Applications*, vol. 38, no. 1, pp. 435–441, 2011.

[12] T.-C. Chiang and W.-H. Hsu, "A knowledge-based evolutionary algorithm for the multiobjective vehicle routing problem with time windows," *Computers and Operations Research*, vol. 45, pp. 25–37, 2014.

[13] B. Ombuki, B. J. Ross, and F. Hanshar, "Multi-objective genetic algorithms for vehicle routing problem with time windows," *Applied Intelligence*, vol. 24, no. 1, pp. 17–30, 2006.

[14] D. Pisinger and S. Ropke, "A general heuristic for vehicle routing problems," *Computers & Operations Research*, vol. 34, no. 8, pp. 2403–2435, 2007.

[15] H. I. Calvete, C. Galé, M.-J. Oliveros, and B. Sánchez-Valverde, "A goal programming approach to vehicle routing problems with soft time windows," *European Journal of Operational Research*, vol. 177, no. 3, pp. 1720–1733, 2007.

[16] S. Elloumi and P. Fortemps, "A hybrid rank-based evolutionary algorithm applied to multi-mode resource-constrained project scheduling problem," *European Journal of Operational Research*, vol. 205, no. 1, pp. 31–41, 2010.

Hindawi Publishing Corporation
Discrete Dynamics in Nature and Society
Volume 2015, Article ID 420581, 11 pages
http://dx.doi.org/10.1155/2015/420581

Research Article

Modeling Mixed Bicycle Traffic Flow: A Comparative Study on the Cellular Automata Approach

Dan Zhou, Sheng Jin, Dongfang Ma, and Dianhai Wang

College of Civil Engineering and Architecture, Zhejiang University, Hangzhou 310058, China

Correspondence should be addressed to Sheng Jin; jinsheng@zju.edu.cn

Received 10 December 2014; Revised 29 April 2015; Accepted 30 April 2015

Academic Editor: Tetsuji Tokihiro

Simulation, as a powerful tool for evaluating transportation systems, has been widely used in transportation planning, management, and operations. Most of the simulation models are focused on motorized vehicles, and the modeling of nonmotorized vehicles is ignored. The cellular automata (CA) model is a very important simulation approach and is widely used for motorized vehicle traffic. The Nagel-Schreckenberg (NS) CA model and the multivalue CA (M-CA) model are two categories of CA model that have been used in previous studies on bicycle traffic flow. This paper improves on these two CA models and also compares their characteristics. It introduces a two-lane NS CA model and M-CA model for both regular bicycles (RBs) and electric bicycles (EBs). In the research for this paper, many cases, featuring different values for the slowing down probability, lane-changing probability, and proportion of EBs, were simulated, while the fundamental diagrams and capacities of the proposed models were analyzed and compared between the two models. Field data were collected for the evaluation of the two models. The results show that the M-CA model exhibits more stable performance than the two-lane NS model and provides results that are closer to real bicycle traffic.

1. Introduction

Traffic flow theories are generally divided into two branches: macroscopic and microscopic theories [1]. The macroscopic traffic flow models are based on fluid dynamics and are mostly used to elucidate the relationships between density, volume, and speed (also called the fundamental diagram) in various traffic conditions. The microscopic traffic models, on the other hand, describe the interaction between individual vehicles. The microscopic traffic models generally include car-following models and cellular automata (CA) models. The car-following model is the most important model, describing the detailed movements of vehicles proceeding close together in a single lane. There have been many car-following models produced in the literature over the past 60 years, such as stimulus-response models, safety distance models, action point models, fuzzy-logic-based models, and optimal velocity models [2–5]. For a broader review, refer to Brackstone and McDonald [6] and Chowdhury et al. [7]. Recently, CA models have emerged as an efficient tool for simulating highway traffic flow because of their easy concept, simple rule, and speed in conducting numerical investigations. The rule-184 model, proposed by Wolfram [8], was the first CA model to be widely used for traffic flow. Nagel and Schreckenberg [9] presented the well-known NS CA model, which is an extension of the rule-184 model allowing the maximal speed of vehicles to be more than one cell/s. The NS model and the many improved versions of it reproduce some basic and complicated phenomena such as stop and go, metastable states, capacity drop phenomena (which means the capacity of road experiences a large drop under critical density conditions), and synchronized flow in real traffic conditions.

Most of the aforementioned microscopic traffic models have been developed only for motorized vehicles. Few of them have been used for modeling non-motorized vehicles such as bicycles, tricycles, electric bicycles, and motorcycles because of the complicated characteristics of such vehicles movements. With the increasing usage of bicycles, some researchers have begun focusing on modeling the operation of bicycle facilities. Jiang et al. [10] introduced two different multivalue CA (M-CA) models in order to model bicycle

flow. Their simulation results showed that, once the randomization effect is considered, the multiple states in deterministic M-CA models disappear and unique flow-density relations exist. They found the transition from free flow to congested flow to be smooth in one model but of second order in the other. Lan and Chang [11] developed inhomogeneous CA models to elucidate the interacting movements of cars and motorcycles in mixed traffic contexts. The car and motorcycle were represented by nonidentical particle sizes, respectively, occupying 6×2 and 2×1 cell units, each of size 1.25×1.25 meters. The CA models were validated by a set of field-observed data and the relationships between flow, cell occupancy (a proxy of density), and speeds under different traffic mixtures and road (lane) widths were elaborated. A M-CA model for mixed bicycle flow was proposed by Jia et al. [12]. Two types of bicycles, with different maximum speeds (1 cell/s and 2 cells/s), were considered in the system. Different results were analyzed and investigated under both deterministic and stochastic regimes. Li et al. [13] presented a multivalue cellular model for mixed nonmotorized traffic flow composed of bicycles and tricycles. A bicycle was assumed to occupy one unit of cell space and a tricycle two units of cell space. The simulation results showed the multiple state effect of mixed traffic flow. Gould and Karner [14] proposed a two-lane inhomogeneous CA simulation model, an improved version of the NS model combining a lane-changing rule, for bicycle traffic, and collected field data from three UC Davis bike paths for comparison with a simulation model. Yang et al. [15] proposed an extended multivalue CA model that permitted the bicycles to move at faster speeds. The simulation results showed that the mixed nonmotorized traffic capacity increased with an increase in the electric bicycle ratio. Zhang et al. [16] used an improved three-lane NS model to analyze the speed-density characteristics of mixed bicycle flow. The simulation results of the CA model were effectively consistent with the actual survey data when the density was lower than 0.225 bic/m^2.

Summarizing the above, none of the aforementioned car-following models have been devoted to mixed traffic with regular bicycles (RBs) and electric bicycles (EBs), but CA models have been widely used for modeling nonmotorized traffic. The modeling of mixed bicycle traffic using CA models can be divided into two branches: NS CA model and M-CA model approaches. The update rules of the NS CA model for bicycle flow are the same as for motorized vehicles, with only the cell size and bicycle speeds being different. As pointed out by Jiang et al. [10] and Jia et al. [12], the M-CA model is more suitable than the NS model for modeling bicycle traffic flow. Because the update rules of the M-CA model do not include direct car-following and lane-changing behavior, it may be appropriate for modeling the nonlane-based behavior of bicycle traffic. The NS CA model and M-CA model have been used for modeling bicycle traffic and mixed bicycle traffic with RBs and EBs. However, there is no evidence in the existing literature as to which model is better for modeling mixed traffic flow, nor as to the differences between these two models. Therefore, a comparison of the NS CA model and the M-CA model in terms of their ability to model mixed bicycle traffic is required so that CA models can be improved efficiently.

This paper attempts to develop two CA models to describe the behaviors of mixed bicycle traffic with RBs and EBs on a separated bicycle path and to compare the characteristics of the NS CA model and the M-CA model. The remaining parts are organized as follows. Section 2 introduces the development of NS and M-CA rules. Section 3 presents the simulation results of these two CA models. Section 4 further discusses differences in the simulation results. Finally, the conclusions and ideas for future studies are addressed.

2. CA Models

2.1. Definition of Cell Size and Bicycle Speed. The main differences encountered when modeling bicycle traffic as opposed to motorized vehicle traffic using a CA model are the cell size and the speed. Mixed bicycle traffic with RBs and EBs on separated bicycle paths is ubiquitous in many Asian countries, such as China, Vietnam, Indonesia, and Malaysia. Because of the different operating speeds of RBs and EBs, mixed traffic produces complicated behavior and characteristics that are likely to lead to safety and efficiency problems. Modeling mixed bicycle traffic is very important for the planning, operation, and management of bicycle facilities. Based on the behavior of cyclists, CA models are the best option for modeling bicycle traffic. The size of cell space and the update rules are two significant aspects of CA models.

Bicycles are shorter and narrower than motorized vehicles. Based on field surveys, the length of most RBs and EBs is 1.7–1.9 m. Meanwhile, bicycle lanes are set at 1 meter wide in both China and the USA [17, 18]. Therefore, the size of a RB or an EB is assumed rectangular, with length 2 m and width 1 m, as is widely used in other CA models [14–16]. The other parameter for modeling bicycle traffic is speed. According to the literature, the reported free flow speed of EBs is larger than that of RBs. Accordingly, in this paper speeds of 2 cells/s (4 m/s or 14.4 km/h) and 3 cells/s (6 m/s or 21.6 km/h) were chosen for RBs and EBs, respectively.

2.2. NS CA Model. The NS CA model used in this paper was proposed by Nagel and Schreckenberg [9]. This model is very widely used in modeling highway traffic and bicycle traffic. The NS CA model includes a car-following rule and a lane-changing rule. The car-following rule is based on four steps, and the lane-changing rule is based on the work of Rickert et al. [19]. Different vehicle behavior rules would lead to different simulation results. With an increase in the number of lanes, the lane-changing logic would become more complicated and make modeling more difficult. Therefore, in this paper only a two-lane bicycle path is simulated and used in the comparison. In the time interval from t to $t+1$, the four basic rules of the NS model evolve according to the following steps.

Step 1 (longitudinal acceleration). Consider

$$v_i(t+1) = \min\left(v_i(t) + 1, v_{i\max}\right), \quad (1)$$

where $v_i(t)$ is the speed of the ith bicycle at updating time t. $v_{i\max}$ is the maximum speed of the ith bicycle. This corresponds to the cyclists' realistic free flow speed.

Step 2 (longitudinal deceleration). Consider

$$v_i(t+1) = \min\left(v_i(t), \text{gap}_i\right), \tag{2}$$

where gap_i is the distance between the ith bicycle and the bicycle in front of it, at updating time t. This step ensures that the bicycle stays safe with no collisions.

Step 3 (random slowing down). Consider

$$v_i(t+1) = \max\left(v_i(t) - 1, 0\right) \quad \text{if rand}() < p_{di}, \tag{3}$$

where rand() is a uniformly distributed random number between 0 and 1 and p_{di} is the random slowing down probability of the ith bicycle. The random slowing down effect, which captures one cyclist's braking maneuver due to a random event (e.g., accident, road, or weather related factors), is one of the most significant parameters of the CA model. This step incorporates the idea of random effects on bicycles that may cause them to slow down.

Step 4 (motion). Consider

$$x_i(t+1) = x_i(t) + v_i(t+1), \tag{4}$$

where $x_i(t)$ is the position of the ith bicycle at time t.

The lane-changing logic is shown below. Before the acceleration step, both lanes are examined to evaluate lane-changing opportunities. The following conditions are checked for each bicycle and must be true in order for it to change lanes.

(1) The speed of the bicycle currently in ith position is larger than or equal to the cell distance to the next bicycle. This condition ensures that this bicycle will need to slow down at the next update:

$$v_i(t) \geq \text{gap}_i(t). \tag{5}$$

(2) The distance to the next bicycle in the lane adjacent to the lane of the ith bicycle ($\text{gap}_i^f(t)$) is larger than the distance to the next bicycle in its current lane ($\text{gap}_i(t)$). This condition ensures that a benefit is derived from changing lanes:

$$\text{gap}_i^f(t) > \text{gap}_i(t). \tag{6}$$

(3) The distance to backward bicycle in the lane adjacent to that of the currently ith bicycle ($\text{gap}_i^b(t)$) is large enough. This condition ensures that, looking backwards, the closest bicycle in the adjacent lane is sufficiently far away:

$$\text{gap}_i^b(t) \geq \min\left[v_{i-1}^b(t) + 1, v_{i-1\max}^b\right]. \tag{7}$$

(4) A uniformly distributed random number between 0 and 1 is less than the probability of a lane change (p_t):

$$\text{rand}() < p_t. \tag{8}$$

$\text{gap}_i^f(t)$ and $\text{gap}_i^b(t)$ can be calculated as follows:

$$\begin{aligned} \text{gap}_i^f(t) &= x_{i+1}^f(t) - x_i(t) - 1 \\ \text{gap}_i^b(t) &= x_i(t) - x_{i-1}^b(t) - 1, \end{aligned} \tag{9}$$

where $x_{i-1}^b(t)$, $v_{i-1}^b(t)$, and $v_{i-1\max}^b(t)$ are the position, speed, and maximum speed of the nearest following bicycle in the lane adjacent to that of the ith bicycle.

The new speed for the bicycle currently in the ith position after lane-changing is calculated as follows:

$$v_i'(t+1) = \min\left[v_i(t) + 1, \text{gap}_i^f(t), v_{i\max}\right], \tag{10}$$

where $v_i'(t+1)$ is the speed of this bicycle after the lane-changing.

The motion of the lane-changing bicycle is

$$x_i'(t+1) = x_i(t) + v_i'(t+1), \tag{11}$$

where $x_i'(t+1)$ is the position of the bicycle after the lane-changing.

2.3. M-CA Model. A family of M-CA models has recently been proposed by Nishinari and Takahashi [20–22]. The basic version of the family is obtained from an ultradiscretization of Burgers' equation. Therefore, it is also called the Burgers CA (BCA). Previously, BCA models were proposed for highway traffic. Recent attempts have included BCA models purported to represent bicycle flow [12, 13] adapted for the unobvious car-following and lane-changing behavior in bicycle traffic. In order to make a comparison with the NS CA model, the M-CA model for mixed bicycle flow is improved upon in this paper.

The numbers of RBs and EBs in location j at time t are $U_j^r(t)$ and $U_j^e(t)$, respectively. As shown in Section 2.1, RBs with a maximum speed of 2 cells/s and EBs with a maximum speed of 3 cells/s are considered in the simulation systems. Therefore, the updating procedures are changed as follows:

(1) all bicycles in location j move to their next location $j+1$ if the location is not fully occupied, and EBs have priority over RBs;

(2) all bicycles that moved in procedure (1) can move to location $j+2$ if their next location is not fully occupied after procedure (1), and EBs again have priority over RBs;

(3) only EBs moved in procedure (2) can move to location $j+3$ if their next location is not fully occupied after procedure (2).

The numbers of RBs and EBs that move one location on from location j at time t in procedure (1) are $b_j^r(t)$ and $b_j^e(t)$, respectively. The numbers of RBs and EBs that move two locations on from location j at time t are $c_j^r(t)$ and $c_j^e(t)$, respectively. $d_j^e(t)$ represents the number of EBs that move three locations on from location j at time t. L is defined as the lane number of the simulation bicycle path. The randomization

effect on the RBs is introduced as follows: $c_j^r(t+1)$ decreases by 1 with probability p_{dr} if $c_j^r(t+1) > 0$. The randomization effect on the EBs is as follows: $d_j^e(t+1)$ decreases by 1 with probability p_{de} if $d_j^e(t+1) > 0$. The updating rules are as follows.

Step 1. Calculation of $b_j^r(t+1)$, $b_j^e(t+1)$, and $b_j(t+1)$ ($j = 1, 2, 3, \ldots, K$) is as follows:

$$b_j^e(t+1) = \min\left(U_j^e(t), L - U_{j+1}(t)\right) \tag{12}$$

$$b_j^r(t+1) = \min\left(U_j^r(t), L - U_{j+1}(t) - b_j^e(t+1)\right) \tag{13}$$

$$b_j(t+1) = b_j^r(t+1) + b_j^e(t+1). \tag{14}$$

Step 2. Calculation of $c_j^r(t+1)$, $c_j^e(t+1)$, and $c_j(t+1)$ is as follows:

$$c_j^e(t+1) = \min\left(b_j^e(t+1), L - U_{j+2}(t) - b_{j+1}(t+1) + b_{j+2}(t+1)\right) \tag{15}$$

$$c_j^r(t+1) = \min\left(b_j^r(t+1), L - U_{j+2}(t) - b_{j+1}(t+1) + b_{j+2}(t+1) - c_j^e(t+1)\right). \tag{16}$$

If rand() $< p_{dr}$, then

$$c_j^r(t+1) = \max\left(c_j^r(t+1) - 1, 0\right)$$
$$c_j(t+1) = c_j^r(t+1) + c_j^e(t+1). \tag{17}$$

In (12) and (15), $b_j^e(t+1)$ and $c_j^e(t+1)$ are calculated first because the EBs have priority over the RBs.

Step 3. Calculation of $d_j(t+1)$ is as follows:

$$d_j(t+1) = \min\left(c_j^e(t+1), L - U_{j+3}(t) - b_{j+2}(t+1) + b_{j+3}(t+1) - c_{j+1}(t+1) + c_{j+2}(t+1)\right). \tag{18}$$

If rand() $< p_{de}$, then

$$d_j(t+1) = \max\left(d_j(t+1) - 1, 0\right). \tag{19}$$

Step 4. Update $U_j^r(t+1)$, $U_j^e(t+1)$, and $U_j(t+1)$:

$$\begin{aligned} U_j^e(t+1) &= U_j^e(t) - b_j^e(t+1) + b_{j-1}^e(t+1) \\ &\quad - c_{j-1}^e(t+1) + c_{j-2}^e(t+1) \\ &\quad - d_{j-2}(t+1) + d_{j-3}(t+1) \\ U_j^r(t+1) &= U_j^r(t) - b_j^r(t+1) + b_{j-1}^r(t+1) \\ &\quad - c_{j-1}^r(t+1) + c_{j-2}^r(t+1) \\ U_j(t+1) &= U_j^r(t+1) + U_j^e(t+1), \end{aligned} \tag{20}$$

where rand() is a uniformly distributed random number between 0 and 1.

3. Simulation Results

For the comparison of the NS CA model against the M-CA model, the simulation parameters in both models should be set to the same values. In the simulations, a two-lane bicycle path ($L = 2$) was selected with length $K = 500$ cells (equal to 1000 m). In the initial conditions, RBs and EBs are randomly distributed on the road using the same random number for both models. The default values of the random slowing down probability (p_d), the probability of a lane change (p_t), and the proportion of EBs (p_e) are 0.2, 0.8, and 0.5, respectively, for the NS CA model (as in previous studies [14]). The default values of the random slowing down probability of RBs (p_{dr}), the random slowing down probability of EBs (p_{de}), and the proportion of EBs are 0.4, 0.4, and 0.5, respectively, for the M-CA model. In the M-CA model, the slowing down probability is the probability that the number of bicycles ($c_j^r(t+1)$) decreases, which means that one bicycle decreases its speed. In this paper, the simulation is based on two lanes ($L = 2$). Therefore, the maximum value of $c_j^r(t+1)$ is 2. If $c_j^r(t+1) = 0$, no bicycle slows down, and the slowing down probability of any bicycle is zero. If $c_j^r(t+1) = 1$, only one bicycle slows down, with probability p. If $c_j^r(t+1) = 2$, this means only one bicycle may slow down with probability p; therefore, the total slowing down probability of bicycles is $0.5p$. By summing the above three cases, we assume these three cases have the same percentage. Therefore, the mean of the three cases' slowing down probabilities is $(0 + p + 0.5p)/3 = 0.5p$. In order to compare the two models, we used a default value for the random slowing down probability for the M-CA model of half that for the NS CA model.

Periodic conditions that are as close as possible to the actual conditions are used so that the bicycles ride on a circuit. The instantaneous positions and speeds for all particles are updated in parallel, per second. The flow, speed, and density of the mixed bicycle traffic flow can be calculated after a given amount of time (20000 simulation steps) [15], and the averages over the last 5000 steps are used for the calculation in order to decrease the random effect.

3.1. Results of the NS CA Model. In order to show the different characteristics of the NS CA model under different model parameters, speed-density and flow-density plots (the fundamental diagram of bicycle traffic flow) were created so that the results could be analyzed. Example plots are shown in Figures 1, 2, and 3. When $p_d = 0$, it is a deterministic case, while $p_d \neq 0$ is a stochastic case. From Figure 1, it can be seen that, with an increase in the slowing down probability p_d, the fundamental diagrams drop quickly, which means that the capacity of the bicycle lane drops quickly with an increase in p_d. When the slowing down probability p_d is equal to one, the stopped RBs will lead bicycle traffic flow to jam, and the speed and flow will both be zero.

Figure 2 shows the speed-density and flow-density relationships under different lane-changing probabilities. In the low-density region, with an increase in the lane-changing probability, the speed of bicycle flow increases. In the high-density region, the speeds of bicycle flow under different

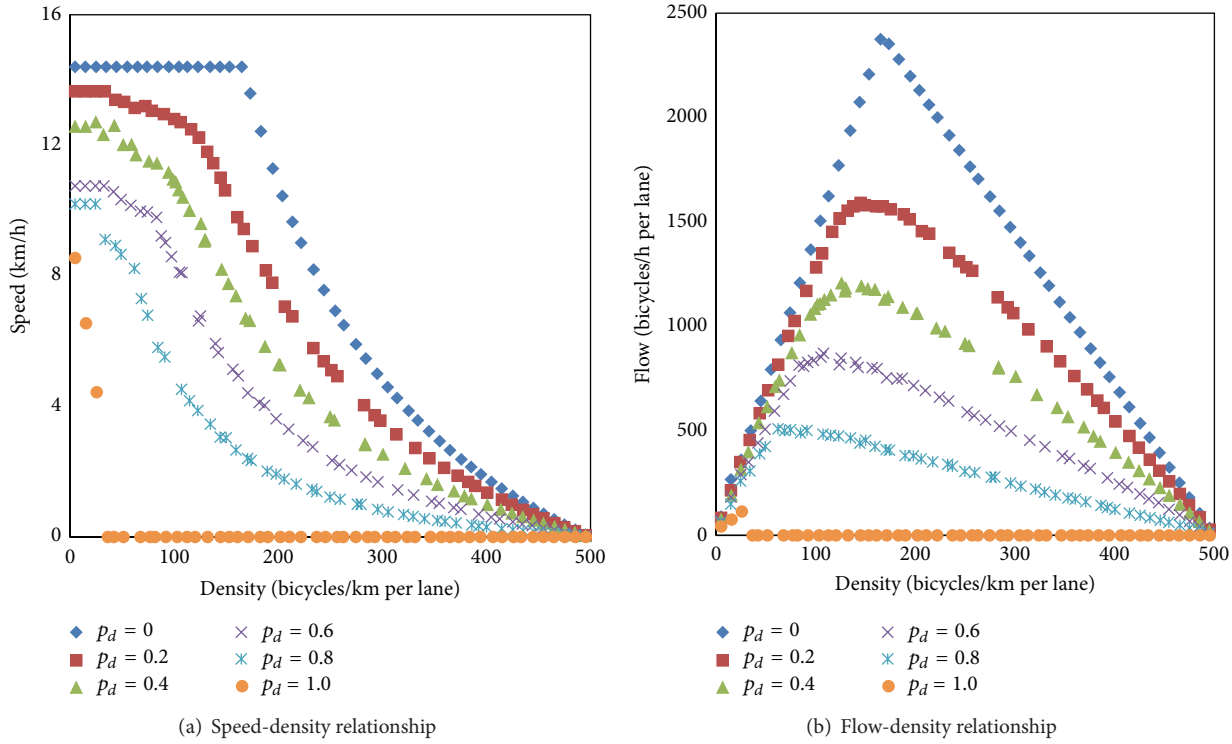

(a) Speed-density relationship (b) Flow-density relationship

FIGURE 1: Speed-density and flow-density relationships under different slowing down probabilities when $p_t = 0.8$ and $p_e = 0.5$.

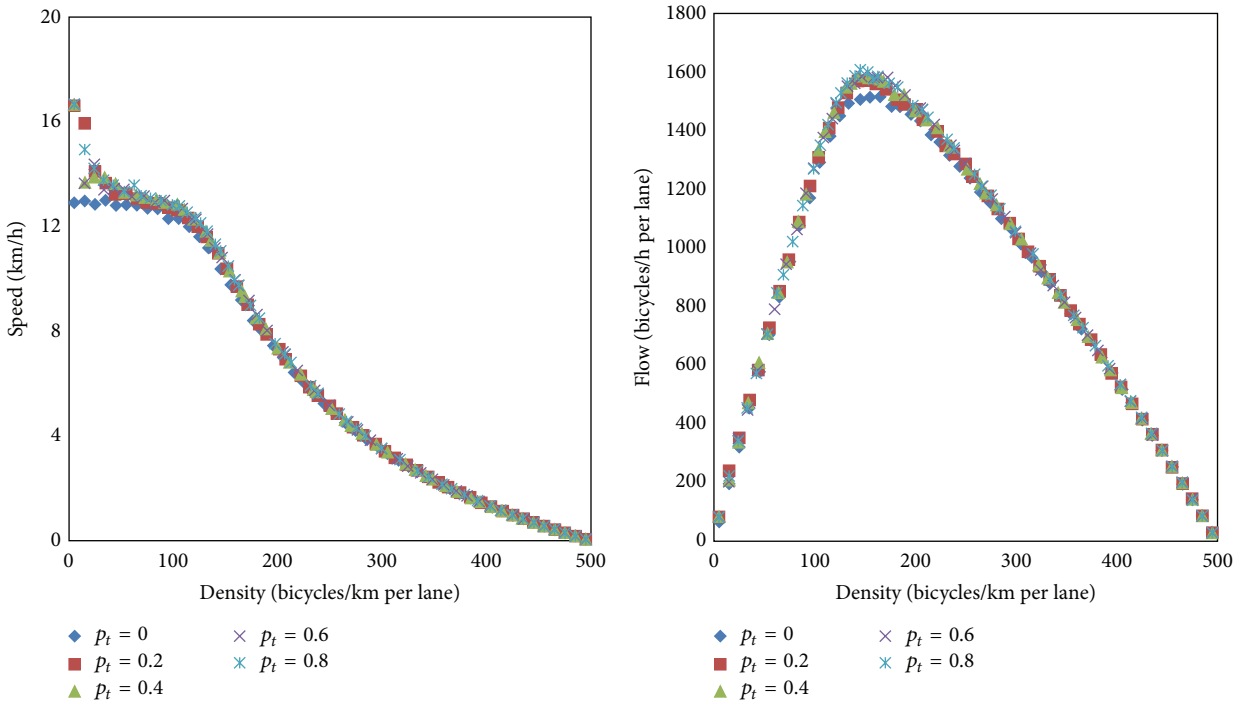

(a) Speed-density relationship (b) Flow-density relationship

FIGURE 2: Speed-density and flow-density relationships under different lane-changing probabilities when $p_d = 0.2$ and $p_e = 0.5$.

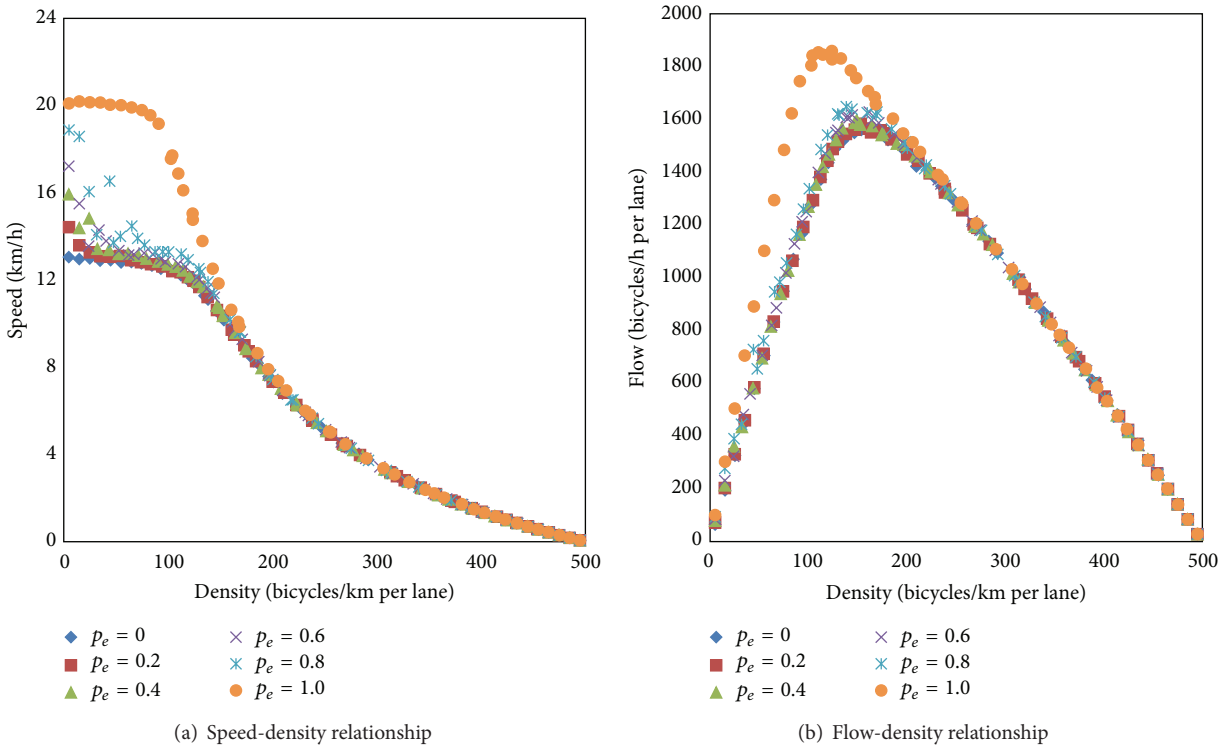

(a) Speed-density relationship

(b) Flow-density relationship

FIGURE 3: Speed-density and flow-density relationships under different proportions of EBs when $p_d = 0.2$ and $p_t = 0.8$.

lane-changing probabilities show smaller differences than in the low-density region. This is due to using the motorized vehicle lane-changing rule for bicycle traffic flow. The lane-changing rule proposed in this paper is very strictly based on gap acceptance theory, and the looking-backward gap should be large in order for lane-changing to happen. However, the driving behavior of bicycles is very different from that of motorized vehicles. The lane-changing rule for motorized vehicles will restrict the lane-changing behavior of higher-speed bicycles (such as EBs in this case) and lead to no significant differences between the fundamental diagrams for different lane-changing probabilities.

The proportion of EBs is one of the most important parameters for mixed bicycle traffic flow. Figure 3 shows the fundamental diagrams for different proportions of EBs in the mixed traffic. It can be seen that, with an increase in the proportion of EBs, speed and capacity increase because of the EBs' higher free flow speed compared to the RBs. Another finding observable in Figure 3 is that, when p_e is small, the influence on capacity is small, and with the increase in p_e, the influence of p_e on capacity becomes larger. This means that the influence of EBs on the bicycle lane capacity is not linear, which may be due to the existence of lower-speed RBs and the strict lane-changing rule, which deter EBs from changing lanes and increasing their speed.

3.2. Results of the M-CA Model. This section presents the simulation results of the M-CA model. In order to compare the results with those of the NS CA model, the slowing down probabilities of RBs and EBs are set to the same value of 0.4. Therefore, only two parameters, p_d and p_e, are analyzed in this simulation case. Figure 4 shows the fundamental diagrams under different p_d values. Similarly to the NS CA model, the capacities drop with the increase in the slowing down probability. However, the capacity drops of the M-CA model are smaller than those of the NS CA model, as will be discussed in detail in the next section.

From Figure 5(a), in the low-density region (density < 200 bicycles/km per lane), the bicycle flow is in the free flow state and most bicycles move independently. Therefore, the average speed of the system equals the free flow speed of mixed bicycles, which increases with the proportion of EBs. As can be seen in Figure 5(b), similar to the case of the NS CA model, with an increase in the proportion of EBs, the bicycle capacity also increases. It is easy to see that the free flow speed of all bicycles will increase with the proportion of EBs. The simulation results from the NS CA model and the M-CA model show the same findings.

4. Discussion

Most of the previous studies on CA models for mixed bicycle flow discuss multiple states and the transition from free flow to congested flow. However, the choice of an appropriate CA model for simulating bicycle traffic is more important than model analysis and calibration. Therefore, we should compare the simulation results of the two CA models presented above and try to draw conclusions about the selection of a CA model.

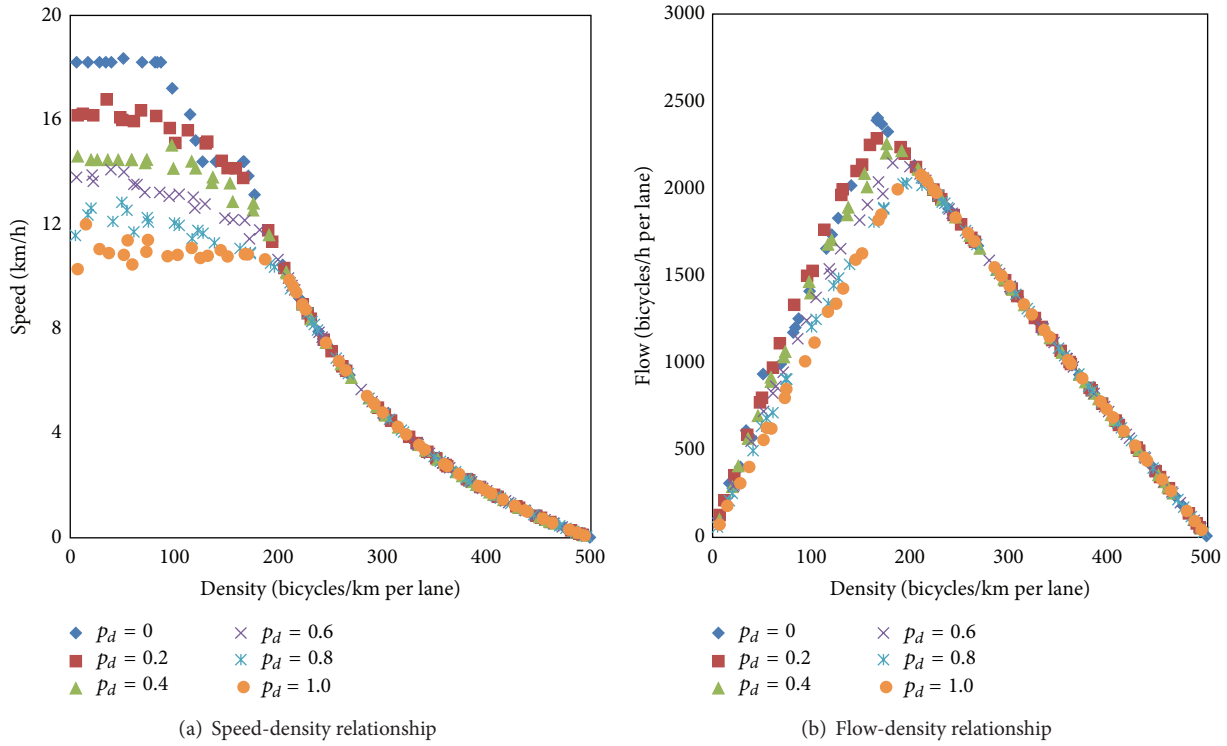

(a) Speed-density relationship (b) Flow-density relationship

FIGURE 4: Speed-density and flow-density relationships under different slowing down probabilities of RBs and EBs when $p_e = 0.5$.

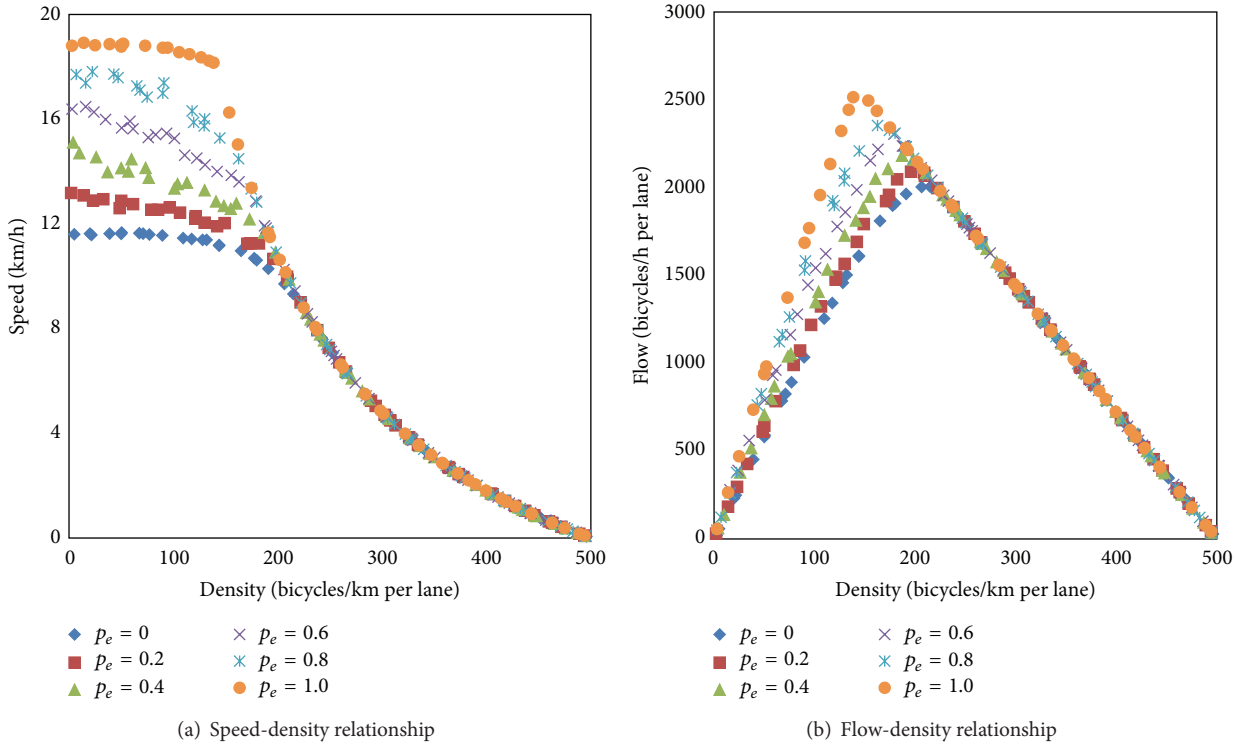

(a) Speed-density relationship (b) Flow-density relationship

FIGURE 5: Speed-density and flow-density relationships under different proportions of EBs when $p_d = 0.4$.

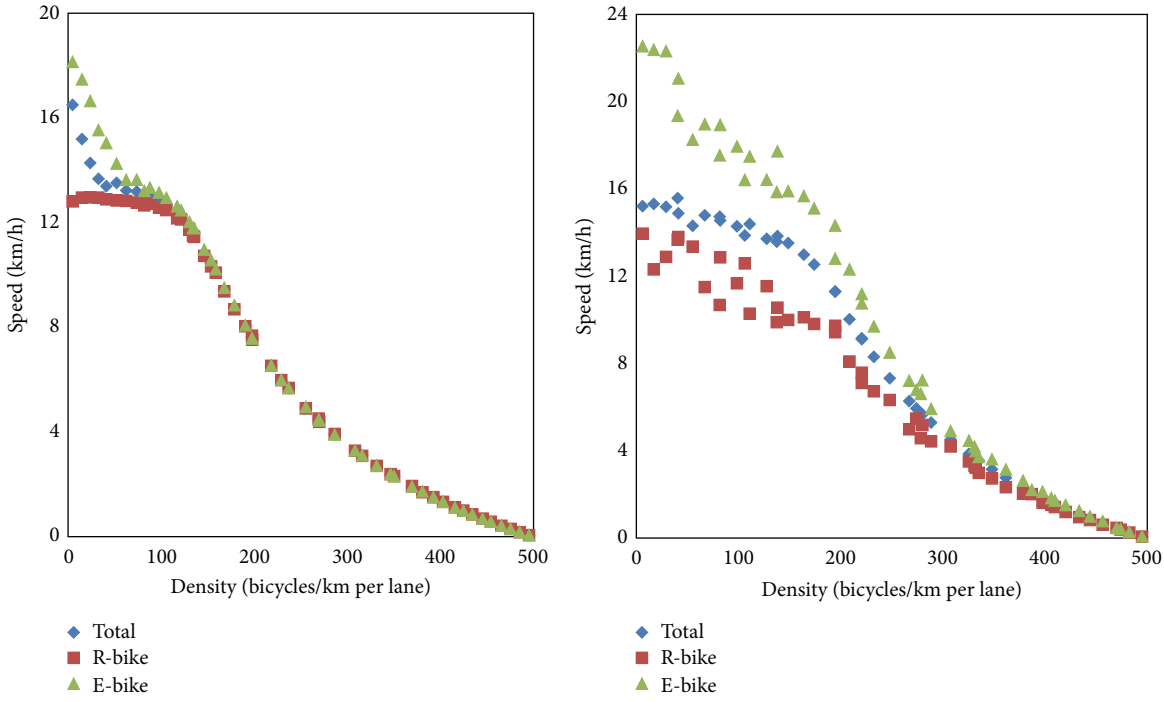

(a) NS CA model (b) M-CA model

Figure 6: Speed-density relationships for different bicycle types.

Because the capacity is a significant parameter for bicycle lane planning and management, capacity and fundamental diagrams can be used for evaluating the CA models [23]. The capacity is defined as the maximum flow under particular road conditions. In the fundamental diagram, the capacity is the peak of the fundamental diagram curve. For simplicity, due to the fact that the simulation densities of bicycle traffic flow cover all traffic conditions, we use the maximum flow of bicycles as the observed capacity of the bicycle path in this paper.

Figure 6 shows the comparisons of the speed-density relationships for the NS CA and M-CA models. It can easily be seen that, for the NS CA model, in the low-density region (approximately 100 bicycles/km per lane or fewer), the speeds of RBs and EBs are very different, while in the high-density region the speeds of RBs and EBs are almost equal. Similar conclusions are found for the M-CA model. However, the critical density distinguishing low from high density is nearly 300 bicycles/km per lane, much larger than that for the NS CA model. The results show that the lane-changing rule of the NS CA model enables the EBs hardly to pass the RBs and the speeds of both bicycle types to quickly become the same.

Figure 7 shows the simulated capacity values obtained from the maximum values of the fundamental diagrams. It can be seen that when the slowing down probability is zero (meaning that both models are deterministic CA models) the two CA models have the same capacity (NS CA model 2387 bicycles/h per lane; M-CA model 2375 bicycles/h per lane). With the increase in the slowing down probability, the capacities of both models drop linearly. Linear regression equations are also shown in Figure 7, and it can clearly be seen that there are strongly linear relationships between the capacities of the two models and the slowing down probabilities. However, the difference between the regression model slopes of the two models is large (−407.27 versus −2045.3). Therefore, when the slowing down probability of the M-CA model equals 1, which means that the slowing down probability of the NS CA model is nearly 0.5, the maximum volumes of the two models are very different (2000 versus 1000 bicycles/h per lane). This means that the slowing down probability has a greater influence on the NS CA model than the M-CA model.

The slowing down probability, as the most significant parameter of the CA model, describes the stochastic effects on bicycle traffic flow. Because of the strict lane-changing rule in the NS CA model, the EBs (fast bicycles) do not find it easy to change lanes and must follow the RBs, which leads to a very low capacity. However, the M-CA model has an implied lane-changing rule in the update rules which has less influence on capacity than in the NS CA model.

Field bicycle data were collected at Jiaogong Road in Hangzhou, China. The width of this bicycle path is 2.27 m, making it nearly a two-lane bicycle path. The field data cover all traffic conditions, and the EB percentages also cover a wide range. The average percentage of EBs is 60.3%, and the capacity of the bicycle path is defined as the maximum volume, with a 30-second sampling interval. Figure 8 shows the observed and simulated speed-density and flow-density relationships, where the percentage of EBs is set to 0.6 (equal to the field sample percentage) and other simulation

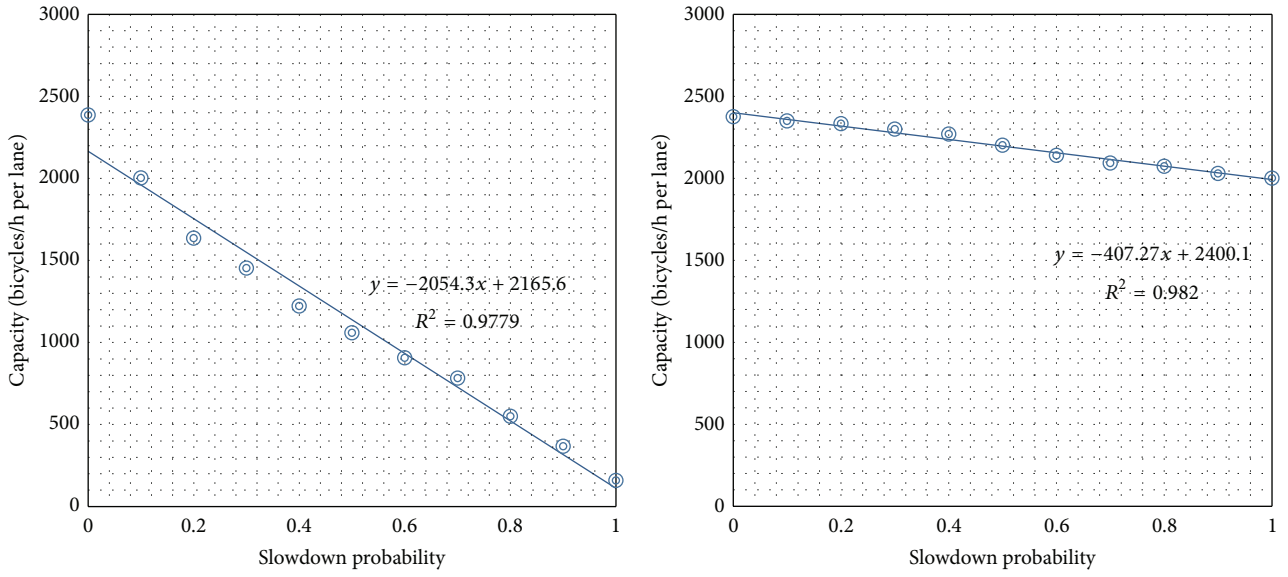

(a) NS CA model (b) M-CA model

Figure 7: Simulated capacities of two CA models under different slowing down probabilities.

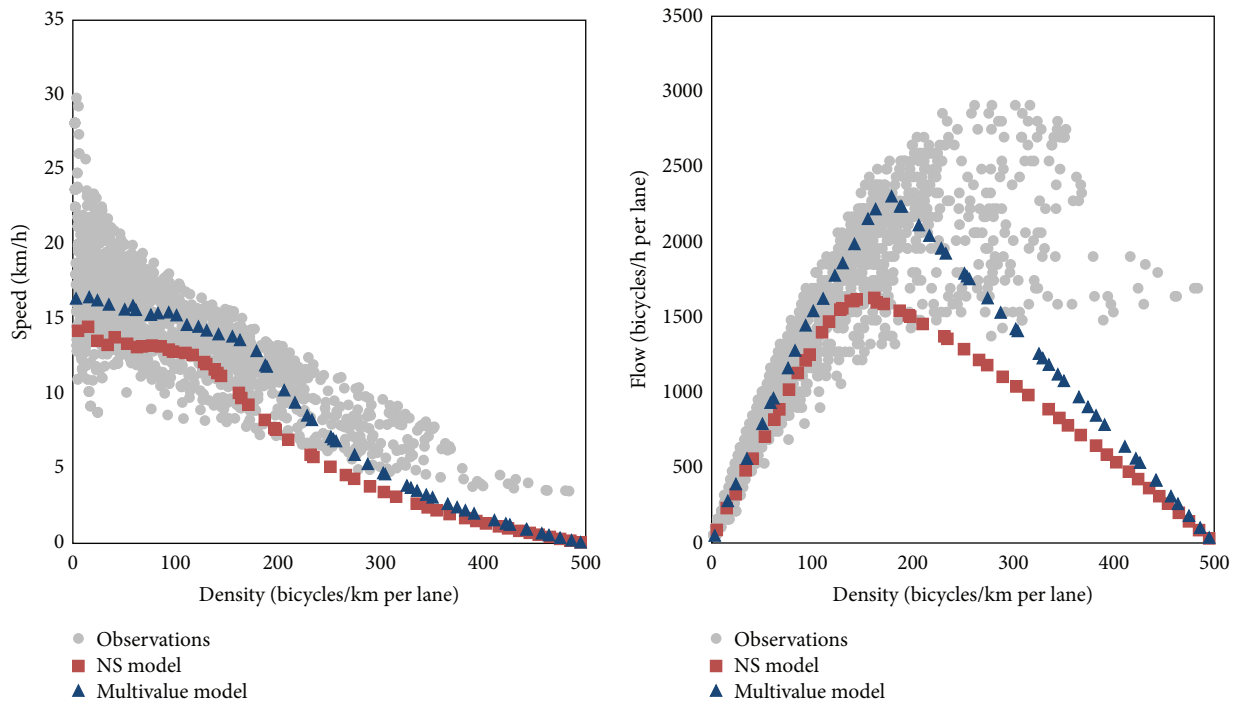

(a) Speed-density relationship (b) Flow-density relationship

Figure 8: Observed and simulated speed-density and flow-density relationships.

parameters are set to the default values presented above. The results imply that the M-CA model performs better than the NS model in fitting the field bicycle observations.

The proportion of EBs describes the proportion of fast bicycles in the mixed bicycle traffic, which affects the free flow speed and the capacity of the bicycle lane. Figure 9 shows the relationships between the proportion of EBs and the lane capacity from observed and simulated results. It can be seen that both models produce the same nonlinear relationship, and the correlation coefficients are both very high. When the proportion of EBs is low, the EBs must slow down their speed and follow the RBs. Therefore, the capacity slowly increases

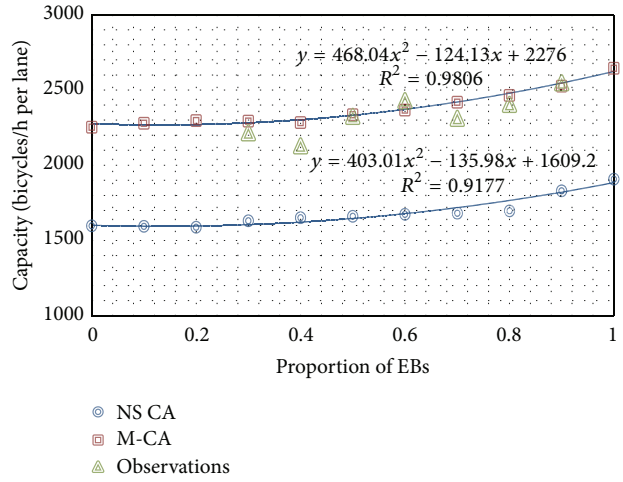

Figure 9: Observed and simulated capacities under different proportions of EBs.

with the proportion of EBs. When the proportion of EBs is large, lane-changing and passing occur more frequently, and the capacity increases quickly with the proportion of EBs. The simulated results of the M-CA model seem more consistent with the observed field bicycle capacity than those of the NS CA model. The root mean square error (RMSE) and the mean absolute percentage error (MAPE) [24, 25] of M-CA model are less than those of NS CA model.

Based on the above comparison and analysis, some conclusions can be drawn. Firstly, CA models can be used for bicycle traffic simulation because of their simple rules and quick simulation. The results for the fundamental diagrams and capacities (about 2000–2500 bicycles/h per lane) are similar to those from the field data and previous studies [26]. Secondly, the slowing down probability has a significant influence on the simulation results for both the NS CA model and the M-CA model. Meanwhile, with an increase in the slowing down probability, the capacity and speed drop more quickly in the NS CA model than in the M-CA model. This may be due to the lane-changing rule of NS CA models that restricts EBs in changing lanes and accelerating. Thirdly, the proportion of EBs in the mixed traffic flow affects the critical density and capacity in both the NS CA model and the M-CA model, as was also reported by some researchers [27, 28]. As the proportion of EBs moves from 0 to 1, the capacities of the NS CA model and the M-CA model increase 19.3% and 17.4%, respectively. Fourthly, for the NS CA model, the probability of lane-changing has less influence on the mixed traffic flow than does the slowing down probability, which may be due to the strict lane-changing rule leading to less lane-changing by bicycles. Lastly, the NS CA model is restricted for multilane bicycle path simulation because more bicycle lanes will lead to more complicated lane-changing rules that are hard to model and calibrate. In contrast, with the M-CA model it is easy to simulate a multilane bicycle path, by simply setting different L values. As can be seen from the above summary, the M-CA model provides more effective performance for modeling bicycle traffic and is more consistent with the field bicycle data than the NS CA model.

5. Conclusions

The modeling and simulation of mixed bicycle traffic flow are becoming increasingly significant because of the increased popularity of regular bicycles and electric bicycles in recent years, due to their greenness and convenience. This paper has proposed two improved CA models for bicycle traffic flow modeling and simulation and has compared their characteristics. The two-lane NS CA model and the multivalue CA model for mixed bicycle traffic flow were introduced and the same parameters set for both models so that a comparison could be made under the same conditions. Speed-density and flow-density relations were obtained so as to compare and analyze the models, and the capacities obtained from the simulation results were also compared under different model parameters. Field data collected from Hangzhou, China, were used for the evaluation of the proposed models. The results show that the M-CA model performs better than the NS CA model in simulating mixed bicycle traffic. The main difference between these two models is the lane-changing and slowing down probability rules, making it harder or easier for EBs to change lanes and accelerate to their free flow speed.

Because of the difficulty of collecting bicycle field data, especially in congested traffic conditions, the calibration and validation of the proposed model using field data were omitted from this paper, and only simulation results were analyzed and compared between the two models. Future work will focus on the calibration of the slowing down probabilities and lane-changing probabilities under different traffic conditions, so as to further validate and evaluate the proposed models.

Conflict of Interests

The authors declare that there is no conflict of commercial or associative interests regarding the publication of this work.

Acknowledgments

This work was supported by the National Natural Science Foundation of China (nos. 51338008, 51278454, 51208462, and 61304191), the Fundamental Research Funds for the Central Universities (2014QNA4018), the Projects in the National Science & Technology Pillar Program (2014BAG03B05), and the Key Science and Technology Innovation Team of Zhejiang Province (2013TD09).

References

[1] A. D. May, *Traffic Flow Fundamentals*, Prentice-Hall, Englewood Cliffs, NJ, USA, 1990.

[2] D. C. Gazis, R. Herman, and R. W. Rothery, "Nonlinear follow-the-leader models of traffic flow," *Operations Research*, vol. 9, no. 4, pp. 545–567, 1961.

[3] S. Jin, D.-H. Wang, Z.-Y. Huang, and P.-F. Tao, "Visual angle model for car-following theory," *Physica A: Statistical Mechanics and Its Applications*, vol. 390, no. 11, pp. 1931–1940, 2011.

[4] S. Jin, D.-H. Wang, and X.-R. Yang, "Non-lane-based car-following model with visual angle information," *Transportation Research Record: Journal of the Transportation Research Board*, no. 2249, pp. 7–14, 2011.

[5] S. Jin, D.-H. Wang, C. Xu, and Z.-Y. Huang, "Staggered car-following induced by lateral separation effects in traffic flow," *Physics Letters A*, vol. 376, no. 3, pp. 153–157, 2012.

[6] M. Brackstone and M. McDonald, "Car-following: a historical review," *Transportation Research F: Traffic Psychology and Behaviour*, vol. 2, no. 4, pp. 181–196, 1999.

[7] D. Chowdhury, L. Santen, and A. Schadschneider, "Statistical physics of vehicular traffic and some related systems," *Physics Reports*, vol. 329, no. 4–6, pp. 199–329, 2000.

[8] S. Wolfram, *Theory and Applications of Cellular Automata*, Advanced Series on Complex Systems, World Scientific, Singapore, 1986.

[9] K. Nagel and M. Schreckenberg, "A cellular automaton model for freeway traffic," *Journal de Physique I France*, vol. 2, no. 12, pp. 2221–2229, 1992.

[10] R. Jiang, B. Jia, and Q.-S. Wu, "Stochastic multi-value cellular automata models for bicycle flow," *Journal of Physics A: Mathematical and General*, vol. 37, no. 6, pp. 2063–2072, 2004.

[11] L. W. Lan and C.-W. Chang, "Inhomogeneous cellular automata modeling for mixed traffic with cars and motorcycles," *Journal of Advanced Transportation*, vol. 39, no. 3, pp. 323–349, 2005.

[12] B. Jia, X.-G. Li, R. Jiang, and Z.-Y. Gao, "Multi-value cellular automata model for mixed bicycle flow," *The European Physical Journal B*, vol. 56, no. 3, pp. 247–252, 2007.

[13] X.-G. Li, Z.-Y. Gao, X.-M. Zhao, and B. Jia, "Multi-value cellular automata model for mixed non-motorized traffic flow," *Acta Physica Sinica*, vol. 57, no. 8, pp. 4777–4785, 2008.

[14] G. Gould and A. Karner, "Modeling bicycle facility operation: cellular automaton approach," *Transportation Research Record*, no. 2140, pp. 157–164, 2009.

[15] X.-F. Yang, Z.-Y. Niu, and J.-R. Wang, "Mixed non-motorized traffic flow capacity based on multi-value cellular automata model," *Journal of System Simulation*, vol. 24, no. 12, pp. 2577–2581, 2012.

[16] S. Zhang, G. Ren, and R. Yang, "Simulation model of speed-density characteristics for mixed bicycle flow—comparison between cellular automata model and gas dynamics model," *Physica A: Statistical Mechanics and Its Applications*, vol. 392, no. 20, pp. 5110–5118, 2013.

[17] Ministry of Housing and Urban-Rural Development of China (MOHURD), "Code for design of urban road engineering," Tech. Rep. CJJ37-2012, MOHURD, 2012.

[18] Transportation Research Board, *Highway Capacity Manual (2010)*, National Research Council, Washington, DC, USA, 2010.

[19] M. Rickert, K. Nagel, M. Schreckenberg, and A. Latour, "Two lane traffic simulations using cellular automata," *Physica A*, vol. 231, no. 4, pp. 534–550, 1996.

[20] K. Nishinari and D. Takahashi, "Analytical properties of ultra-discrete Burgers equation and rule-184 cellular automaton," *Journal of Physics A*, vol. 31, no. 24, pp. 5439–5450, 1998.

[21] K. Nishinari and D. Takahashi, "A new deterministic CA model for traffic flow with multiple states," *Journal of Physics A*, vol. 32, no. 1, pp. 93–104, 1999.

[22] K. Nishinari and D. Takahashi, "Multi-value cellular automaton models and metastable states in a congested phase," *Journal of Physics A: Mathematical and General*, vol. 33, no. 43, pp. 7709–7720, 2000.

[23] X. Qu, S. Wang, and J. Zhang, "On the fundamental diagram for freeway traffic: a novel calibration approach for single-regime models," *Transportation Research Part B: Methodological*, vol. 73, pp. 91–102, 2015.

[24] S. Jin, D.-H. Wang, C. Xu, and D.-F. Ma, "Short-term traffic safety forecasting using Gaussian mixture model and Kalman filter," *Journal of Zhejiang University SCIENCE A*, vol. 14, no. 4, pp. 231–243, 2013.

[25] Y. Kuang, X. Qu, and S. Wang, "A tree-structured crash surrogate measure for freeways," *Accident Analysis & Prevention*, vol. 77, pp. 137–148, 2015.

[26] S. Jin, X. Qu, D. Zhou, C. Xu, D. Ma, and D. Wang, "Estimating cycleway capacity and bicycle equivalent unit for electric bicycles," *Transportation Research Part A*, vol. 77, pp. 225–248, 2015.

[27] D. Wang, D. Zhou, S. Jin, and D. Ma, "Characteristics of mixed bicycle traffic flow on conventional bicycle path," in *Proceedings of the 94th Annual Meeting of the Transportation Research Board*, Washington, DC, USA, 2015.

[28] D. Zhou, C. Xu, D. Wang, and S. Jin, "Estimating capacity of bicycle path on urban roads in Hangzhou, China," in *Proceedings of the 94th Annual Meeting of the Transportation Research Board*, Washington, DC, USA, 2015.

Hindawi Publishing Corporation
Discrete Dynamics in Nature and Society
Volume 2015, Article ID 206149, 11 pages
http://dx.doi.org/10.1155/2015/206149

Research Article

Recycler Reaction for the Government Behavior in Closed-Loop Supply Chain Distribution Network: Based on the System Dynamics

Xi gang Yuan[1] and Xiao qing Zhang[2]

[1]*School of Statistics, Southwest University of Financial and Economics, Chengdu, Sichuan 611130, China*
[2]*School of Management, Guangxi University of Science and Technology, Liu Zhou, Guangxi 545006, China*

Correspondence should be addressed to Xi gang Yuan; 1038223569@qq.com

Received 17 December 2014; Accepted 25 January 2015

Academic Editor: Essam Radwan

With system dynamics, we establish three-closed-loop supply chain distribution network system model which consists of supplier, manufacturer, two retailers, and products (parts) recycler. We proposed that recycler make reflect for the government policy by adjusting the recycling ratio and recycling delay. We use vensim software to simulate this model and investigate how the products (parts) recyclers behavior influences the loop supply chain distribution system. The result shows that (1) when recyclers respond positively to government policies, recycling will increase the proportion of recyclers. When recyclers respond negatively to government policy making, recycling will reduce the proportion of recyclers. (2) When the recovery percentage of recyclers improves, manufacturers, Retailer 1, and Retailer 2 quantity fluctuations will reduce and the bullwhip effect will diminish. (3) When the proportion of recycled parts recyclers is lowered, manufacturers, Retailer 1, and Retailer 2 inventory fluctuation will increase and the bullwhip effect will be enhanced. (4) When recyclers recycling product delays increased, volatility manufacturers order quantity will rise, but there is little change in the amount of fluctuation of orders of the two retailers. (5) When recycling parts recyclers delay increases, fluctuations in the supplier order quantity will rise, but there is little change in the amount of fluctuation of orders of the two retailers.

1. Introduction

Nowadays, closed-loop supply chain distribution network system has become a new research point since people pursue circular economy and social sustainable development. Closed-loop supply chain distribution system is a new supply chain form in circular economy. van Wassnhove et al. [1] and Guide Jr. et al. [2] have researched the closed-loop supply chain; they think that we can build a complete closed-loop supply chain distribution network system which includes supply, manufacturing, retail, and recycling and is based on the traditional supply chain and adds to products (parts) recycler.

With products (parts) recycler adding to the supply chain distribution network system, it makes the nature of the supply chain distribution network system gradually changed. Domestic and foreign scholars deeply discuss cooperation mechanism between various members in the supply chain distribution network system. Savaskan et al. [3] and Savaskan and van Wassenhove [4] research the cooperation mechanism problem between manufacturers and retailers under symmetric information with the recycler participating in the supply chain. Forrester [5], Sterman [6], and Baik [7] mainly discuss the cooperative factors and competitive factors in the supply chain distribution network system and come up with the corresponding cooperation strategy. Then, Liu et al. [8] consider competitive factors in different supply chain distribution network system and establish appropriate cooperation model and propose effective solving measure.

Based on the abovementioned articles, many scholars research the bullwhip effect problem in the closed-loop supply chain distribution network system. Based on the two-stage supply chain [8], Wan and Li [9] increase recycling logistics, and they research the bullwhip effect in the closed-loop supply chain distribution network system. Because the recycler participates in the supply chain, it causes the bullwhip effect in the supply chain distribution network system. Forrester [10] analyzes a traditional supply chain and observes how a small change in a customer's demand pattern amplifies as it flows through distribution, production, and replenishment processes. Burbidge [11, 12] presents the so-called PBC (period batch control), which develops the five golden rules to avoid bankruptcy. Subsequently, Towill [13] integrates Forrester and Burbidge's concepts to develop a series of improved communication and materials flow practices in the supply chain. Lee et al. [14] research how the structure of different supply chain types influences the bullwhip effect. Holmström [15] analyzes the bullwhip effect in a supply chain of the grocery industry; Towill and McCullen [16] study the bullwhip effect in a clothes supply chain, while Daganzo [17] unveils the core causes of the bullwhip effect and describes control methods for eliminating all instabilities without increasing supplier costs. However, Sterman [18] provides the best illustration of the bullwhip effect, investigating how human errors affect the dynamics of a system through its well-known business game, the so-called Beer Game, from the performance science perspective, but did not consider the circumstances under asymmetric information.

As can be seen from the abovementioned articles, the shortage of normal research is as follows. Firstly, most articles are limited to accessing the single closed-loop supply chain distribution system; few scholars research the bullwhip effect in the supply chain distribution network system which consists of multiple manufacturers and multiple retailers. And then, few scholars research recycler's reaction to the government policy in the supply chain distribution network system.

Based on the above research, we establish a three-closed-loop supply chain distribution system dynamics model which consists of supplier, manufacturer, two retailers, and products (parts) recycler. We research the influence of each member in supply chain distribution system under different recycling ratios and different recycling delay, thus revealing the impact of product (parts) recycler's behavior on the entire closed-loop supply chain distribution system.

The rest of this paper is organized as follows. In Section 2 we establish a closed-loop supply chain distribution system dynamics model. In Section 3 we illustrate our model using numerical examples. Concluding remarks are given in Section 4.

2. Closed-Loop Supply Chain Distribution System Dynamics Model

In the paper, we establish a closed-loop supply chain distribution system dynamics model by vensim PLE. The model consists of a supplier, a manufacturer, two retailers, and a products (parts) recycler. The supply chain starts from supplier supplying new parts and recycling old parts, manufacturer sailing some products to two retailers, products (parts), and recyclers recycling old products, thus constituting a complete closed-loop supply chain distribution system.

2.1. Model Assumption. The assumption in supply chain distribution system model is as follows.

(1) Suppliers' products (parts) capacity, manufacturers' production capacity, retailers' sale capacity, and transport capacity all have no restriction; products (parts) recyclers recycling products and components capacity have no restriction.

(2) The price of recycling products and parts is equal to new products price; old parts and products are recycled by the manufacturer; manufacturer or supplier is not recycling old parts or old products.

(3) Customer does not discriminate the remanufacturing products and remanufactured parts; customer has the same demand for new products and remanufactured products (parts).

(4) In the paper, using two retailers' market rates, we measure the customer's demand; if two retailers' market rate is high, it indicates that customer's demand is high.

2.2. System Dynamics Model. In the paper, closed-loop supply chain distribution system consists of a supplier, a manufacturer, two retailers, and a products (parts) recycler; in the middle, any link does not appear out of stock. We establish the supply chain distribution system as shown in Figure 1.

In Table 1 and Figure 1, we can find that suppliers' inventory is decided by suppliers' products delay time, parts productivity, recycled parts remanufacturing rate, and suppliers' delivery rate. Manufacturers' inventory is decided by suppliers' delivery rate, recycled products remanufacturing rate, manufacturers' products delay time, and manufacturers' shipment ratio to two retailers. Retailer 1 inventory is decided by market sale's rate and transportation delay time 1. Retailer 2 inventory is decided by market sale's rate and transportation delay time 2. Order of Retailers 1 and 2, the needs for manufacturer's products, and the needs for suppliers' products (parts) are decided by sales forecast, inventory adjustment, and inventory adjustment time. The recycler recycles the waste products (parts) from market. Some recovered products (parts) are directly discarded, some recovered products (parts) for are kept further processing, recycling old products directly flow to the manufacturer, recycling old parts directly flow to the supplier, then parts go through distribution and transport to reach the hands of customers, and this cycle forms a complete closed-loop. We can establish the flow chat of the supply chain distribution network in Figure 2 and the system dynamics model in Figure 3.

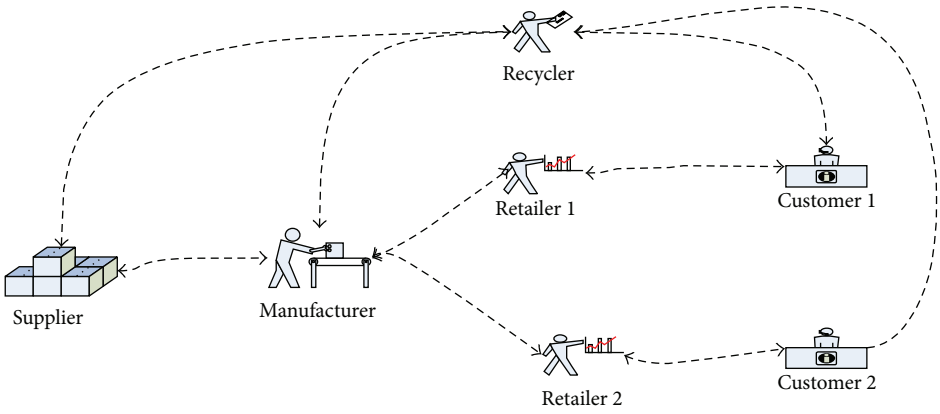

Figure 1: Supply chain distribution system conceptual model.

Table 1: Model constants set.

Parameters	Value	Parameters	Value
Inventory adjustment time	28	Manufacturer product delay	14
Supplier product delay	14	Retailer 2 transportation delay	14
Retailer 1 transportation delay	14	Moving average period number	14
Expect inventory sustainable time	21	Manufacture delivery delay	14
Recycling product adjustment time	14	⟨Time2⟩	12
⟨Time1⟩	12	Supplier delivery delay	14

3. Main Parameters and System Dynamics Equation

3.1. Supplier's Main Equation. Supplier inventory is a stock variable, inflow variables are parts productivity and recycled parts remanufactured rate, and the out of flow variable is delivery rate from supplier to manufacturer. Delivery rate from supplier to manufacturer is based on manufacturer's production orders. Parts productivity is equal to supplier production order. Supplier's expected inventory and supplier's sale forecast are based on the sustainable time of expected inventory. Supplier's parts production consists of supplier's new product and recycled parts remanufacturing product. Supplier's new production order is equal to supplier's production demand rate minus recycled parts remanufactured rate. Supplier's sale forecast is the smoothing function for supplier delivery rate. The function is as follows:

$$\begin{aligned}&\text{Supplier inventory}\\&\quad=\text{DELAY3I}\left(\text{Parts productivity, Delivery delay of the supplier's, Supplier production delays time}\right)\\&\qquad+\text{Recycled parts remanufactured rate}\\&\qquad-\text{Delivery rate from supplier to manufacturer;}\end{aligned}$$

$$\begin{aligned}&\text{Supplier production demand rate}\\&\quad=\text{MAX}\left(0,\text{Supplier's sale forecast}+\frac{\text{Supplier's expect inventory}}{\text{Inventory adjustment time}}-\frac{\text{Supplier inventory}}{\text{Inventory adjustment time}}\right);\end{aligned}$$

$$\begin{aligned}&\text{Supplier's sale forecast}\\&\quad=\text{SMOOTH}\left(\text{Delivery rate from supplier to manufacturer, Average moving period time}\right);\end{aligned}$$

$$\begin{aligned}&\text{Delivery rate from supplier to manufacturer}\\&\quad=\text{DELAY3}\left(\text{Manufacturer production order, Delivery delay of the supplier's}\right);\end{aligned}$$

$$\begin{aligned}&\text{Supplier production orders}\\&\quad=\text{Supplier production demand rate}\\&\qquad-\text{Recycled parts remanufactured rate;}\end{aligned}$$

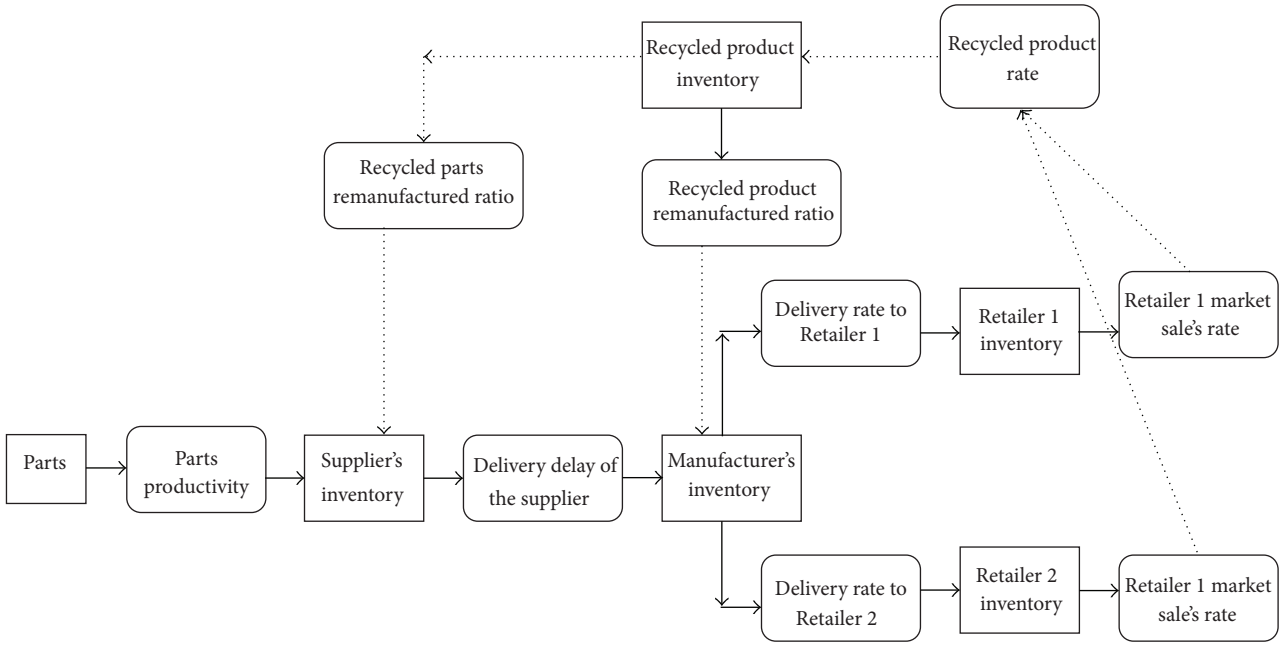

Figure 2: Flow chat of the supply chain distribution system.

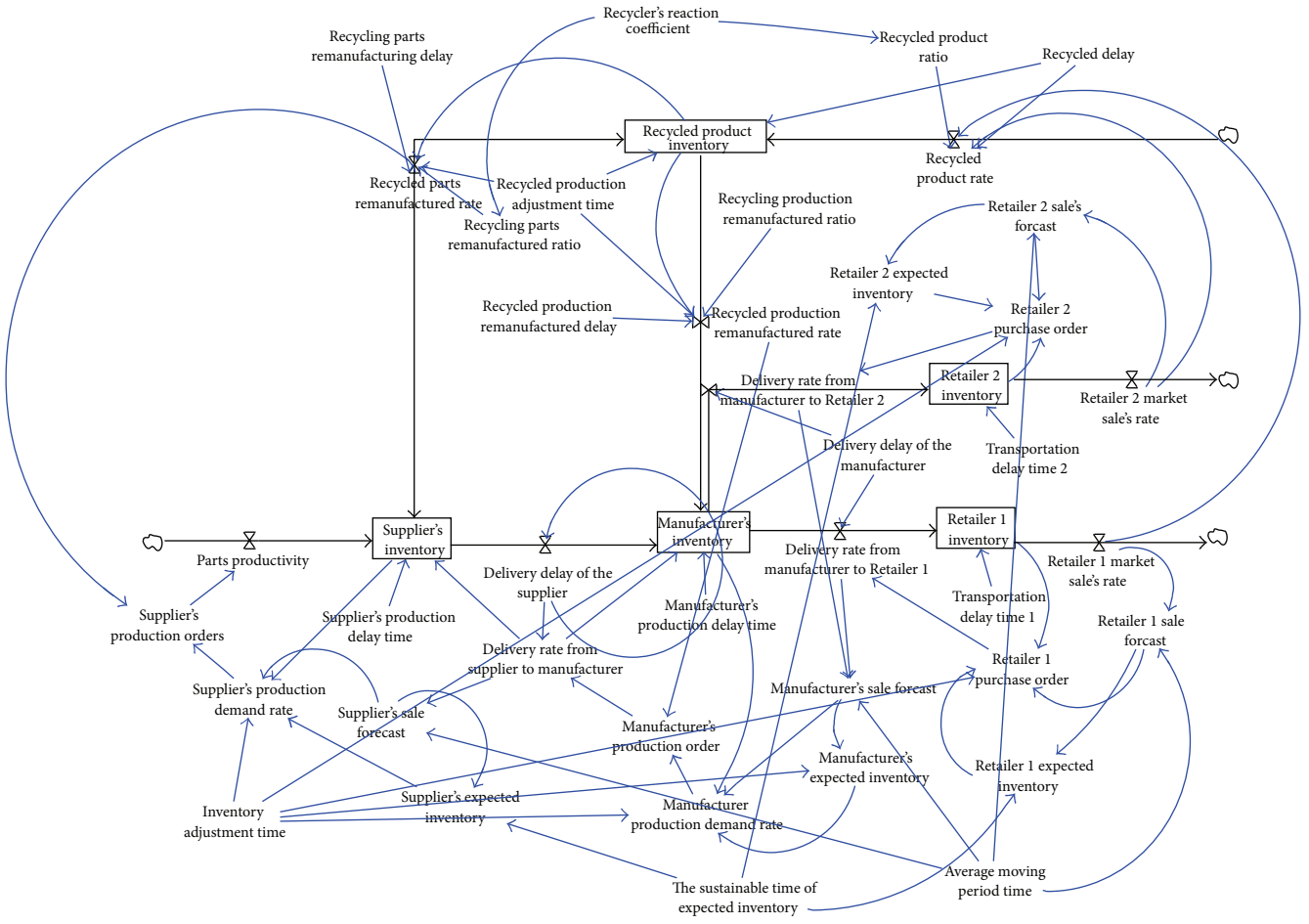

Figure 3: Closed-loop supply chain distribution network system dynamics flow diagram.

Supplier's expect inventory

= Supplier's sale forecast

∗ the sustainable time of expect inventory;

Parts productivity = Supplier production orders. (1)

3.2. Manufacturer's Main Equation. Manufacturer inventory is a stock variable, inflow variables are delivery rate from supplier to manufacturer and recycled production remanufactured rate, and the out of flow variables are delivery rate from manufacturer to Retailer 1 and delivery rate from manufacturer to Retailer 2. Delivery rate from manufacturer to Retailer 1 is based on Retailer 1 sale orders. Delivery rate from manufacturer to Retailer 2 is based on retailer 2 sale orders. Manufacturer's expected inventory and manufacturer's sale forecast are based on the sustainable time of expect inventory. Manufacturer production order is equal to manufacturer production demand rate minus recycled production remanufactured rate. Manufacturer sale forecast is the smoothing function for manufacturer delivery rate. The function is as follows:

Manufacturer inventory

= DELAY3I (Delivery rate from

supplier to manufacturer,

Manufacturer production delays time,

Delivery delay of the supplier's)

+ Recycled production remanufactured rate

− Delivery rate from manufacturerto retailer 1

− Delivery rate from manufacturer to retailer 2;

Manufacturer production order

= MAX (0, Manufacturer production demand rate

−Recycled production remanufactured rate);

Manufacturer production demand rate

$$= \mathrm{MAX}\left(0, \text{Manufacturer's sale forecast} + \frac{\text{Manufacturer expect inventory}}{\text{Inventory adjustment time}} - \frac{\text{Manufacturer inventory}}{\text{Inventory adjustment time}}\right);$$

Manufacturer expect inventory

= Inventory adjustment time

∗ Manufacturer's sale forecast;

Manufacturer's sale forecast

= SMOOTH3I (Delivery rate from

manufacturer to retailer 1,

Delivery rate from manufacturer

to retailer 2,

Average moving period time). (2)

3.3. Retailer 1 and Retailer 2 Main Equation. Retailer 1 inventory and Retailer 2 inventory are all stock variable, inflow variables are delivery rate from manufacturer to Retailer 1 and delivery rate from manufacturer to Retailer 2, and the out of flow variables are Retailer 1 market sale's rate and Retailer 2 sale's rate. Retailer 1 expected inventory and Retailer 1 sale forecast are based on the sustainable time of expect inventory. Retailer 2 expected inventory and Retailer 2 sale forecast are based on the sustainable time of expect inventory. Retailer 1 purchase order is related to Retailer 1 sale forecast, Retailer 1 expected inventory, and inventory adjustment time. Retailer 2 purchase order is related to Retailer 2 sale forecast, Retailer 2 expected inventory, and inventory adjustment time. Retailer 1 sale forecast is the smoothing function for Retailer 1 market sale's rate. Retailer 2 sale forecast is the smoothing function for Retailer 2 market sale's rate. The function is as follows:

Retailer 1 inventory

= DELAY3 (Delivery rate from manufacturer

to retailer 1, Transportation delay 1)

− Retailer 1 market sale's rate;

Delivery rate from manufacturer to retailer 1

= DELAY3 (Retailer 1 purchase order, Delivery

delay of the manufacturer's);

Retailer 1 expect inventory

= Retailer's 1 sale forecast

∗ the sustainable time of expect inventory;

Retailer 1 purchase order

$$= \mathrm{MAX}\left(0, \text{Retailer's 1 sale forecast} + \frac{\text{Retailer 1 expect inventory}}{\text{Inventory adjustment time}} - \frac{\text{Retailer 1 inventory}}{\text{Inventory adjustment time}}\right);$$

Retailer's 1 sale forecast

$$= \text{SMOOTH}\left(\text{Retailer 1 market sale's rate}, \text{Average moving period time}\right);$$

Retailer 2 inventory

$$= \text{DELAY3}\left(\text{Delivery rate from manufacturer to retailer 2}, \text{Transportation delay 2}\right) - \text{Retailer 2 market sale's rate};$$

Retailer 2 purchase order

$$= \text{MAX}\left(0, \text{Retailer 2 sale's forecast} + \frac{\text{Retailer 2 expect inventory}}{\text{Inventory adjustment time}} - \frac{\text{Retailer 2 inventory}}{\text{Inventory adjustment time}}\right);$$

Retailer's 2 sale forecast

$$= \text{SMOOTH}\left(\text{Retailer 2 market sale's rate}, \text{Average moving period time}\right);$$

Delivery rate from manufacturer to retailer 2

$$= \text{DELAY3}\left(\text{Retailer 2 purchase order}, \text{Delivery delay of the manufacturer's}\right);$$

Retailer 2 expect inventory

$$= \text{Retailer's 2 sale forecast} * \text{the sustainable time of expect inventory}. \quad (3)$$

3.4. Recycler's Main Equation. Recycled product inventory is a stock variable, inflow variables are recycled product rate and recycled production adjustment time, and the out of flow variables are recycled production remanufactured rate and recycled parts remanufactured rate. Recycled production remanufactured rate is based on the recycled production remanufactured delay. Recycled production rate is based on recycled product ratio, Retailer 1 market sale's rate, recycled product ratio, and Retailer 2 market sale's rate. Recycled parts remanufactured rate is mainly based on the recycled production remanufactured delay and recycling parts remanufactured ratio. The function is as follows:

Recycled product inventory

$$= \text{DELAY3}\left(\text{Recycled delay}, \text{Recycled product rate} * \text{Recycled production adjustment time}\right) - \text{Recycled production remanufactured rate} - \text{Recycled parts remanufactured rate};$$

Recycled production remanufactured rate

$$= \text{DELAY3}\left(\text{Recycled product inventory} * \frac{\text{Recycling production remanufactured ratio}}{\text{Recycled production adjustment time}}, \text{Recycled production remanufactured delay}\right);$$

Recycled product rate

$$= \text{DELAY1}\left(\text{Recycled product ratio} * \text{Retailer 1 market sale's rate}, \text{Recycled product ratio} * \text{Retailer 2 market sale's rate}, \text{Recycled delay}\right);$$

Recycled parts remanufactured rate

$$= \text{DELAY3}\left(\text{Recycled product inventory} * \frac{\text{Recycling parts remanufactured ratio}}{\text{Recycled production adjustment time}}, \text{Recycling parts remanufacturing delay}\right). \quad (4)$$

4. System Dynamics Simulation Model Which Is Recycler's Reaction to the Government Policy in Closed-Loop Supply Chain Distribution Network

In closed-loop supply chain distribution network, recycler's products recycled rate is based on the recycled ratio. We assume that recycler recycles the old product at a certain proportion. When the manufacturer produces products, recycler predicts the manufacturer's remanufacturing order, according to the manufacturer's remanufacturing rate, and determines their own recycling ratio. The higher the remanufacturing order, the higher the recycling ratio. In 2009, "the circular economy promotion law of China" can be promulgated. In 2011, the regulation of the waste electrical electronic products recycling and dealing can be promulgated. It is more important for us to protect the environment around us. Our government comes up with the "producer responsibility system"; it asks the producer not only to be responsible for the environment pollution in the process of production but they should also be responsible for the environment pollution in the whole life cycle. Based on above, we propose recycler's reaction coefficient to respond for the environment policy such as the law or policy of mentioned above. We assume that the recycler reaction coefficients are $-1, 0, 1$. When recycler makes positive response to the government environment policy, the recycler reaction coefficient is 1; when recycler

makes no response to the government environment policy, the recycler reflection coefficient is 0; when recycler makes negative response to the government environment policy, the recycler reflection coefficient is −1.

Recycler's products recycled rate = DELAY1(products recycled ratio ∗ Retailer 1 market sale's rate and recycling delay time) + DELAY1(products recycled ratio ∗ Retailer 2 market sale's rate and recycling delay time). As can be seen from the above equation, recyclers recycling behavior is mainly affected by the recycled ratio and recycled delay time.

Based on the above research, we assumed the following.

Assumption 1. When recycler makes positive response to the government policy, recycler will increase the recycling rate; when recycler makes negative response to the government policy, recycler will decrease the recycling rate.

Assumption 2. When recyclers increase the recycling rate, manufacturers, Retailer 1, and Retailer 2 will decrease inventory, and the bullwhip effect will be weak.

Assumption 3. When recyclers decrease the recycling rate, manufacturers, Retailer 1, and Retailer 2 will increase inventory, and the bullwhip effect will be enhanced.

4.1. Numerical Examples. Based on the above assumptions, we establish system dynamics model verifying the accuracy of the above assumptions. In the paper, the set for mathematical equations about recycling ratio are as follows:

$$\begin{aligned}&\text{Product recycling ratio}\\&\quad=\text{recyclers' reaction coefficient}\\&\qquad*\left(\text{baseline product recycling ratio}\right.\\&\qquad\quad\left.+\alpha_1*\text{product reproduction ordering ratio}\right)^{1/2},\\&\text{Parts recycling ratio}\\&\quad=\text{recyclers' reaction coefficient}\\&\qquad*\left(\text{baseline parts recycling ratio}\right.\\&\qquad\quad\left.+\alpha_2*\text{parts reproduction ordering ratio}\right)^{1/2}.\end{aligned}\tag{5}$$

When we use the system dynamics simulation, the baseline product recycling ratio is 0.1, the baseline parts recycling ratio is 0.2, parts recycling delay time is 14 days, product recycling delay time is 21 days, and recycler reaction coefficients are −1, 0, and 1. When recycler makes positive response to the government policy, the recycler reaction coefficient is 1; when recycler makes no response to the government policy, the recycler reflection coefficient is 0; when recycler makes negative response to the government policy, the recycler reflection coefficient is −1. We can get

$$\begin{aligned}\alpha_1&=\left(\frac{\text{product recycling ratio}^2}{\text{recyclers' reaction coefficient}}\right.\\&\qquad\left.-\text{baseline product recycling ratio}\right)\\&\qquad\cdot\left(\text{product reproduction ordering rate}\right)^{-1},\\\alpha_2&=\left(\frac{\text{parts recycling ratio}^2}{\text{recyclers' reaction coefficient}}\right.\\&\qquad\left.-\text{baseline parts recycling ratio}\right)\\&\qquad\cdot\left(\text{parts reproduction ordering rate}\right)^{-1}.\end{aligned}\tag{6}$$

Combination with the simulation result of specific model, $\alpha_1 = 0.000001$, and $\alpha_2 = 0.000002$ results in

$$\begin{aligned}&\text{Product recycling ratio}\\&\quad=\text{recyclers' reaction coefficient}\\&\qquad*\left(\text{baseline product recycling ratio} + 0.000001\right.\\&\qquad\quad\left.*\text{product reproduction ordering rate}\right)^{1/2},\\&\text{Part recycled ratio}\\&\quad=\text{recyclers' reaction coefficient}\\&\qquad*\left(\text{baseline parts recycling ratio} + 0.000002\right.\\&\qquad\quad\left.*\text{parts reproduction ordering rate}\right)^{1/2}.\end{aligned}\tag{7}$$

4.2. Research on Recycler Reaction Coefficient in System Dynamics. Simulation setting is as follows: INITIAL TIME = 0 days, FINALTIME = 4000 days, TIME STEP = 1 day, SAVEPER = TIME STEP; the simulation period is 4000 days, one day for a step.

4.2.1. The Change of Recycling Ratio under Different Reaction Coefficient

(1) Product Recycling Ratio under Different Recyclers Reflection Coefficient. As can be seen from Figure 4, run 1 is product recycling ratio when recycler reaction coefficient is 1; run 2 is product recycling ratio when recycler reaction coefficient is 0; run 3 is product recycling ratio when recycler reaction coefficient is −1. This also shows that when recycler makes positive response to the government policy, recycler will increase recycling ratio and when recycler makes negative response to the government policy, recycler will reduce the recycling ratio.

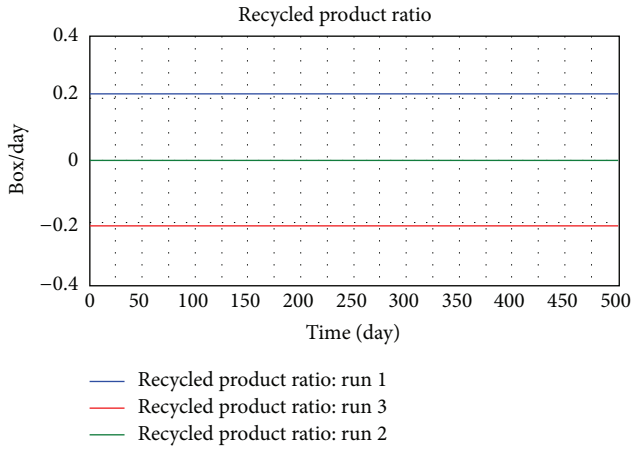

Figure 4: Product recycling ratio under different recycler reaction coefficients.

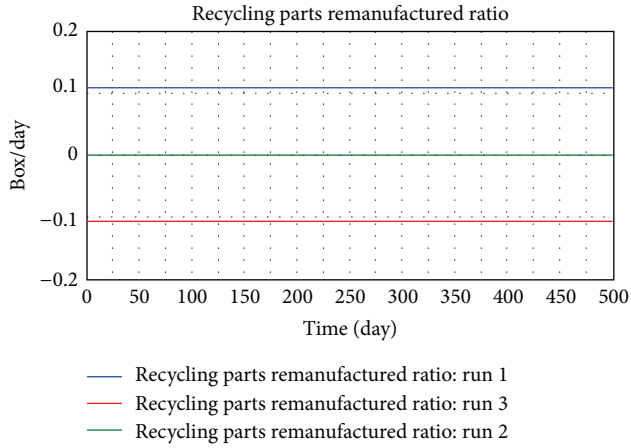

Figure 5: Parts recycling ratio under different recycler reaction coefficients.

4.2.2. Parts Recycling Ratio under Different Recycler Reaction Coefficient. As can be seen from Figure 5, and Table 2 run 1 is parts recycling ratio when recycler reaction coefficient is 1; run 2 is parts recycling ratio when recycler reaction coefficient is 0; run 3 is parts recycling ratio when recycler reaction coefficient is −1. This also shows that when recyclers make positive response to the government policy, recycler will increase recycling ratio and when recyclers make negative response to the government policy and the various members' order changes in the supply chain distribution network under different recyclers reflection coefficient and recycling delay.

(1) Various Members' Order Changes in the Supply Chain Distribution Network under Different Recyclers Reflection Coefficient. The main difference between the traditional supply chain model and the supply chain distribution network model established in this paper is that we add two retailers. As a result, the relationship is more complex in this supply chain. We consider when recycler reaction coefficient changes, how the order changes in manufacturer and two retailers.

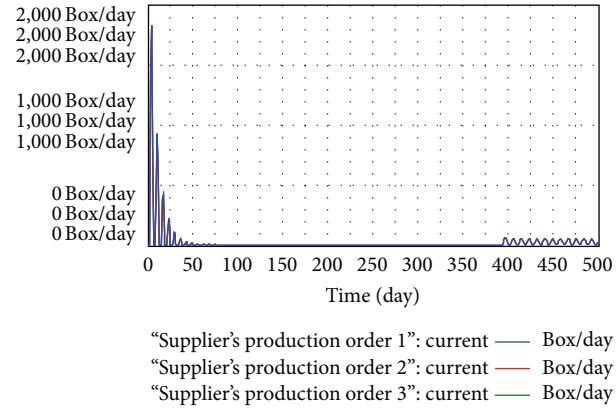

Figure 6: The members' order quantity changes when recycler reaction coefficient is 1.

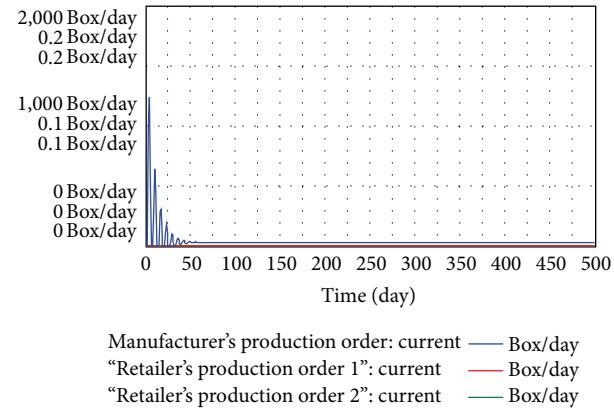

Figure 7: The members' order quantity changes when recycler reaction coefficient is 2.

As can be seen from the Figures 6, 7, and 8, when recycler reaction coefficient is 1, the fluctuation of order quantity is very large in each of the members, range bound between 0 and 2000. When recycler reaction coefficient is 2, the fluctuation of order quantity in each member is decreased; when recycler reaction coefficient is 3, the fluctuation of order quantity in each member reduces between 0 and 1000. With recycler reaction coefficient increasing, order quantity in each member gradually reduces.

We introduce the variation coefficient in the financial management and quantify the bullwhip effect in the closed-loop supply chain distribution network:

$$\text{Bullwhip effect} = \frac{\delta(x_i)/E(x_i)}{\delta(y_i)/E(y_i)}, \tag{8}$$

where $\delta(x_i)$ is said to be the standard of the order rate, $E(x_i)$ is said to be the expectation of the order rate, $\delta(y)$ is said to be the standard of the market sailor rate, and $E(x)$ is said to be the expectation of the market sailor rate.

(2) The Effect of Recycled Products Delay on the Order Quantity in Manufacturers and Two Retailers. As can be seen from the Figures 9, 10, and 11, and Table 3 with the increase of

Table 2: Bullwhip effect of the order quantity of each member under different recycler's coefficient.

	Recycler reaction coefficient is 1	Recycler reaction coefficient is 2	Recycler reaction coefficient is 3
Manufacturer order quantity	105.32	100.08	98.24
Retailer 1 order quantity	85.24	79.201	68.204
Retailer 2 order quantity	83.054	77.204	65.38

Table 3: The bullwhip effect when product recycling delay times are different (3) parts recycling delay's influence on supplier and two retailers.

	Recyclers reflection coefficient is 1	Recyclers reflection coefficient is 2	Recyclers reflection coefficient is 3
Manufacturer order quantity	105.32	120.52	140.25
Retailer 1 order quantity	85.24	86.32	88.27
Retailer 2 order quantity	83.56	84.22	86.57

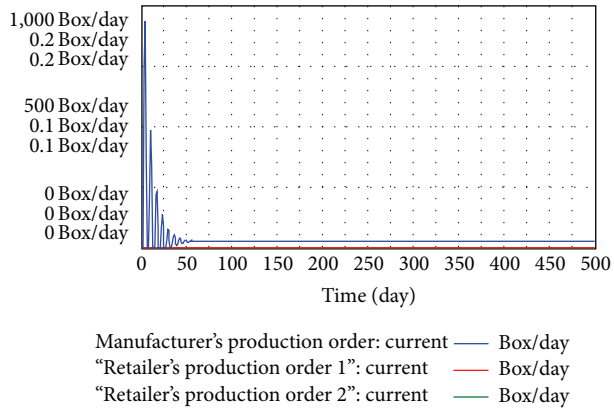

Figure 8: The members' order quantity changes when recycler reaction coefficient is 3.

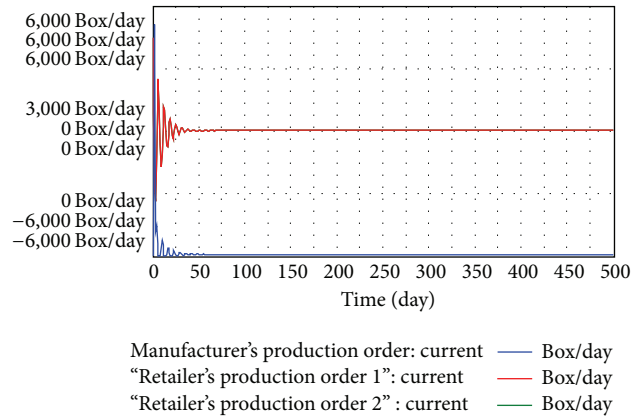

Figure 9: Changes of the order quantity of each member when recycled product delay time is 14.

recycling product delay time, fluctuations of the order in the two retailers did not change much; at the same time, with the increasing of the recycled product delay time, fluctuation of the order in manufacturer gradually increases. This is mainly due to the recycling product delay time directly affecting changes in the manufacturer's order.

(3) Parts Recycling Delay's Influence on Supplier and Two Retailers. As can be seen from the Figures 12, 13, and 14, and Table 4 with the parts recycling delay time increasing, fluctuations of the order in two retailers did not change much; at the same time, with the parts recycling delay time increasing, fluctuation of the order in manufacturer gradually increases. This is mainly due to the parts recycling delay time directly affecting changes of the manufacturer's order.

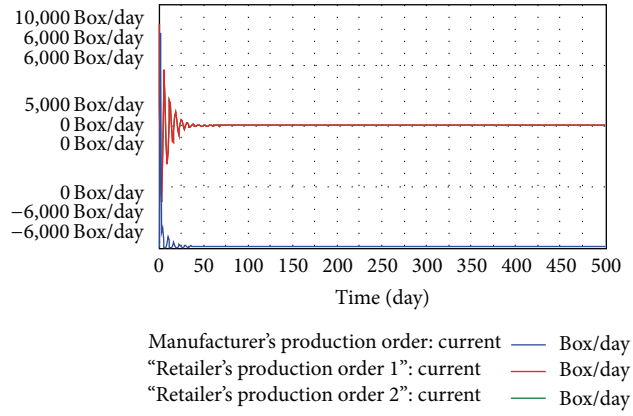

Figure 10: Changes of the order quantity of each member when recycled product delay time is 21.

5. Conclusion

In this paper, we research the different reflection of recyclers on the government policy. We can get the conclusion that (1) when recyclers respond positively to government policies, recycling will increase the proportion of recyclers. When recyclers respond negatively to government policy making, recycling will reduce the proportion of recyclers. (2) When the recovery percentage of recyclers improves, manufacturers, Retailer 1, and Retailer 2 order quantity fluctuations will reduce and the bullwhip effect will diminish. (3) When the proportion of recycled parts recyclers is lowered, manufacturers, Retailer 1, and Retailer 2 inventory fluctuation will increase and the bullwhip effect will be enhanced. (4) When recyclers recycling product delays increased, volatility manufacturers order quantity will rise, but there is little change in the amount of fluctuation of orders of two retailers. (5) When recycling parts recyclers delay increases, fluctuations in the

Table 4: The bullwhip effect when parts recycling delay times are different.

	Recyclers reflection coefficient is 1	Recyclers reflection coefficient is 2	Recyclers reflection coefficient is 3
Supplier order quantity	102.412	118.521	147.502
Retailer 1 order quantity	88.21	89.21	92.01
Retailer 2 order quantity	86.204	88.024	89.2817

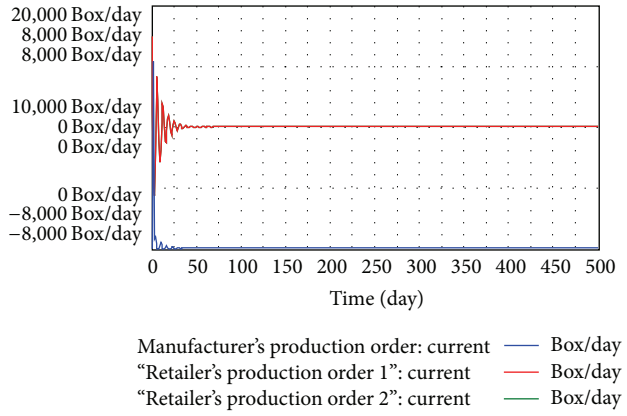

Figure 11: Changes of the order quantity of each member when recycled product delay time is 42.

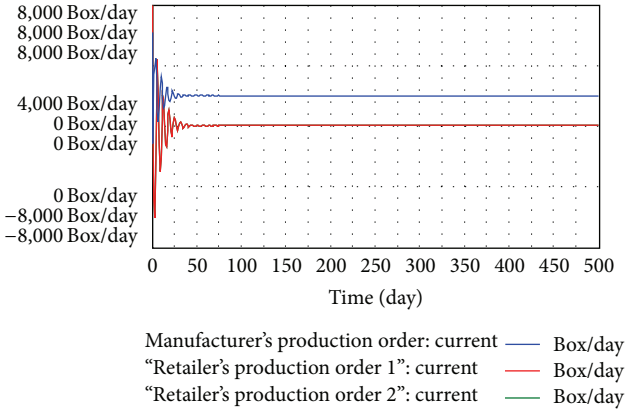

Figure 12: Changes of the order quantity of each member when parts recycling delay time is 14.

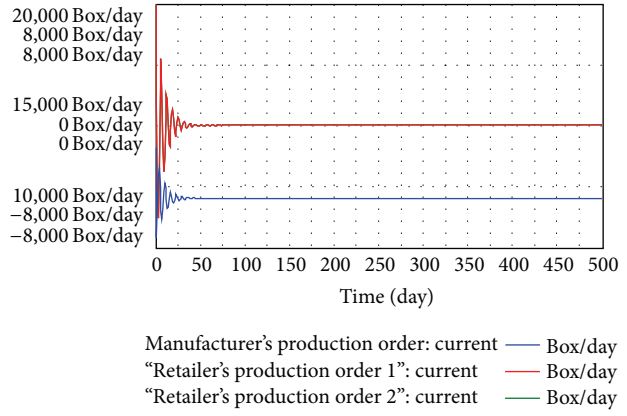

Figure 13: Changes of the order quantity of each member when parts recycling delay time is 21.

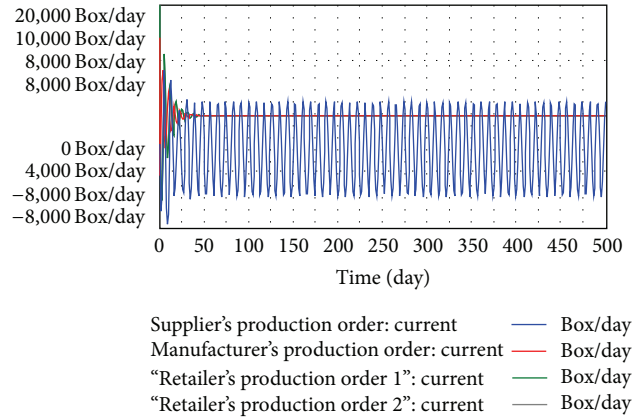

Figure 14: Changes of the order quantity of each member when parts recycling delay time is 42.

supplier order quantity will rise, but there is little change in the amount of fluctuation of orders of two retailers.

Disclosure

The research interests are supply chain management, distribution network, and regional logistics. Some papers of Xi gang Yuan is published in Logistics Technology Journal and Journal of Information Technology.

Conflict of Interests

The authors declare that there is no conflict of interests regarding the publication of this paper.

References

[1] L. N. van Wassnhove, H. R. Krikke, and J. Q. Bloemhof-Ruwaard, "Design of closed-loop supply chains: a production and return network for refrigerators," *Erasmus Research Institute of Management*, vol. 17, no. 8, pp. 312–319, 2001.

[2] V. D. R. Guide Jr., V. Jayaraman, and J. D. Linton, "Building contingency planning for closed-loop supply chains with product recovery," *Journal of Operations Management*, vol. 21, no. 3, pp. 259–279, 2003.

[3] R. C. Savaskan, S. Bhattacharya, and L. N. van Wassenhove, "Closed-loop supply chain models with product remanufacturing," *Management Science*, vol. 50, no. 2, pp. 239–252, 2004.

[4] R. C. Savaskan and L. N. van Wassenhove, "Reverse channel design: the case of competing retailers," *Management Science*, vol. 52, no. 1, pp. 1–14, 2006.

[5] J. Forrester, *Industrial dynamics*, The M.I.T.Press, Cambridge, UK, 1961.

[6] J. Sterman, *Business Dynamics: System Thinking and Modeling for a Complex World*, McGraw-Hill/Irwin, 2000.

[7] Y. Baik, *Control in the Extended Enterprise*, University of Waterloo, 1997.

[8] X. L. Liu, J. H. Ji, and J. L. Li, "The network structure in the supply chain based on the system dynamics simulation," *System Engineer*, vol. 24, no. 6, pp. 40–45, 2006.

[9] Z. Wan and B. Li, "The bullwhip effect in the closed-loop supply chain based on system dynamics," *Computer Integrated Manufacturing Systems*, vol. 18, no. 5, pp. 1093–1098, 2012.

[10] J. W. Forrester, "Industrial dynamics: a breakthrough for decision makers," *Harvard Business Review*, vol. 8, no. 9, pp. 37–66, 1958.

[11] J. L. Burbidge, "The new approach to production," *Production Engineer*, vol. 40, no. 12, pp. 769–784, 1961.

[12] J. Burbidge, "Five golden rules to avoid bankruptcy," *Production Engineer*, vol. 62, no. 10, pp. 13–14, 1983.

[13] D. R. Towill, "Forridge-Principles of good practice in material flow," *Production Planning and Control*, vol. 8, no. 7, pp. 622–632, 1997.

[14] H. L. Lee, V. Padmanabhan, and S. Whang, "Information distortion in a supply chain: the bullwhip effect," *Management Science*, vol. 43, no. 4, pp. 546–558, 1997.

[15] J. Holmström, "Product range management: a case study of supply chain operations in the European grocery industry," *Supply Chain Management*, vol. 2, no. 3, pp. 107–115, 1997.

[16] D. R. Towill and P. McCullen, "The impact of an agile manufacturing on supply chain dynamics," *International Journal of Logistics*, vol. 11, no. 10, pp. 83–96, 1999.

[17] C. F. Daganzo, *A Theory of Supply Chains*, Institute of Transportation Studies and Department of Civil and Environment Engineering University of California, Berkeley, Calif, USA, 2002.

[18] J. D. Sterman, "Modeling managerial behavior: misperceptions of feedback in a dynamic decision making experiment," *Management Science*, vol. 35, no. 3, pp. 321–339, 1989.